

PERFORMANCE BASED SEISMIC DESIGN OF REINFORCED CONCRETE
TALL BUILDINGS

A THESIS SUBMITTED TO
THE GRADUATE SCHOOL OF NATURAL AND APPLIED SCIENCES
OF
MIDDLE EAST TECHNICAL UNIVERSITY

BY

ERHAN BUDAK

IN PARTIAL FULFILLMENT OF THE REQUIREMENTS
FOR
THE DEGREE OF MASTER OF SCIENCE
IN
CIVIL ENGINEERING

SEPTEMBER 2015

Approval of the thesis:

**PERFORMANCE BASED SEISMIC DESIGN OF REINFORCED
CONCRETE TALL BUILDINGS**

Submitted by **ERHAN BUDAK** in partial fulfillment of the requirements for the degree of **Master of Science in Civil Engineering Department, Middle East Technical University** by,

Prof. Dr. Gülbin Dural Ünver
Dean, Graduate School of **Natural and Applied Sciences**

Prof. Dr. Ahmet Cevdet Yalçiner
Head of Department, **Civil Engineering**

Prof. Dr. Haluk Sucuoğlu
Supervisor, **Civil Engineering Dept., METU**

Examining Committee Members:

Prof. Dr. H. Polat Gülkan
Civil Engineering Dept., Çankaya University

Prof. Dr. Haluk Sucuoğlu
Civil Engineering Dept., METU

Prof. Dr. Barış Binici
Civil Engineering Dept., METU

Prof. Dr. Murat Altuğ Erberik
Civil Engineering Dept., METU

Assoc. Prof. Dr. Afşin Sarıtaş
Civil Engineering Dept., METU

Date: 10.11.2015

I hereby declare that all information in this document has been obtained and presented in accordance with academic rules and ethical conduct. I also declare that, as required by these rules and conduct, I have fully cited and referenced all material and results that are not original to this work.

Name, Last name : Erhan BUDAK

Signature :

ABSTRACT

PERFORMANCE BASED SEISMIC DESIGN OF REINFORCED CONCRETE TALL BUILDINGS

Budak, Erhan

M.S., Department of Civil Engineering

Supervisor: Prof. Dr. Haluk Sucuoğlu

September 2015, 150 pages

Cities, their economies and populations are steadily increasing all over the world. In parallel, the land prices in those cities are rising enormously, hence the need for new living spaces has been arisen. These results bring some obligations and new perspectives for those cities in order to address their needs. In addition, improvements and developments in technological equipment, material science and analyses methods have opened great opportunities to construct new life areas by rising the vertical direction instead of horizontal direction. Considering all these facts, the need for tall buildings are growing up and the design of tall buildings are increasing gradually day by day. However, most of those buildings are located in the regions of high seismicity. Unfortunately, the behaviour of tall buildings, especially under the effect of seismic loading, is one of the most sophisticated problems in earthquake engineering. In this study, the behaviour of tall buildings under seismic

loading is investigated by utilizing performance based seismic design (PBSD) approach.

Unlike regular buildings, tall buildings are special due to their specific architectural properties and building configurations. Accordingly, the behaviour of tall buildings under the effect of seismic actions is different since the contribution of higher mode effects is significant on the dynamic behaviour of tall buildings. Moreover, there exist some important differences from design to analysis to construction. In addition, current prescriptive seismic codes are too restrictive and inadequate to understand the anticipated behaviour of tall buildings and apply a reasonable design. In this study, all of these problems are explained elaborately and addressed. On the other hand, alternative high strength materials and innovative structural systems have growingly employed to resist unique challenges introduced by these structures in the regions of high seismicity. Considering all these facts, several institutions and building officials have proposed and published alternative consensus guidelines which are based on performance based design concepts by conducting nonlinear time history analysis. The methodology of these alternative non-prescriptive guidelines is investigated and compared with each other.

Nowadays, performance based seismic design of tall buildings by conducting nonlinear dynamic analysis is being used increasingly for tall buildings. Some building departments and seismic codes obligate designer to use this method on tall buildings. PBSD approach is quite sophisticated and a time consuming process from creating nonlinear modelling to the interpretation of results. However, there are also a variety of uncertainties from modelling of the component to the selection of ground motions to define performance target levels. All of these issues are also examined in the scope of this study. Finally, a reinforced concrete unsymmetrical-plan tall building with 34 stories is designed according to the Turkish Seismic Code under design level earthquake. For both service level and collapse prevention levels, nonlinear time history analysis is employed by using a suite set of seven ground motions for checking the results in compliance with the determined target

performance levels. The results have indicated that satisfactory seismic performance can be obtained through the use of performance based seismic design procedures.

Keywords: Tall buildings, reinforced concrete tall buildings, performance based seismic design, seismic performance, nonlinear time history analysis

ÖZ

BETONARME YÜKSEK YAPILARIN PERRFORMANS ESASLI SİSMİK TASARIMI

Budak, Erhan
Yüksek Lisans, İnşaat Mühendisliği Bölümü
Tez Yöneticisi: Prof. Dr. Haluk Sucuoğlu

Eylül 2015, 150 Sayfa

Dünya genelinde şehirlerin ekonomileri ve nüfusları sürekli artmaktadır. Buna paralel olarak şehirlerdeki arsa fiyatları da aşırı derecede değerlenmekte ve yeni yaşam alanları için gereksinimler ortaya çıkmaktadır. Bu sonuçlar neticesinde şehirlerdeki barınma gereksinimlerini karşılamak üzere bazı yükümlülükler ve yeni perspektifler geliştirilmesi gerekmiştir. Ek olarak teknolojik donanımlarındaki, malzeme bilimindeki ve analiz metotlarındaki gelişmeler ve ilerlemeler yatay yönde yaşam alanları inşa etmek yerine düşey yönde oluşturmaya imkan sağlamıştır. Tüm bu gerçekler göz önüne alındığında, yüksek bina ihtiyacı artmakta ve yüksek bina tasarımları her geçen gün giderek artmaktadır. Ancak, bu binaların çoğu yüksek sismik bölgelerde bulunmaktadır. Ne yazık ki, özellikle deprem yükleri etkisindeki yüksek binaların davranışı, deprem mühendisliğinde en karmaşık sorunlardan biridir. Bu çalışmada, deprem yükleri altında yüksek binaların davranışı performans esaslı sismik tasarım (PEST) yaklaşımı kullanılarak incelenmiştir.

Normal binaların aksine, yüksek binalar kendi özel mimari özellikleri ve bina yapılandırmaları nedeniyle özellerdir. Buna göre, yüksek mod etkilerinin katkısı yüksek binaların dinamik davranışı üzerinde önemli olduğundan sismik etkiler altında yüksek binaların davranışı farklıdır. Ayrıca, tasarım, analiz ve inşaaşamalarında da bazı önemli farklılıklar vardır. Buna ek olarak, yürürlükteki sismik kodlar yüksek binaların davranışlarını anlamak ve makul bir tasarım için çok kısıtlayıcı ve yetersizdirler. Bu çalışmada, tüm bu sorunların özenle ele alınıp açıklanacaktır. Öte yandan, alternatif yüksek mukavemetli malzemeler ve yenilikçi yapı sistemleri yüksek sismik tehlikeye sahip bölgelerde bu yapı tiplerinin yapımını kolaylaştırmak için daha yoğun bir şekilde kullanılmaktadır. Tüm bu gerçekler göz önüne alındığında, birçok kurum ve yetkili kişi zaman tanım alanında doğrusal olmayan analizlerle gerçekleştirilen performans esaslı tasarım ilkelerine dayalı alternatif kurallar yayınlamaktadır. Bu alternatif kurallardaki metodolojiler incelenerek ve birbirleriyle karşılaştırılacaktır.

Günümüzde, yüksek binaların tasarım aşamasında doğrusal olmayan dinamik analiz kullanılarak gerçekleştirilen performans esaslı sismik tasarım daha çok kullanılmaktadır. Bazı bina bölümleri ve sismik kodlar, yüksek binalar üzerinde bu yöntemi kullanmak için tasarımcıyı zorunlu tutmaktadır. PEST yaklaşımı model oluşturmasından sonuçların yorumlanmasına kadar oldukça sofistike ve zaman alıcı bir süreci içermektedir. Ancak, aynı zamanda performans hedef seviyelerini tanımlamak için zemin hareketlerinin seçimi ve bileşen modellemedeki belirsizlikler gibi çok farklı belirsizlikler de PEST yaklaşımında bulunmaktadır. Bütün bu sorunlar da bu çalışma kapsamında incelenmiştir. Son olarak, 34 katlı simetrik olmayan plana sahip bir betonarme bina tasarım düzeyi depremi etkisi altında Türk Deprem Şartnamesindeki hükümlere uygun olarak tasarlanmıştır. Hem hizmet seviyesi hem de göçme düzeyleri için, doğrusal olmayan zaman tanım alanında analizler kullanılarak yedi farklı zemin hareketi etkisi altında belirlenen hedef performans seviyesi kontrolleri gerçekleştirilmiştir. Sonuçlar tatmin edici sismik performansın, performans esaslı sismik tasarım prosedürlerinin kullanılmasıyla elde edilebildiğini göstermiştir.

Anahtar Kelimeler: Yüksek Yapılar, betonarme yüksek yapılar, performans esaslı sismik tasarım, sismik performans, zaman tanım aralığında doğrusal olmayan analiz

To my honourable teacher Erdal Can and my big family

ACKNOWLEDGMENT

I have completed this project with the help and believe of many precious and respectful people in my life .I am thankful to all of them but firstly I would like to thank to my supervisor Prof. Dr. Haluk Sucuođlu for his guidance, patience, wisdom, encouragement and valuable friendship during this tough but pleasant process.

Very special thanks to dear Alper Aldemir for being a supportive big brother, teacher and friend to me. He also deserves my appreciation as he has always been with me in my hard times with his knowledge and guidance. I have learnt a lot from his friendship and character.

I would also like to thank my precious colleagues İsmail Ozan Demirel, Gizem Mestav Sarıca, Baran obanođlu, Beyazıt Bestami Aydın, Ali Gharibdoust, Dr. Ali Kerimzade for their support, encouragement and patience in this period.

I would like to express special thanks to my real friends Cankat Tanriverdi and Rehber Akdođan with whom I set off this journey ten years ago with nice and promising dreams.

Finally, my deepest gratitude goes to my family and Semra Uđurlu for their constant support and encouragement in all respects with love. This dissertation would not have been possible without them.

TABLE OF CONTENTS

ABSTRACT.....	V
ÖZ	VIII
ACKNOWLEDGMENT.....	XII
LIST OF TABLES	XVI
LIST OF FIGURES	XVII
LIST OF SYMBOLS / ABBREVIATIONS	XXV
CHAPTERS	
1 INTRODUCTION	1
1.1 PROBLEM STATEMENT.....	1
1.2 SEISMIC DESIGN GUIDELINES ON THE PERFORMANCE BASED DESIGN OF TALL BUILDINGS	5
1.2.1 Definition of Tall Buildings	8
1.2.2 Why NLTHA is used for Tall Buildings?.....	9
1.3 OBJECTIVES AND SCOPE	13
2 SEISMIC PERFORMANCE ASSESSMENT.....	15
2.1 INTRODUCTION.....	15
2.2 TYPES OF NONLINEAR MODELS.....	16
2.3 MATERIAL MODELS	20
2.3.1 Uniaxial Reinforcement Steel Models for Fiber Models	21
2.3.2 Uniaxial Unconfined and Confined Concrete Models for Fiber Sections	26
2.3.3 Shear Material Model for Fiber Element	29
2.4 NONLINEAR MODELING OF REINFORCED CONCRETE MEMBERS	30
2.4.1 Nonlinear Modeling Parameters for Reinforced Concrete Beam and Column Members	31
2.4.2 Nonlinear Modeling of Beam Elements.....	38

2.4.2.1 Exact Model	40
2.4.2.2 Finite Element Model.....	40
2.4.2.3 Plastic Hinge Model	42
2.4.2.4 Plastic Zone Model.....	42
2.4.3 Nonlinear Modeling of Reinforced Column Members	43
2.4.4 Modeling of Reinforced Concrete Shear walls	43
2.4.5 Nonlinear Modeling of Reinforced Concrete Coupling Beams	48
2.5 P-DELTA EFFECTS	50
2.6 GRAVITY LOAD EFFECTS IN NONLINEAR ANALYSIS	51
2.7 GROUND MOTIONS SELECTION.....	51
2.8 DESCRIPTION OF PERFORMANCE LEVELS AND ACCEPTANCE CRITERIA FOR TALL BUILDINGS	53
2.8.1 Summary of Performance Levels and Acceptance Criteria According to TEC-2007	54
2.8.1.1 Description of Performance Levels.....	54
2.8.1.2 Damage Limits (acceptance criteria) for reinforced concrete members	56
2.8.2 Summary of Performance Levels and Acceptance Criteria According to ASCE-SEI 41-13	57
2.8.3 Performance Levels and Acceptance Criteria for Tall Buildings .	62
2.8.3.1 Performance Levels.....	62
2.8.3.2 Acceptance Criteria at the Component Level	63
2.8.3.2.1 Force-Controlled Actions.....	64
2.8.3.2.2 Non – Critical Force Controlled Actions	66
2.8.3.2.3 Deformation controlled Actions.....	66
2.8.3.3 Acceptance Criteria for the Overall Building Behavior.....	67
3 CASE STUDY	69
3.1 INTRODUCTION	69
3.2 GENERAL PROPERTIES OF THE CASE STUDY BUILDING	69
3.2.1 Eigenvalue (Free Vibration) Analysis.....	72
3.3 NONLINEAR MODELING OF THE CASE STUDY BUILDING	75

3.4 GROUND MOTION SELECTION	79
3.5 PRESENTATION OF RESULTS FOR THE CASE STUDY	83
3.5.1 Inter Story Drift Ratios.....	83
3.5.2 Average Shear Stress and Axial Load Level of Shear Walls.....	87
3.5.3 Axial Forces in Columns.....	92
3.5.4 Axial Strain of Shear Walls.....	94
3.6 PRESENTATION OF RESULTS FOR THE REVISED CASE STUDY	98
3.6.1 Inter Story Drift Ratios.....	100
3.6.2 Average Shear Stress and Axial Load Level of Shear Walls.....	103
3.6.3 Axial Forces in Columns.....	106
3.6.4 Axial Strain of Shear Walls.....	107
3.6.5 Beam-end Average Curvature.....	112
3.6.6 Coupling Beam Results.....	120
3.7 COMPARISON OF RESULTS FROM THE ORIGINAL AND REVISED CASE STUDIES	121
3.7.1 Comparison of Drift Results	122
3.7.2 Comparison of Average Shear Stress and Axial Loads and Axial Strain of Shear Walls	124
4 SUMMARY AND CONCLUSIONS	131
4.1 SUMMARY	131
4.2 CONCLUSIONS.....	133
REFERENCES.....	137
APPENDICES	
APPENDIX A.....	143
A. SERVICE LEVEL EARTHQUAKE GROUND MOTIONS TIME SERIES.....	143
B. MAXIMUM CONSIDERED EARTHQUAKE GROUND MOTIONS TIME SERIES	145
C. SELECTED CRITICAL SECTION DETAILS.....	147

LIST OF TABLES

TABLES

Table 1.1. Tall buildings taller than 100 meters in regions until 2015	2
Table 2.1. Effective stiffness values according to ASCE/SEI 41-06	36
Table 2.2. Reinforced concrete members stiffness properties (LATBSDC, 2015)...	37
Table 2.3. Minimum building performance objectives expected for different earthquake levels according to TEC-2007	55
Table 2.4. Modeling Parameters and Numerical Acceptance Criteria for Nonlinear Procedures—Reinforced Concrete Beams	59
Table 2.5. Modeling Parameters and Numerical Acceptance Criteria for Nonlinear Procedures—Reinforced Concrete Columns	60
Table 2.6. Modeling Parameters and Numerical Acceptance Criteria for Nonlinear Procedures—R/C Shear Walls and Associated Components Controlled by Flexure	61
Table 2.7. Expected minimum performance regions for different earthquake levels	62
Table 2.8. Typical Classification of Component Actions According to LATBSDC 2015	63
Table 3.1. Section properties of the coupling beams (I_n/h)	72
Table 3.2. The section dimensions of shear walls (centimeters).....	72
Table 3.3. Free vibration properties of the building for the first twelve modes.....	73
Table 3.4 Reference ground motion properties	83
Table 3.5. Free vibration properties of the revised case study for the first twelve modes	99

LIST OF FIGURES

FIGURES

Figure 1.1. Completions and under construction of tall buildings (+100m) until 2015	2
Figure 1.2. Completed tall buildings (+200m) in 2009 and 2015 with respect to material.....	2
Figure 1.3. The reduced and minimum base shear forces according to TEC 2007 ..	10
Figure 1.4. Outrigger braces and viscoelastic dampers connecting coupled walls ...	11
Figure 2.1. Outrigger braces and viscoelastic dampers connecting coupled walls (NEHRP, 2013).....	17
Figure 2.2. Idealized cross section for fiber model and elevation of shear wall.....	18
Figure 2.3. Ibarra –Krawinkler monotonic backbone model and its key parameters (Ibarra et al., 2005).....	19
Figure 2.4. Cycling degradation and unloading stiffness parameters	23
Figure 2.5. Comparison of Menegotto-Pinto steel model with two different Perform3D Models (1 % strain hardening).....	23
Figure 2.6. Comparison of web concrete model with boundary concrete model	24
Figure 2.7. Comparison of analytical models and Thomsen and Wallace RW2 specimen test results for rectangular wall section.....	24
Figure 2.8. Comparison of different idealized steel models under monotonic loading.....	25
Figure 2.9. Comparison of different idealized steel models under cyclic loading....	25
Figure 2.10. Comparison of test results (Thomsen and Wallace RW2) and models using different steel models for a rectangular wall section.....	26
Figure 2.11. Orakcal and Wallace Concrete models (ATC-72, 2010).....	27
Figure 2.12. Comparison of Saatçioğlu Razvi unconfined concrete model with the idealized trilinear models	28
Figure 2.13. An application of unconfined concrete model in Perform3D under cycling loading	28

Figure 2.14. Comparison of Saatçioğlu Razvi confined concrete model with the idealized trilinear models	29
Figure 2.15. An application of confined concrete model in Perform3D under cycling loading.....	29
Figure 2.16. Shear force-deformation backbone curve bases on ASCE-41-13	30
Figure 2.17. Monotonic capacity curve and hysteretic model (FEMA P440A, 2009)	32
Figure 2.18. Options for component modelling (ATC-72, 2010)	34
Figure 2.19. Comparison force-deformation relationship of Perform 3D, Ibarra-Krawinkler, ASCE/SEI 41-06, TEC-2007	34
Figure 2.20. Comparison of proposed effective stiffness values by Haselton and Elwood (ATC-72, 2010)	37
Figure 2.21. Inelastic and idealized moment curvature (Priestly et al., 2007).....	39
Figure 2.22. Comparison of inelastic and idealized moment curvature relationship.	41
Figure 2.23. Finite element models (Perform 3D, 2011)	41
Figure 2.24. Plastic Hinge Model and its implementation to beam and reduced beam section.....	42
Figure 2.25. Plastic zone Model.....	43
Figure 2.26. Comparison of actual and idealized section for fiber model	44
Figure 2.27. Strain distribution of the base of the wall element for 6 elements	45
Figure 2.28. Strain distribution of the base of the wall element for 48 elements	45
Figure 2.29. The effect of fiber size on the wall element for different axial load levels and interaction diagram	47
Figure 2.30. Rigid lumped plasticity and shear displacement hinge model with their backbone curves for coupling beams (ATC-72, 2010)	48
Figure 2.31. Cantilever columns and moment diagram for a) First-order effects only and, b) P- Δ effects only.	50
Figure 2.32. Damage limits and region for reinforced concrete section according to TEC-2007	57
Figure 2.33. Generalized force-deformation relation for reinforced concrete flexural elements or components with performance levels	58
Figure 3.1. (a) 3-D view and (b) typical floor plan of the building	70

Figure 3.2. TEC-2007 design and elastic spectrum	71
Figure 3.3. Labels of shear walls	72
Figure 3.4. The first mode shape ($T_1=3.08$ sec).....	73
Figure 3.5. The second mode shape ($T_2=2.73$ sec)	74
Figure 3.6. The third mode shape ($T_3=1.43$ sec).....	74
Figure 3.7. The fourth mode shape ($T_4=0.86$ sec)	74
Figure 3.8. Comparison of inelastic and idealized (used) moment curvature relationship.....	76
Figure 3.9. Number of wall elements for core shear wall.....	77
Figure 3.10. The characteristic backbone curve of coupling beams (CB3).....	78
Figure 3.11. Acceleration response spectra of generated ground motions, mean acceleration spectrum, target spectrum and TEC2007 design spectrum for SLE.....	81
Figure 3.12. Acceleration response spectra of generated ground motions, mean acceleration spectrum, target spectrum and TEC2007 design spectrum for MCE	81
Figure 3.13. Maximum transient interstory drift ratios for each ground motion with maximum average transient interstory drift ratios obtained from a set of SLE shaking in X direction.....	84
Figure 3.14. Maximum transient interstory drift ratios for each ground motion with maximum average transient interstory drift ratios obtained from a set of SLE shaking in Y direction.....	85
Figure 3.15. Maximum transient interstory drift ratios for each ground motion with maximum average transient interstory drift ratios obtained from a set of MCE shaking in X direction	86
Figure 3.16. Maximum transient interstory drift ratios for each ground motion with maximum average transient interstory drift ratios obtained from a set of MCE shaking in Y direction	87
Figure 3.17. Max average shear stress and axial load on shear wall SW2 under SLE shaking	90
Figure 3.18. Max average shear stress and axial load on shear wall SW3 under SLE shaking	90
Figure 3.19. Max average shear stress and axial load on shear wall SW6 under SLE shaking	90

Figure 3.20. Max average shear stress and axial load on shear wall SW2 under MCE shaking	91
Figure 3.21. Max average shear stress and axial load on shear wall SW3 under MCE shaking	91
Figure 3.22. Max average shear stress and axial load on shear wall SW6 under MCE shaking	91
Figure 3.23. C10, C11 and C12 columns	92
Figure 3.24. Average axial load level on C800*1500 columns (C1, C7, C19, C20 and the first six floors of C2 to C6) under (a) SLE, and (b) MCE shakings.....	93
Figure 3.25. Average axial load level on C1000*1000 columns (from C8 to C18) under (a) SLE and (b) MCE shakings	93
Figure 3.26. Average axial load level on C700*1400 columns (from C2 to C6 between 7th and 29th floor) under (a) SLE and (b) MCE shakings.....	93
Figure 3.27. Average axial load level on C700*1200 columns (the four upper stories of C3, C4, C5 and C6) under (a) SLE and (b) MCE shakings	94
Figure 3.28. Axial strain at edge I (internal edge) and edge J (external edge) of shear wall SW2 under SLE shaking	96
Figure 3.29. Axial strain at edge I (internal edge) and edge J (external edge) of shear wall SW2 under MCE shaking	96
Figure 3.30. Axial strain at edge I (internal edge) and edge J (external edge) of shear wall SW3 under SLE shaking	97
Figure 3.31. Axial strain at edge I (internal edge) and edge J (external edge) of shear wall SW3 under MCE shaking	97
Figure 3.32. Axial strain at edge I (internal edge) and edge J (external edge) of shear wall SW6 under SLE shaking	98
Figure 3.33. Axial strain at edge I (internal edge) and edge J (external edge) of shear wall SW6 under MCE shaking.....	98
Figure 3.34. Maximum transient interstory drift ratios for each ground motion with maximum average transient interstory drift ratios obtained from a set of SLE shaking in X direction.....	100

Figure 3.35. Maximum transient interstory drift ratios for each ground motion with maximum average transient interstory drift ratios obtained from a set of SLE shaking in Y direction.....	101
Figure 3.36. Maximum transient interstory drift ratios for each ground motion and maximum average transient interstory drift ratios obtained from a set of MCE shaking in X direction	102
Figure 3.37. Maximum transient interstory drift ratios for each ground motion with maximum average transient interstory drift ratios obtained from a set of MCE shaking in Y direction.	103
Figure 3.38. Average shear stress and axial load on shear wall SW2 under SLE shaking	104
Figure 3.39. Average shear stress and axial load on shear wall SW3 under SLE shaking	104
Figure 3.40. Average shear stress and axial load level on shear wall SW6 under SLE shaking	105
Figure 3.41. Average shear stress and axial load on shear wall SW2 under MCE shaking	105
Figure 3.42. Average shear stress and axial load on shear wall SW3 under MCE shaking	105
Figure 3.43. Average shear stress and axial load on shear wall SW6 under MCE shaking	106
Figure 3.44. Average axial load level on all columns under SLE shaking	107
Figure 3.45. Average axial load level on all columns under MCE shaking.....	107
Figure 3.46. Axial strain at edge I (internal edge) and edge J (external edge) of shear wall SW2 under SLE shaking	109
Figure 3.47. Axial strain at edge I (internal edge) and edge J (external edge) of shear wall SW2 under MCE shaking.....	109
Figure 3.48. Axial strain at edge I (internal edge) and edge J (external edge) of shear wall SW3 under SLE shaking	110
Figure 3.49. Axial strain at edge I (internal edge) and edge J (external edge) of shear wall SW3 under MCE shaking.....	110

Figure 3.50. Axial strain at edge I (internal edge) and edge J (external edge) of shear wall SW6 under SLE shaking	111
Figure 3.51. Axial strain at edge I (internal edge) and edge J (external edge) of shear wall SW6 under MCE shaking	111
Figure 3.52. Selected critical beams and direction of earthquake horizontal components.....	112
Figure 3.53. Sign convention	112
Figure 3.54. The distribution of positive moments and curvatures at the end I, negative moments and curvatures at the end I, positive moments and curvatures at the end J and negative moments and curvatures at the end J along the height of the building under SLE shaking (Beam B1).	114
Figure 3.55. The distribution of positive moments and curvatures at the I end, negative moments and curvatures at the I end, positive moments and curvatures at the J end and negative moments and curvatures at the J end along the height of the building under MCE shaking (Beam B1).....	115
Figure 3.56. The distribution of positive moments and curvatures at the end I, negative moments and curvatures at the end I, positive moments and curvatures at the end J and negative moments and curvatures at the end J along the height of the building under SLE shaking (Beam B2)	116
Figure 3.57. The distribution of positive moments and curvatures at the end I, negative moments and curvatures at the end I, positive moments and curvatures at the end J and negative moments and curvatures at the end J along the height of the building under MCE shaking (Beam B2).....	117
Figure 3.58. The distribution of negative moments and curvatures at the end I, positive moments and curvatures at the end J and negative moments and curvatures at the end J along the height of the building under SLE shaking (Beam B3)	118
Figure 3.59 The distribution of negative moments and curvatures at the end I, positive moments and curvatures at the end J and negative moments and curvatures at the end J along the height of the building under MCE shaking (Beam B3).....	119
Figure 3.60 Maximum average positive chord displacement hinge for CB3 under SLE shaking.	120

Figure 3.61 Maximum average negative chord displacement for CB3 under SLE shaking.	120
Figure 3.62 Maximum positive chord displacement for CB3 under MCE shaking.	121
Figure 3.63 Maximum negative chord displacement for CB3 under MCE shakings.	121
Figure 3.64 Comparison mean interstory drift results of original case study with revised case study under SLE shakings in X direction	122
Figure 3.65 : Comparison mean interstory drift results of original case study with revised case study under SLE shaking in Y direction.....	123
Figure 3.66 : Comparison mean interstory drift results of original case study with revised case study under MCE shakings in X direction.....	123
Figure 3.67 Comparison mean interstory drift results of original case study with revised case study under MCE shakings in Y direction.....	124
Figure 3.68 Comparison average shear stress and axial load level of shear wall SW2 results of case study model with revised case study model under SLE shaking	125
Figure 3.69 Comparison average shear stress and axial load level of shear wall SW3 results of case study model with revised case study model under SLE shaking	125
Figure 3.70 Comparison average shear stress and axial load level of shear wall SW6 results of case study model with revised case study model under SLE shaking	125
Figure 3.71 Comparison average shear stress and axial load level of shear wall SW2 results of case study model with revised case study model under MCE shaking....	126
Figure 3.72 Comparison average shear stress and axial load level of shear wall SW3 results of case study model with revised case study model under MCE shaking....	126
Figure 3.73 Comparison average shear stress and axial load level of shear wall SW6 results of case study model with revised case study model under MCE shaking....	126
Figure 3.74 Comparison mean axial strain results of case study model with revised case study model under SLE shaking.....	127
Figure 3.75 Comparison max fiber compressive and tensile strain of SW2 under MCE shaking.....	127
Figure 3.76 Comparison max fiber compressive and tensile strain of SW3 under SLE shaking.	128

Figure 3.77 Comparison max fiber compressive and tensile strain of SW3 under MCE shaking.....	128
Figure 3.78 Comparison max fiber compressive and tensile strain of SW6 under SLE shaking.	129
Figure 3.79 Comparison max fiber compressive and tensile strain of SW6 under MCE shaking.....	129
Figure A.1 Selected critical beam section details at the support region	147
Figure A.2 Selected column section details	147
Figure A.3 Shear wall SW3 section details.....	148
Figure A.4 Section details of parametric case study	149
Figure A.5 The detailed fiber properties of parametric case study	150

LIST OF SYMBOLS / ABBREVIATIONS

AB-083...	Administrative Bulletin No: 083
ACI	American Concrete Institute
ASCE SEI...	American Society of Civil Engineers Structural Engineering Institute
ATC	Applied Technology Council
CTBUH	The Council on Tall Buildings and Urban Habitat
IMM	Istanbul Metropolitan Municipality
LATBSDC	Los Angeles Tall Buildings Structural Design Council
NLTHA	Nonlinear Time History Analysis
PEER	Pacific Earthquake Engineering Research
SEINEHRP	National Earthquake Hazards Reduction Program
SEONAC	Structural Engineers Association of California
SFDBI	San Francisco Department of Building Inspection
TBI	Tall Buildings Initiative
TEC	Turkish Earthquake Code
MCE	Maximum Considered Earthquake
SLE	Service Level Earthquake

CHAPTER 1

INTRODUCTION

1.1 Problem Statement

The first modern tall building, 119 meter tall Park Row Building, built in 1899 at New York came up by the economic reasons to increase the rentable area by receiving natural light as much as possible. Most of the tall buildings in the late nineteenth and early twentieth century comprised of steel frames with wind bracings. In spite of the deficiency of advanced structural analysis methods and technological equipment and lack of knowledge about structural materials, Empire State Building has reached 381 meters in 1931 by using excessive structural materials similar to the ones at the same time [M.M.Ali and K.S.Moon, 2007]. Since that time to today and then, the cities, their economies and populations have been growing dramatically. In parallel, the land prices in cities are increasing enormously. These results lead to some obligations and new perspectives for those cities. In addition, improvements and developments in technological equipment, material science and analyses methods have enabled great possibilities to construct new life areas that reveal modern tall buildings. As a result, the need for tall buildings has been going up and the design of modern tall buildings has risen incredibly day by day. According to The Council on Tall Buildings and Urban Habitat (CTBUH) interactive data base, as it is seen from Table 1.1, approximately seven thousand buildings over 100 meters were constructed and a thousand buildings are being constructed and thousands of buildings are planned to be designed. In addition, nearly equal percentages of buildings were erected in North America and Asia but a major percentage of buildings (57.13 %) under construction are being built in Asia as a result of increasing population and economic growth there. Whereas most of the tall buildings in the late nineteenth and early twentieth century comprised of steel frames with wind bracing as it is seen from the first pie chart (Figure 1.1), a major part of tall buildings (51%) consists of primarily concrete structural systems in the light of developed material science. However 38 tall buildings taller than 200 meters have been built until 2009 and this number has increased to 97 in 2014. As it is observed

from Figure 1.2, the number of buildings whose primary structural systems consist of concrete dropped to 38.1 % in 2014 from 74 % in 2009. In addition, composite structural systems have been utilized in a majority of tall buildings (53.6 %) completed in 2014 [CTBUH, interactive database site]. It follows that as the height of tall buildings increase, the primary structural system change from concrete to composite.

Table 1.1. Tall buildings taller than 100 meters in regions until 2015

Region	# of Countries	Completed		Under Construction	
		# of Buildings	Percent %	# of Buildings	Percent %
North America	3	2508	36.74	178	17.23
Asia	32	2480	36.33	592	57.31
Europe	48	672	9.84	84	8.13
Middle East	13	413	6.05	69	6.68
South America	11	216	3.16	39	3.78
Oceania	5	322	4.72	52	5.03
Center America	18	118	1.73	14	1.36
Africa	39	98	1.44	5	0.48
Total	169	6827		1033	

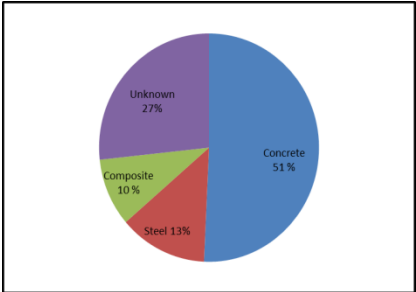


Figure 1.1. Completions and under construction of tall buildings (+100m) until 2015

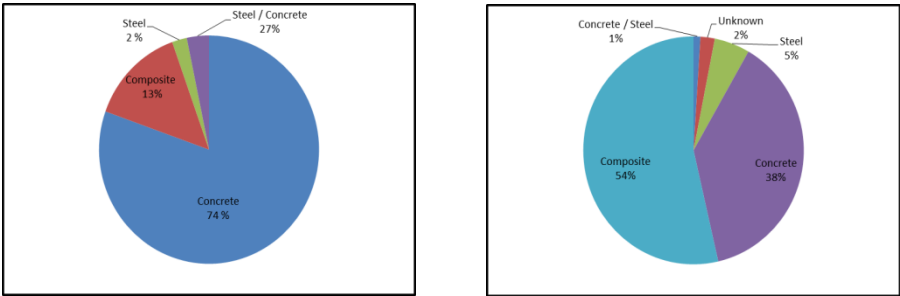


Figure 1.2. Completed tall buildings (+200m) in 2009 and 2015 with respect to material

The majority of the world's population is concentrated in the regions with high seismicity and tall buildings are increasing in these regions such as China, West Coast of North America, Japan, and Turkey [CTBUH interactive database]. The statistical data shows that nowadays, the need for tall buildings is increasing gradually and most of those buildings are in seismic regions. According to CTBUH database, 84 of 100 tall buildings taller than 100 meters constructed in Turkey are located in the regions of high seismicity (Istanbul and Izmir). These types of buildings are special (unique and pioneering) buildings, therefore unlike regular buildings; they need to be paid more attention at the design stage.

A core wall composed of a reinforced concrete shear wall along with a frame structure having a low redundancy have been more prevalent for the design of tall buildings. Unlike conventional regular buildings, shear walls are desired to withstand not only all of the lateral forces (seismic and wind) but also a considerable amount of gravity forces due to having less redundant structural systems. In other words, the safety factor for preventing collapse of a tall building is low and it may collapse if a major component of the primary structural system is subjected to heavy damage or collapse.

Performance based design concepts have been increasingly used to understand the behavior of tall buildings. Tall buildings are generally designed on a mentality which consists of a preliminary design stage based on the capacity design principles under design earthquakes with a return period of 475 years (moderate earthquakes), followed by two performance evaluation stages, service level and collapse prevention checks, respectively. Service level evaluation stage is to check structure under the high probability of occurrence (frequent) earthquakes with return periods of 43~72 years (small to moderate earthquakes). Collapse prevention evaluation stage is to check the structure under the low probability of occurrence (rare) earthquakes with a return period of 2475 years (severe earthquakes). In the first evaluation stage, it is generally desirable that the tall buildings remain essentially elastic. Linear response spectrum analysis is generally utilized for this stage since a permanent damage is not appreciated but nonlinear response history analysis may also be utilized [TBI-PEER, 2010]. In the second evaluation stage, the target is that tall buildings maintain their

stability under expected strong earthquakes, namely collapse of the structures should be prevented. Instead of these, limited damage in specified locations and a specific stress limit is permitted for reasonable designs. Current conventional seismic codes do not allow estimating distribution of the expected damage level and internal forces accurately since these codes are based on linear elastic analysis where nonlinear behavior is considered implicitly and approximately. In addition, current prescriptive seismic codes are too restrictive on structural height, period and minimum base shear requirement etc. Accordingly, alternative non-prescriptive consensus guidelines which are based on performance based design concepts (especially based on using nonlinear time history analysis) have arisen since the need has grown. Unlike conventional linear elastic procedures, nonlinear response history analysis considers nonlinear behavior explicitly and it gives quite reasonable results under design and maximum considered earthquake shaking if it is utilized properly [Moehle, 2005]. However this method is more sophisticated and time consuming compared to linear elastic methods. Where nonlinear response history analysis is used, there are three important steps, modeling, analysis and assessment, respectively. The first step is modeling where selection of correct inelastic component types for each structural member is carried out. Inelastic component types are mainly categorized in three groups, continuum finite element models, fiber models and lumped plasticity models. Each of these models has some advantages and shortcomings but fiber models can be generally used for shear wall elements and lumped plasticity models for frame elements in practice since current analytical modeling and computer analysis software and their capabilities are mostly based on these models [ATC-72, 2010]. In addition, unlike linear elastic analyses, the results of nonlinear analyses are influenced and depend on the gravity load effects directly, therefore the selection of appropriate expected gravity load is important. It is generally taken as dead load $[G]$ and some portion of the design live load $[0.2\sim 0.3Q]$. The second step of analysis is where a suitable suite of representative ground motion sets and suitable damping values are chosen. They are long period structures so it might be troublesome to detect appropriate ground motion records to obtain accurate response from these structures. Either spectrum matching or scaling method based on the target linear response spectrum obtained from either site specific hazard analysis or general standard response spectrum shape in the seismic codes is used to choose and

manipulate ground motions for expected performance levels. If uniform hazard spectrum is utilized then spectrum matching is preferred for tall buildings. On the other hand, tall buildings are special structures thus scaling procedure with conditional mean spectrum from site-specific seismic hazard analysis generally can be done by considering all of the properties of site conditions and the fundamental periods of the structure. This method is being widely employing for tall buildings. One of the most important parameter that must be selected is the viscous damping ratio. It is generally taken as 2~5 % for concrete structures and 2~3 % for steel structures with respect to the target performance level. In addition, P-Delta effects must be considered not only at the design stage but also at the performance evaluation stages. The last part is assessment stage where the interpretation of the results and checking the building behavior in compliance with the determined target performance criteria are performed.

Consequently, the need for tall buildings has been growing steadily. Unlike regular buildings, the contribution of higher mode effects influences the behavior of tall buildings under external lateral forces. In addition, tall buildings have some important differences from design to analysis to construction. Current prescriptive seismic codes are inadequate and too restrictive, so alternative non-prescriptive consensus guidelines based on performance based design concepts using nonlinear time history analysis have been applied to estimate the performance of structures under expected earthquakes.

1.2 Seismic Design Guidelines on the Performance Based Design of Tall Buildings

Due to the increasing number of tall buildings, the need of alternative non-prescriptive seismic design guidelines has grown for the reasons explained in the oncoming paragraphs. San Francisco Building Code (2013) and ASCE SEI 41-13 (2013) documents allow employing alternative materials, analysis procedures and construction methods whereas alternative materials are verified by laboratory tests to provide at least minimum strength, effectiveness, fire resistance, durability and safety in these codes. In addition, analysis and construction methods are approved by

certified authorities. Performance based design has resulted in a new vision to seismic design of tall buildings, pioneering to a smart shift in analysis and assessment methods from the prescriptive force-based design method which is based on linear elastic analysis under reduced seismic loads and capacity design principles, to non-prescriptive displacement-based design methods which are based on nonlinear analysis and checking performance evaluations with respect to expected demand parameters. Accordingly, several institutions (task groups) or building officials have proposed improved building codes and published non-prescriptive seismic design guidelines for tall buildings based on displacement based methods in the last decade. The first guideline was published by the Los Angeles Tall Buildings Seismic Design Council (LATBSDC) in 2005. It has been updated several times in the light of developments in performance based design (2005, 2008, 2011, 2013, and 2014, 2015). It is a consensus document between structural (design) engineers and certified authorities which is “an alternative procedure for seismic analysis and design of tall buildings located in the Los Angeles Region”. One of the other guideline which is a recommendation for the seismic design of high-rise buildings was published by Council on Tall Buildings and Urban Habitat (CTBUH, 2008) which is a non-profit organization and an international group in the area of tall buildings and sustainable urban design. This guideline is also a consensus document. One of the other guidelines “Administrative Bulletin NO: AB-083” was prepared for the San Francisco Department of Building Inspection (SFDBI) in 2007 by Structural Engineers Association of Northern California (SEONAC). Then it was updated in 2014. The objective of this administrative bulletin was to show requirements and recommendations for the seismic design of new tall buildings located in the San Francisco region. The most comprehensive and favorable guideline, “Tall Buildings Initiative (TBI)” was prepared by the Pacific Earthquake Engineering Research (PEER) Center working group between 2007 and 2010. It consists of twelve specific tasks and five reports on the developing consensus from performance objectives to modeling and acceptance criteria for seismic design and analysis to the instrumentation of tall buildings. It is a pioneering guideline and aims to offer an alternative non-prescriptive procedure for the next generation of seismic codes instead of the prescriptive procedures for seismic design of tall buildings. Another seismic design guideline was prepared by Kandilli Observatory and Earthquake

Research Institute for Istanbul Metropolitan Municipality (IMM) in 2008. “Istanbul seismic design code for tall buildings” was not published officially, but has been used in practice.

As explained earlier, these modern guidelines for seismic designs of tall buildings are based on displacement based design methodology basically. They consist of a preliminary design stage and one or two performance evaluation stages, service level and collapse prevention evaluation levels. As it is known, structural elements must be preliminarily proportioned and detailed in order to employ NLTHA procedures. NLTHA is a time consuming process where it is aimed to predict inelastic zones or elements where an acceptable yielding mechanism is expected to occur at the preliminary design stage. Capacity design concepts by using linear elastic analysis is a good approach to start achieving target yielding mechanism over the structural members for a ductile response. Although these guidelines make use of capacity design concepts and current prescriptive provisions, apart from the exceptions of seismic codes basically at the preliminary design stage, they differ from each other at this point since two different approaches have been developed.

The first approach is a two-stage process consisting of a preliminary design stage and two performance evaluation stages. Tall buildings are long period structures and base shear demand according to seismic codes are generally controlled by minimum base shear requirements. Accordingly, structural members may or may not be proportioned and reinforced in line with the prescriptive provisions of seismic codes. In other words, things to do at this stage are entirely left to the structural engineers and their experience. The second stage is to analyze the building with either nonlinear time history analysis or linear response spectrum analysis for checking service level performance and to analyze the building with nonlinear time history analysis for checking the collapse prevention safety in compliance with the pre-determined target performance levels. If the target performance levels are not satisfied, preliminary design has to be revised. It is continued until achieving the performance objectives. TBI and LATBSDC utilize this approach.

The second approach is a three-stage process consisting of a preliminary design stage and two performance evaluation stages similar to the first approach but there are significant differences at the preliminary design stage. In the preliminary design stage, structural members are being proportioned and reinforced properly in line with capacity design principles by using linear elastic analysis. In other words, all applicable prescriptive provisions of seismic codes such as minimum base shear requirement must be fulfilled. Inapplicable provisions are expressed explicitly. The second stage is similar to the second stage of the first approach. SEONAC, SFDBI and IMM (comparatively) utilize this approach. However, IMM is more complicated in practice than the others. It is a rough guideline that categorizes tall building as normal tall buildings and special tall buildings by height, with over 60 meters and 75 meters, respectively. In addition, minimum base shear requirements may go up to 6-7 % of the seismic weight of the structure depending on the soil type and earthquake zone. Unlike these guidelines, previous edition of LATBSDC 2005 suggests 2.5 % of the seismic weight as sufficient in preliminary design respectively [LATBSDC 2005]. Afterward it was updated to 3% of the seismic weight in the 2005 edition of LATBSDC. In the last four editions since 2008, minimum base shear requirement has been eliminated at the preliminary design stage. According to current seismic code, the provision of minimum base shear requirement must be employed in order to eliminate uncertainties and assumptions when calculating period of structure and generating analytical model of structure. Although the minimum base shear requirement directly affects design of tall buildings, this step is arguable between guidelines and researchers for design of tall buildings.

1.2.1 Definition of Tall Buildings

What do you visualize when it is said tall buildings? There is no exact description of what forms a tall building. As it is understood from the “tall”, it comes to mind that it is about the height of the building. But what is the height limit of the building to be considered as tall building? Tall buildings have been identified differently by alternative seismic design codes of modern tall buildings. According to LATBSDS, AB-083 and PEER/TBI, it is defined as buildings exceeding 160 feet (~50 meter) in height. On the other hand, Istanbul seismic design code for tall buildings categorizes

tall buildings into two groups. It is identified as the ones whose height taller than 60 meters above ground surface but extra analysis must be needed to assess performance of the building if it is taller than 75 meters. However, In CTBUH, a tall building is not just defined according to the height. It may be categorized as a tall building if the proportion of building which might be slender sufficiently to give the view of a tall building. If used, an innovative technology product could be attributed as being a product of “tall”, and the context in which the building stands. Buildings are also categorized (called) as “supertall” and “mega tall” in CTHBUH. If the height of a building exceeds 300 meters, it is defined as “supertall” and if a building height goes beyond 600 meters, it is defined as ‘mega tall’. Whereas these guidelines are based upon modeling and assessment criteria, Toronto Tall Building Design Guideline (TTBDG) contains additional supporting architectural criteria. In contrast to these guidelines, In TTBDG, it is described that “tall buildings are generally defined as buildings with height that is greater than the width of the adjacent street right-of-way or the wider of two streets if located at an intersection”. Typical height in Toronto changes from 20 to 36 meters. This height limit is for the architectural properties of structure not for analysis procedures.

One of the most important questions in earthquake engineering is why a building is needed to be considered in a tall building category or not. There are several reasons. For instance, in contrast to low to mid rise construction, as the building height increases, the architectural properties of the structure are dramatically changed and the effects of lateral forces because of higher modes and gravity forces grow. Accordingly, traditional structural engineering approaches from design to construction become insufficient. The other reasons explained elaborately in the following paragraphs are about why NLTHA should be used for performance-based design of tall buildings.

1.2.2 Why NLTHA is used for Tall Buildings?

Nowadays, as mentioned previously, structural systems of tall buildings have been growingly improved. NLTHA is also increasingly used for performance based design of tall buildings. One of the most important questions that comes to mind is why

NLTHA should be used for performance-based design of tall buildings as an analysis tool. The reasons may be examined from two different perspectives.

First of all, we should consider the limitations of the current official seismic codes based on linear elastic principles to understand why NLTHA should be performed for tall buildings. As a basis, it is not sensible to design a building to remain entirely elastic under the design and maximum considered earthquake hazard levels. For this reason, some inelastic deformations should be expected during analysis. Seismic design codes are force-based methods that account for inelastic response indirectly by dividing the results of linear elastic response with a force reduction factor R . The value of R which is dependent on structural system and the level of ductility as explained in seismic design codes is used to reduce linear elastic forces to inelastic forces under the actual seismic actions. Nonlinear behavior is considered indirectly by this approach. However, the required strength is controlled by minimum base-shear requirements for a tall building. After all, as it can be seen from Figure 1.3 which describes design base shears from the Turkish Seismic Code (2007) for a typical site, the effective base shear force is minimized from the value specified in seismic code for that structural system to a smaller value depending on building period, seismic zone and other factors.

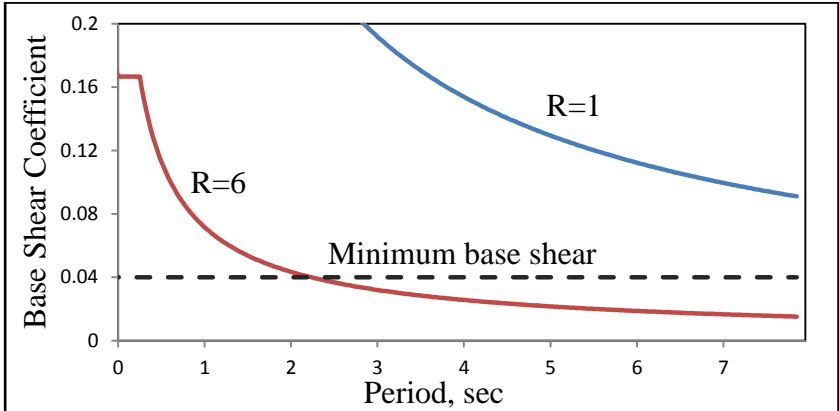


Figure 1.3. The reduced and minimum base shear forces according to TEC 2007

One of the other reasons why NLTH is used for tall buildings is that nonlinear behavior is considered directly in the NLTHA which is considered the best approach

to understand the response of the building and measure directly the damage of building when subjected to different levels of ground motion intensity. The level of damage might give us an idea whether the buildings could continue serviceability functions or need to be repaired or collapse after an earthquake shaking.

One of the other reasons why NLTH is used for tall buildings is that alternative structural analysis methods are required for innovative structural systems which is used increasingly. Although special building configurations and structural systems have been employed to satisfy the functional requirements of tall buildings, prescriptive provisions of current official seismic codes are based upon being extremely restrictive, resulting in pressure to design outside the limits of code provisions. Structural systems that are used for those buildings are also less redundant compared to conventional buildings. Under these circumstances, many tall buildings which have unusual configurations with innovative structural systems using specialized products that are not recognized in current building code are being designed and many of them are to be designed in the future. One of these examples which consists of concrete core walls with buckling-restrained steel outrigger braces along one axis, under construction in San Francisco, is illustrated in Figure 1.4. (a). Other examples about using a pioneering innovative structural system in tall buildings are also illustrated in Figure 1.4. (b). In this building, Viscoelastic coupling dampers were used at some specified floors instead of conventional coupling concrete beams to enhance seismic performance of the building [Christopoulos, 2015].

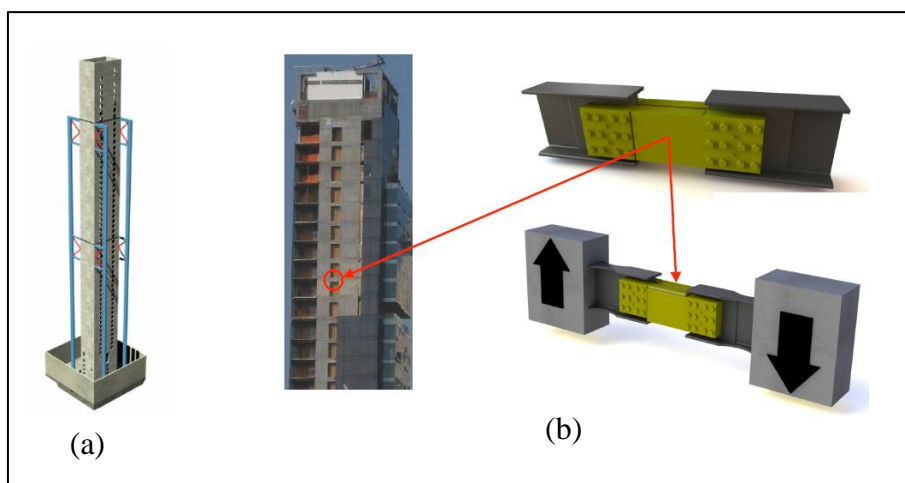


Figure 1.4. Outrigger braces and viscoelastic dampers connecting coupled walls

Construction cost is one of the other reasons. There are some alternative design criteria which are mentioned in the previous chapter to apply NLTHA for tall buildings. These alternative codes commonly indicate some deviations from prescriptive provisions of seismic codes. Some seismic code requirements could be eliminated by using NLTHA. For instance, it is stated in ASCE SEI 7-10 section 12.2.1 that the selected structural system has to be in compliance with the limitations on the structural system and the restriction on structural height. ASCE SEI 7-10 also puts limitation on period T_n . Other limitations such as minimum base shear requirement, additional requirements for systems with structural irregularity, diverse detailing requirements might not be provided if objectives of performance evaluation levels are ensured. Furthermore, alternative and high strength materials are growingly used to withstand the unique challenges introduced by these structures in high seismicity regions. In addition to specialized products, using these materials increases the construction costs of tall buildings compared with conventional buildings. As it is mentioned before, NLTHA is not a procedure to design but a method to check design whether it is sufficient or not. Dimensions of members could be revised if NLTHA is applied. As a result, NLTHA provides an optimum solution for better and reasonable cost designs with respect to other analysis methods.

Nonlinear analysis can be mainly categorized as nonlinear static analysis (pushover), and nonlinear time history analysis. Among these methods, there are variety of procedures in the implementation of nonlinear static analysis such as conventional pushover analysis, multi-mode pushover analyses, modal pushover analysis, generalized pushover analysis etc. depending on the application of a pseudo-dynamic (static) lateral force vector to push structure until the desired target level is reached. Each of these methods is rational and has some advantages and also shortcomings from modeling to analysis to assessment. Among nonlinear static analysis methods, conventional pushover analysis is generally used for conventional regular buildings. In this method, since fundamental period of these buildings are governed by the first mode, it is accepted that the applied lateral force vector is the first modal force vector of the structure which is found by the principle of eigenvalue analysis. After obtaining the capacity curve of the structure, the expected demand of the structure is obtained by nonlinear response history analysis of the equivalent single degree of

freedom systems in order to calculate the expected nonlinear response of structure. However, when the participation of higher mode effects are significant, conventional pushover analysis is insufficient to capture expected inelastic behavior of structures. As it is known, tall buildings are long period structures and the contribution of higher modes are significant, so using this method is not convenient. Accordingly alternative pushover analyses have been improved by several researchers [Chopra and Goel (2002), Goel and Chopra (2005), Poursha et al. (2009), Gupta and Kunnath (2000), Sucuoğlu and Günay (2011) etc.] to consider participation of all important modes to inelastic response. However, all multi-mode pushover analyses in the literature have two common important shortcomings [Soner, 2013]. First of all, the adaptive pushover methods cannot be put into practice with available software analysis program since they require eigenvalue analysis at each loading increment. In other words, these methods are more complicated to utilize since the mathematic model of tall buildings may be quite large and this requires more and more computation time. Secondly, although they predict inter-story drifts quite accurately, they have shortcomings to capture internal forces and deformations since the participation of all important modes are combined by statistical rules (CQC and SRSS) under the design and maximum earthquake shaking. This is also an important problem for tall buildings. For instance, axial load level of columns and shear walls may control the behavior of tall buildings. However sophisticated pushover analysis methods such as Generalized Pushover Analysis developed by Sucuoğlu and Günay (2011) eliminate such effects but these methods are also not standard. To sum up, because of these reasons are explained, nonlinear dynamic analysis procedure would be preferred instead of linear elastic analysis and nonlinear static analyses methods for the analysis of tall buildings.

1.3 Objectives and Scope

Performance based seismic design of a tall building by using nonlinear time history is presented in this study. This study begins with a general view of need for tall buildings. This is followed by recognition of current alternative non-prescriptive consensus seismic design guidelines and definition of tall building by different guidelines. After that, shortcomings and imperfections of conventional seismic

design codes for tall building design is explained and why NLTHA should be used among others analysis methods for performance-based seismic design of tall buildings as an analysis tool is justified. Then, nonlinear model types are described and compared with regard to the strengths and weaknesses aspects. Afterward material models are explained and calibrated according to the commercial software, PERFORM 3D V5 (2011) for fiber models. Different structural member modelling and the kind of nonlinear model (component) types to be used for different structural members is presented in order to predict the member and building behavior accurately when subjected to different levels of ground motion intensity. In addition, performance levels and acceptance criteria for tall buildings are explained. This is followed by a discussion on the importance of the selection and manipulation of ground motions to obtain reasonable results for predicting the seismic performance of tall buildings under specified earthquake hazard levels. The effects of gravity loads, damping and P-delta effects are also discussed. Finally, a reinforced concrete unsymmetrical-plan tall building with 34 stories and 115 meter in height is designed according to the Turkish Seismic Code under design earthquake. Both service level and collapse prevention level, NLTHA is employed by using a set of seven ground motions and checking the results in compliance with the determined target performance levels. Several performance targets are not satisfied, hence the preliminary design is revised. The case study is reanalyzed and evaluated to achieve the objectives of performance evaluation levels. The results for both of the initial and revised cases are presented.

Main objective of this study is to examine the necessity of performance based seismic design concepts through using NLTHA for tall buildings. For this purpose, a tall building is designed according to the prescriptive provisions of Turkish Seismic Code and NLTHA is applied for two performance levels. The result of this study reveals that utilizing NLTHA is essential for tall buildings as an analysis tool if they are designed in compliance with the current prescriptive provisions of seismic codes. Moreover, this study is an application on the evaluation of tall buildings by using NLTHA with the only commercially available software, PERFORM 3D.

CHAPTER 2

SEISMIC PERFORMANCE ASSESSMENT

2.1 Introduction

This chapter begins with a general review of nonlinearity sources in a structure. It is followed by introduction of the inelastic component types and comparison of their advantages and shortcomings. Then, types of material models for fiber models are explained. Material models are demonstrated for the implementation of nonlinear time history analysis to tall buildings through the commercial software, PERFORM 3D. Afterward, nonlinear modeling of reinforced concrete components is described. The importance of the selection and modification of ground motion pairs are explained. Gravity load effects on the nonlinear analysis are also mentioned. In addition, accounting P-delta effects in nonlinear analysis is discussed. Finally, performance levels and acceptance criteria on the basis of member behavior and overall response of the structure are indicated.

Nonlinear time history analysis is employed for determining the seismic performance of tall structures. A designed structure generally does not necessarily remain entirely elastic under the design and maximum earthquake excitations. Some inelastic deformations are expected to occur. The basic nonlinearity sources in a structure are material nonlinearity and geometric nonlinearity. For a realistic analytical simulation of the structure, both geometric and material nonlinearity should be taken into consideration. Material nonlinearity occurs because of the changing of material properties under the expected loading, which is considered in the model either explicitly (finite and fiber model) or implicitly (lumped plasticity model). Geometrical nonlinearity occurs due to initial imperfection of members and P-Delta effects, etc. Initial imperfection of members generally can be neglected but P-Delta effects must be considered especially in the analysis of tall buildings to predict the seismic performance of structure accurately.

2.2 Types of Nonlinear Models

NLTHA aims to simulate building behavior accurately under gravity and seismic loads. It mainly consists of three steps: modeling, analysis and assessment. Modeling phase is the most important step as it directly affects the other steps and it can change from one type of a nonlinear model to another. The first question comes to mind is how an appropriate model should be formed to predict structural response. There are several parameters that need to be taken into consideration during the selection of a favorable inelastic model. These are the type of structural system, types of member which comprise the structural system, materials of the members, expected overall response of the members or components, governing and controlling type of actions desired to be captured during analysis, unknowns and uncertainties which comes from inherent nonlinear behavior, the analysis objectives and necessary demand parameters, design and construction (stage construction), time and effort, computer analysis software and its capabilities etc. [ATC-72, 2010].

A variety of inelastic structural component types are available in practice but they can be mainly categorized into three groups which depend on the degree of idealization in the model. The term “degree of idealization” refers to where and how inelastic action is modeled in a member such as integrated inelastic behavior of a member idealized at a point (lumped plasticity model) or a zone (fiber model) or distributed by a specific characteristic length over the entire length, finite element model, (ATC-72, 2010 and NEHRP report, 2013). Figure 2.1 illustrates idealized types of component models used for beam-column member behavior. Each of the nonlinear models has a phenomenological basis as they are based on mathematical logic and they are verified by laboratory and analytical tests.

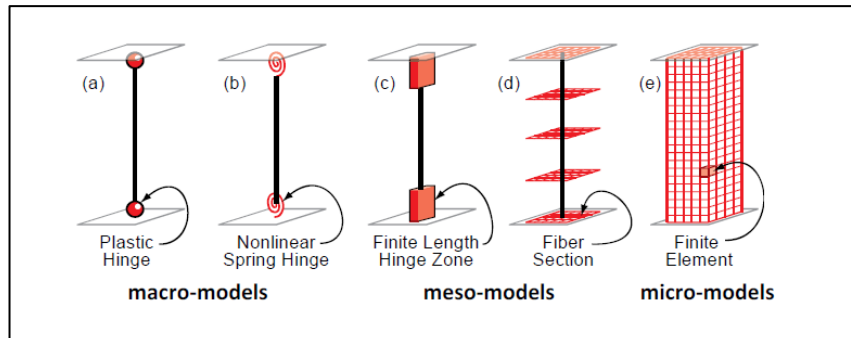


Figure 2.1. Outrigger braces and viscoelastic dampers connecting coupled walls
(NEHRP, 2013)

The first nonlinear model type is continuum finite element model. Required parameters for continuum finite models are defined in terms of the basic material properties and a specific characteristic finite mesh size. Either uniaxial or biaxial or tri-axial, basic material properties for concrete and reinforcement are used. Material properties and mesh size parameter should be well defined to predict a reasonable response in this type of modeling.

A second type of nonlinear model is the fiber (distributed inelasticity) model. It can be said that it is a simple form of finite element. Required parameters for fiber model are similar to the finite element model but it is simpler with respect to the finite element model. In fiber and continuum finite element models, expected nonlinear behavior of the component is captured explicitly by the nonlinear behavior of the material that constitutes the component. Whereas finite element models are based on more complex material constitutive relationships, fiber models are based on simpler basic uniaxial material properties to capture the overall response of the structure in practice. Unlike continuum finite element model, cross section of a member is divided into steel and concrete fibers according to steel or concrete included in the fiber model. Figure 2.2 illustrates an example of a reinforced concrete (RC) shear wall fiber model. Continuum finite element models divide a RC member by a characterized finite mesh with explicitly including longitudinal and shear reinforcement over the entire height and width (3D). Fiber models divide cross section of the member into sufficient number of concrete and steel fibers by a simple way with characterized element length over the entire height. But using adequate

number of fibers along the cross section and adequate number of elements over the height of the member is crucial to capture the overall member behavior. For this purpose, continuum finite elements are being used to find adequate numbers of fibers along the cross section. One of the implementations is shown in the case study section of this thesis. Besides, wall element length is taken nearly equal to the estimated plastic length which might be taken as the smaller value of one-half of the wall length or story height.

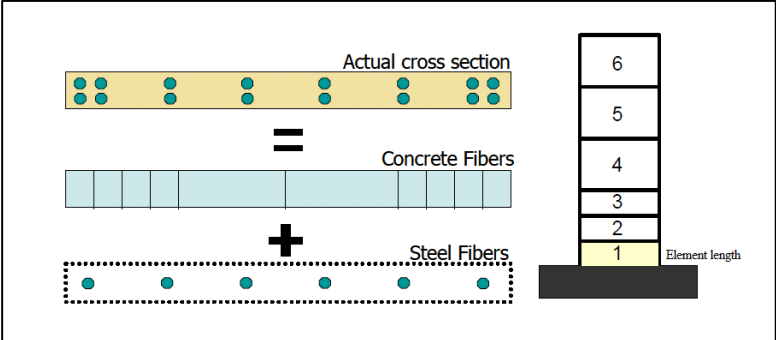


Figure 2.2. Idealized cross section for fiber model and elevation of shear wall

The last type of nonlinear model is the concentrated hinge model which is based on the overall response of prismatic components. Concentrated hinge model consists of quasi-elastic element implicitly accounting for concrete cracking, bond slip, etc. with concentrated plastic hinges where they best represent the integrated effects of distributed inelastic action. As it can be seen from Figure 2.3, Ibarra –Krawinkler concentrated plastic hinge model is characterized by force and deformation relationships. This is the backbone curve of component that identifies the capacity of the component under monotonic loading. This action is changeable from a component type to others and depends on the expected behavior of member under the expected loading. The main objective of the backbone model for a component is to capture the basic features of the component behavior, namely the initial stiffness, strain hardening, ultimate strength, strength loss and relating deformation capacity, which is shown in Figure 2.3 (Ibarra, 2005). The key parameters of the backbone curve of a concentrated plastic hinge model are;

- Effective yield strength and deformation (F_y and δ_y)
- Effective elastic stiffness, $K_e = F_y / \delta_y$
- Strength cap and associated deformation for monotonic loading (F_c and δ_c)
- Pre-capping plastic deformation for monotonic loading, δ_p
- Effective post-yield tangent stiffness, $K_p = (F_c - F_y) / \delta_p$
- Post-capping deformation range δ_{pc}
- Effective post-capping tangent stiffness, $K_{pc} = F_c / \delta_{pc}$
- Residual Strength, Effective post-yield tangent stiffness, $F_r = \kappa F_c$
- Ultimate deformation, Effective post-yield tangent stiffness, δ_u

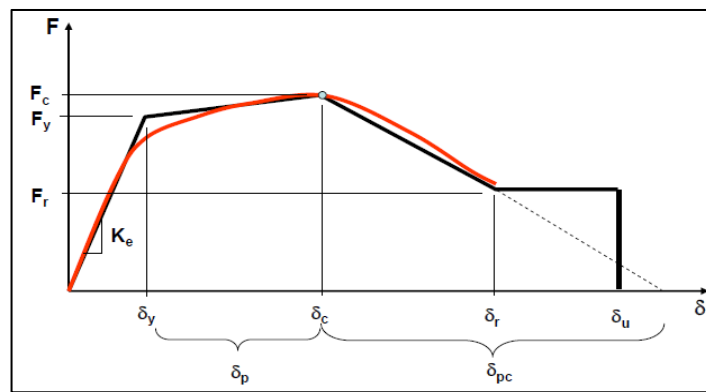


Figure 2.3. Ibarra –Krawinkler monotonic backbone model and its key parameters (Ibarra et al., 2005)

In finite element and fiber models, these key parameters are not needed during the modeling phase as they are inherently derived from material relations and characteristic length or mesh size. The effect of axial load level on the response (neutral axis changes during analysis) is directly considered. This is one of the most powerful features of these models. Moreover, one of the positive aspects of these models is capturing the initiation of cracking, crushing and steel yielding. On the other hand, they can be limited to capture cyclic stiffness and strength degradation, reinforcing bar buckling, bond slip and shear failure.

In concentrated hinge models, the effects of reinforcing bar buckling and bond slip are taken into consideration implicitly by using effective stiffness. In-cycle strength

degradation also can be defined approximately by imposing a backbone curve. While cyclic degradation can be considered as material cyclic behavior in fiber and finite element models, it can be considered as either explicitly or implicitly by imposing a backbone curve in concentrated hinge models, which is explained elaborately in Chapter 2.4.

As a result, use of continuum finite element models is neither practical nor available in current analysis software for performance based design of tall buildings. Nonlinear analysis is very sensitive to uncertainties and assumptions of the nonlinear behavior so the simplest models are used in order to obtain reasonable results. For this purpose, concentrated hinge model is used generally for frame member types such as columns, beams etc. There are two reasons of this. First, it is not practical to use fiber models in the modeling of frame members as it requires so much time during analysis if existing computer analysis programs are utilized. Second, current analytical models and acceptance criteria that are specified in codes for frame type member are based on lumped plasticity (concentrated hinge) models. However, fiber models can be generally used for shear wall elements. It is accepted that this model represents the behavior of shear walls more accurately than the others since it also may not be realistic to model complex core shear walls by simple concentrated hinge models by integrating the inelastic behavior of a member at a point. Use of more concentrated hinges for a complex shear wall is also not a simple and practical task in practice.

2.3 Material Models

In continuum finite element models and fiber models, effective stiffness, strength and deformation parameters of the component and expected inelastic behavior of the structure under external loads are directly obtained from material stress-strain relationships specified for the components. Accordingly, efficient and reliable hysteresis material models are needed. As explained earlier, whereas multi-axial basic material properties for concrete and steel are generally available in 2D and 3D finite element models, the uniaxial basic material properties of the material are employed in fiber models. The selection of material model parameters depends on

the selected inelastic model types, structure types, the expected and desired accuracy, simplicity and sufficiency, the capabilities of analysis tool used for analysis. Considerable amount of studies has been conducted on the modeling material models. Consequently, favorable material models for concrete and steel from the simple and efficient to quite sophisticated and more complex models have been improved. The studies in this area are quite extensive but the scope of material models in this study is limited to fiber models and its implementations in the current commercial software for tall buildings.

Nonlinear dynamic analysis depends on the expected material properties instead of nominal, characteristic or design material properties which are employed in design or linear assessment stages in order to predict accurately the performance of structure. In other words, using expected material properties in the NLTHA is essential for simulating, measuring and interpreting the expected structural performance more realistically and unbiasedly [ATC-72, 2010]. Expected material properties (strength and stiffness) are median values of the results obtained from a large group of material and component tests. If there is not enough test results, alternative consensus non-prescriptive seismic guidelines suggest some values to impose directly on the characteristic strength of material, which also affect deformation and stiffness properties of the components. According to ATC-72, expected strengths are taken as $1.2 f_y$ for the yield strength of reinforcement steel and $1.25 f_c$ for the compressive strength of concrete where f_y and f_c are the characteristic strengths of steel and concrete respectively. However these values change to 1.17 for reinforcement steel and 1.3 for concrete in LATBSDC 2015 and IMM 2008.

2.3.1 Uniaxial Reinforcement Steel Models for Fiber Models

Steel is a ductile material which can experience significant inelastic deformations without any substantial strength loss under the uniaxial cyclic loading. In reinforced concrete members, the reinforcing steel is thin and long thus the governing effect is uniaxial. Accordingly, it is enough to use a uniaxial steel material model for reinforced concrete members [Saritaş, course notes 2013]. A number of sophisticated uniaxial material models have been enhanced by considering some important

material effects such as yielding, hardening, cyclic degradation and buckling of steel. The model which was proposed by Menegotto and Pinto (1973), as modified by Filippou (1983) shown in Figure 2.4 has been widely used among the other models [ATC-72, 2010]. These models are incorporated directly in some analysis program, such as OPENSEES but it is not feasible to employ this software for tall buildings. On the other hand, relatively simple strain-stress relations for steel models have been used by Perform 3D software which is generally employed for performance based seismic assessment of tall buildings. Hence these implementation types of the materials are examined elaborately.

The reinforcement steel material models in Perform 3D has a special modelling format. It is modelled as bilinear or trilinear whether with considering strain hardening, cyclic degradation and stiffness degradation or not. For this purpose, Perform 3D has cycling degradation and unloading stiffness coefficients (energy and stiffness degradation factors) depending on the maximum strain that can be reached in every cycle [Figure 2.4]. A relation is established between several specific strain point of the material and the corresponding factors to determine the amount of dissipated energy in every cycle. If there is energy dissipation in a loop, Perform 3D conforms these factors to reduce and balance the loop area (energy capacity). It is suggested to calibrate these coefficients by comparing test results with analysis results by using simplified material models until achieving reasonable results under cycling loading before a structure is modelled in perform 3D (ATC-72, 2010). Wall tests are generally used to obtain these parameters since the self-behavior of reinforcement steel maybe different from the reinforcement steel in the reinforced concrete section under cycling loading because of interaction concrete and steel in reinforced concrete section. Comparison of Menegotto-Pinto steel model with two different Perform3D models (degradation model by using factors in Figure 2.4 and no degradation model) is illustrated in Figure 2.5. Web and boundary concrete model which are used both model are illustrated in Figure 2.6. The comparison of the test result with analysis results by using these models is shown in Figure 2.7. As it can be seen, the behavior of no degradation reinforcement steel model is more close to Menegotto-Pinto model under cycling loading but the results by using degradation parameters in the model is better correlated with the test results (Thomsen and

Wallace, 2004) since the behavior of reinforcement steel in the reinforced concrete section is different from the other.

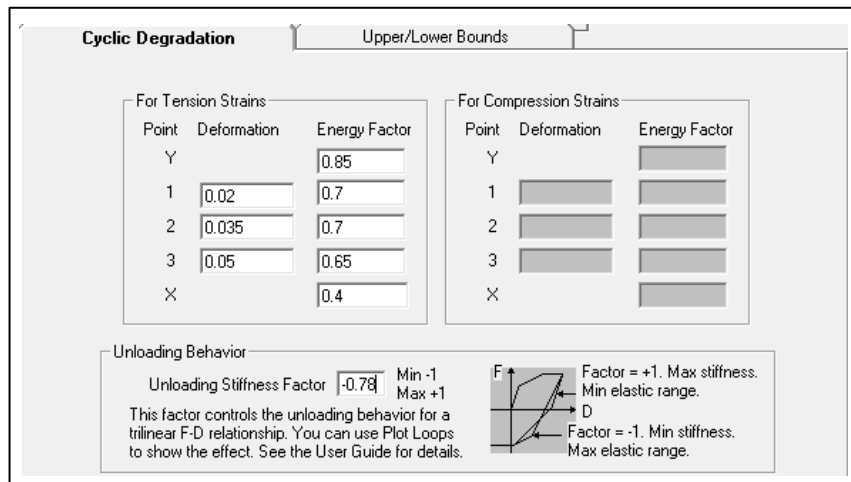


Figure 2.4. Cycling degradation and unloading stiffness parameters

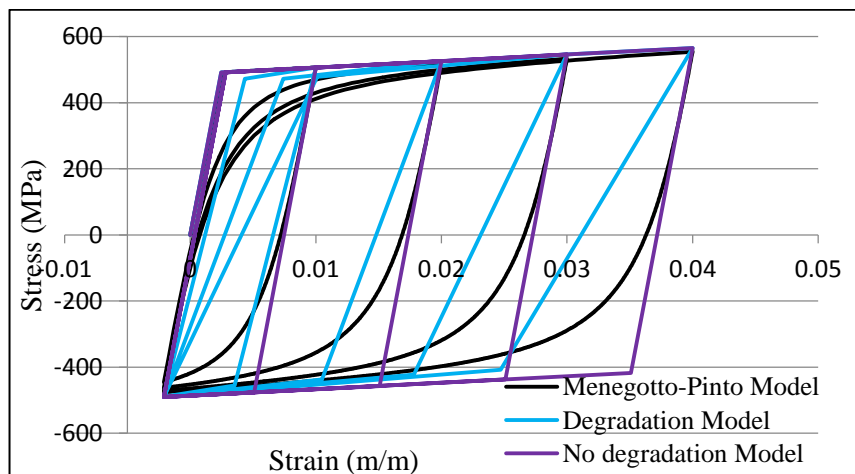


Figure 2.5. Comparison of Menegotto-Pinto steel model with two different Perform3D Models (1 % strain hardening)

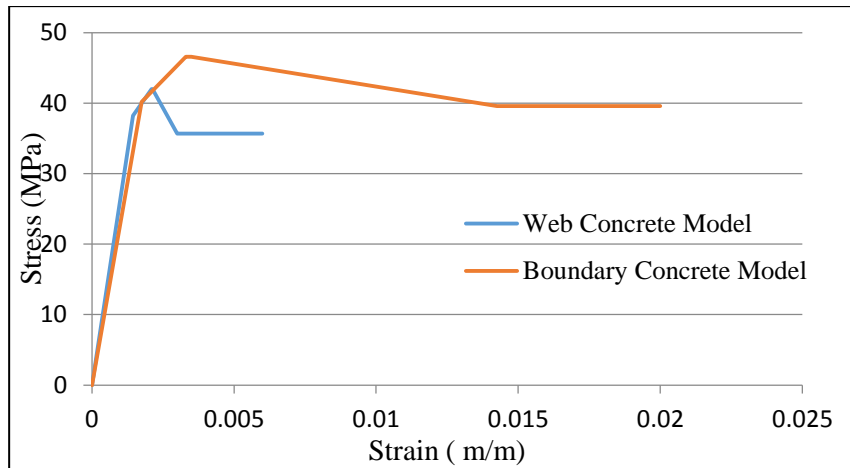


Figure 2.6. Comparison of web concrete model with boundary concrete model

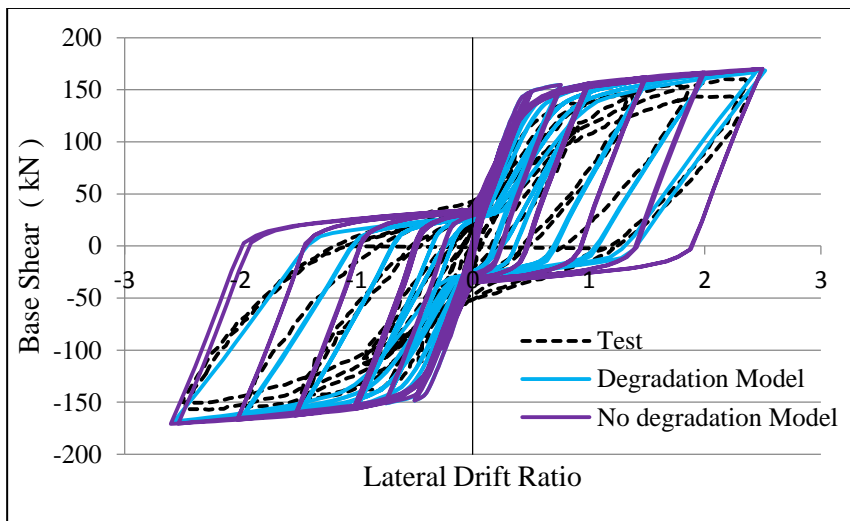


Figure 2.7. Comparison of analytical models and Thomsen and Wallace RW2 specimen test results for rectangular wall section

As explained earlier, relatively simple basic uniaxial stress-strain relation is employed in the software thus the influence of the variation of these effects must be known on the analysis results. For this purpose, test results are compared with the analysis results by using different types of uniaxial steel material models given for same six wall elements with four concrete fibers and twelve steel fibers, cyclic degradation parameters which is shown in Figure 2.4, concrete models which is shown in Figure 2.6 and loading-unloading protocols. Three types of material models results have been compared with the test results and presented in Figures 2.8 and

2.10. In the first model (ITM %1 St. Hard.), assuming 1 % post yield strain hardening slope is suggested by LATBSDC 2015. In the second model (ITM %3.6 St. Hard.), assuming 3.6% strain hardening slope is offered by PEER's ATC-72 document. The last model is the elastic-perfectly plastic (EPP) steel model. Ultimate strength of elastic perfectly plastic model assumes half of the sum of expected yield and ultimate strength of the steel.

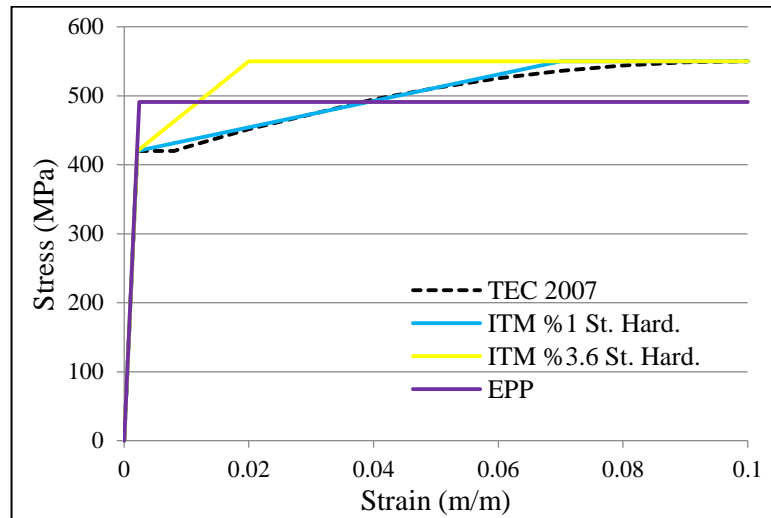


Figure 2.8. Comparison of different idealized steel models under monotonic loading

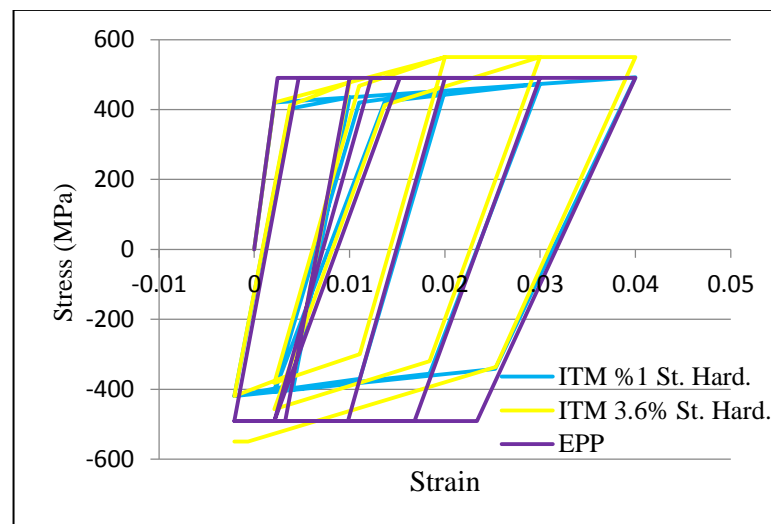


Figure 2.9. Comparison of different idealized steel models under cyclic loading

As it can be seen in Figure 2.10, the first model gives closer results when compared with the test results and other models. On the other hand, the second model has overestimated the capacity when compared with the test results. Results have also showed that quite relevant results have been acquired with the elastic-perfectly plastic model. However, a significant difference has been observed near the yield region among them. Elastic perfectly plastic model has estimated yield capacity further. The reason of this is possibly sudden changing stiffness, incapability of the analysis method and other uncertainties. Using a feasible strain hardening slope is also important to preclude convergence problems due to sudden changing stiffness in NLTHA. According to Ruiz-Garcia and Miranda (2003) and Chopra and Chintakanapakdee (2004), using a moderate post yield stiffness hardening results in drops in the peak displacement by less than 5 % for moderate normal and long period structures. In addition, Ruiz-Garcia and Miranda (2006a), and Pampanin et al. (2002) have emphasized that using a moderate post yield stiffness hardening slope causes an important drop in residual drift in all structures. As it is known, residual drift is one of the important parameters to evaluate the performance of tall buildings under earthquake excitation.

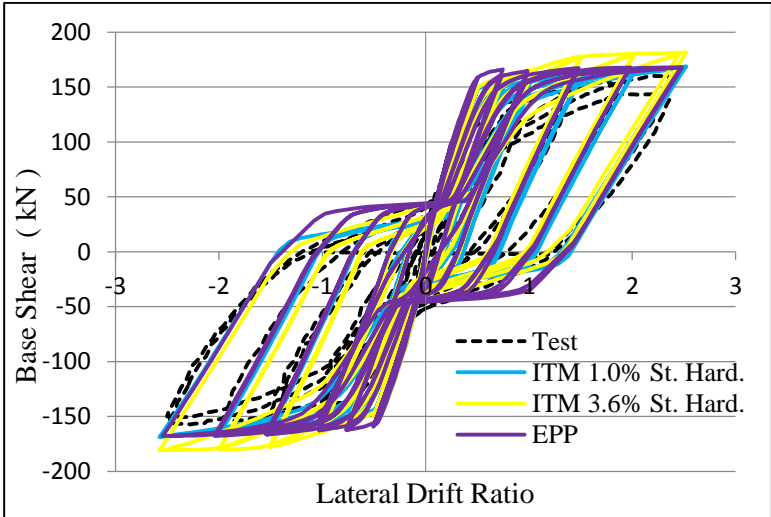


Figure 2.10. Comparison of test results (Thomsen and Wallace RW2) and models using different steel models for a rectangular wall section

2.3.2 Uniaxial Unconfined and Confined Concrete Models for Fiber Sections

Unlike reinforcing steel material, the behavior of concrete is fairly complicated and depends on imposed loading. Although concrete behaves as a quasi-brittle material

under uniaxial compressive loading, it may behave like a ductile material under multi-axial compressive loading. Several studies have been conducted for unconfined and confined concrete models by considering the confinement effects depending on the properties of the lateral reinforcement, diameter, spacing, yield strength, configuration of lateral and longitudinal reinforcement steel and section size. Modified Kent Park [1982], Saatçioğlu and Razvi [1982], Sheikh and Uzumeri (1983), Yassin [1984], Mander et al. [1988], Orakcal and Wallace [2004] have developed well defined and useful models for unconfined and confined concrete.

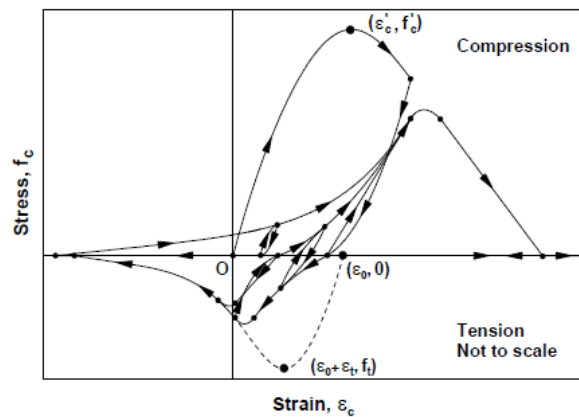


Figure 2.11. Orakcal and Wallace Concrete models (ATC-72, 2010)

Orakcal and Wallace model is more sophisticated among other models but it has a fairly complex loading and reloading behavior as shown in Figure 2.11. More sophisticated concrete models are generally used for research studies and it is not practical to employ in practice for performance based design of tall buildings. These models are more reliable to capture gradual opening and closing of cracks when compared with the test results, but it is applied only for a member or a small structure [ATC-72, 2010]. However, in a tall building model, in addition to having much larger number of components and connection, these material models have much more integration points in a model with many global degrees of freedom so that they require much more run time during nonlinear time history analysis. They also have not been adapted in commercially available software. On the other hand, the aim of nonlinear time history analysis for tall buildings is to capture the general expected behavior of the structure and members with a high degree of reliability. For this purpose, the most important stage is to choose the correct simplified material models

compatible with an acceptable material model proposed above. An example of the simplified uniaxial material model for unconfined and confined concrete is illustrated in Figures 2.12-2.15. The comparison of test results and analysis results which are used with these models were illustrated in Figure 2.7 and 2.10. It can be seen that the results obtained by using relatively simple concrete models are satisfactory. Results have also showed that using confined concrete models for wall boundaries and unconfined concrete models for wall web in the fiber modeling is sufficient to predict building behavior under cycling loading.

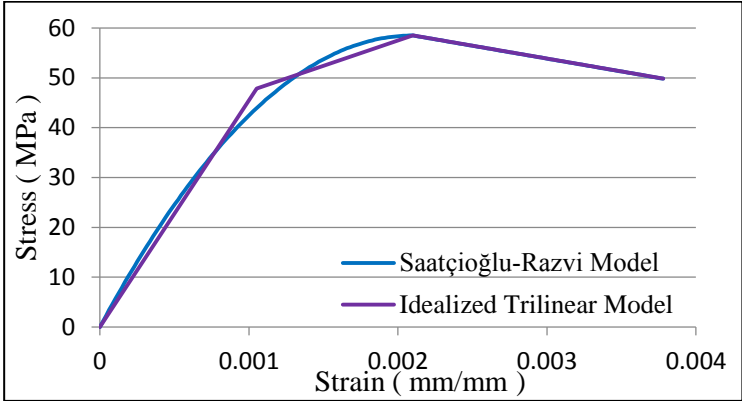


Figure 2.12. Comparison of Saatçioğlu Razvi unconfined concrete model with the idealized trilinear models

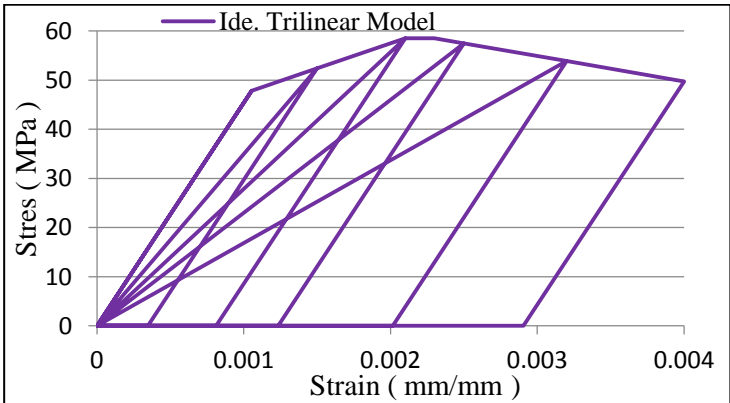


Figure 2.13. An application of unconfined concrete model in Perform3D under cycling loading

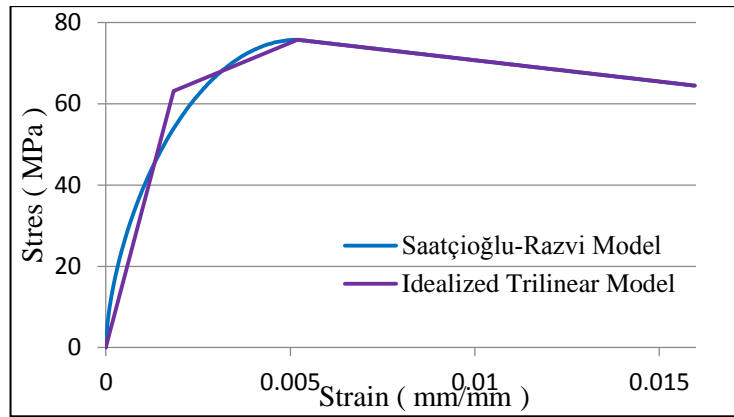


Figure 2.14. Comparison of Saatçioğlu Razvi confined concrete model with the idealized trilinear models

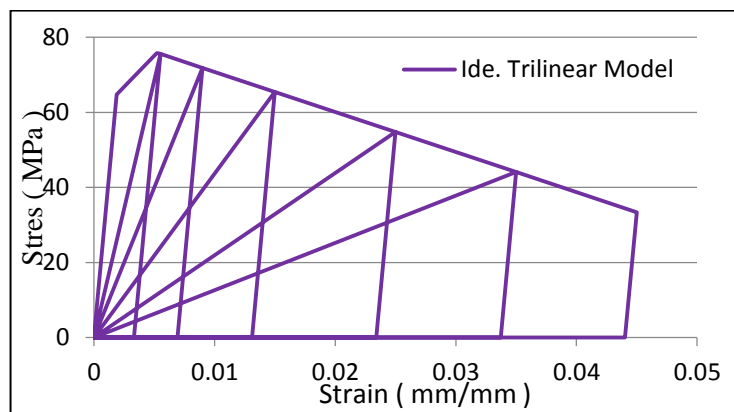


Figure 2.15. An application of confined concrete model in Perform3D under cycling loading

2.3.3 Shear Material Model for Fiber Element

Shear force – deformation behavior of shear walls can be modelled as either elastic or inelastic depending on the expected behavior of members under seismic loading and properties of members. In this part, shear behavior of reinforced concrete shear wall members is mentioned. Shear failure of shear walls is not a desired behavior under the seismic loading thus it is generally assumed to remain elastic at the design stage of these members. However, reinforced concrete tall shear walls do not remain elastic under the seismic loading because of the probable cracking due to the excessive moment demands on these members. Accordingly, linear elastic

assumption is not a realistic approach for them. Studies show that, the shear force deformation behavior of shear walls show some inelastic action even if it is not as ductile behavior as steel materials. Figure 2.16 shows the shear force-deformation relation provided in ASCE-41-13. As it can be seen, the backbone curve includes a pre-cracked stiffness and strength, subsequent to post-cracked stiffness up to the nominal shear strength and followed by sudden strength loss and remaining some residual strength. However, using appropriate secant stiffness up to yield (nominal) shear strength is widely employed in practice. These models are an uncoupled model, which do not consider the effect of shear-flexural interaction and axial force. However, according to Massone et al. (2006) and Wallace et al. reports (2006), there is a shear-flexural interaction. Their studies show that shear-flexural interaction causes an increase in flexural deformations and a member yields at lower shear force levels with respect to an uncoupled model. But coupled material models are not standard so these models have not been incorporated in commercially available programs.

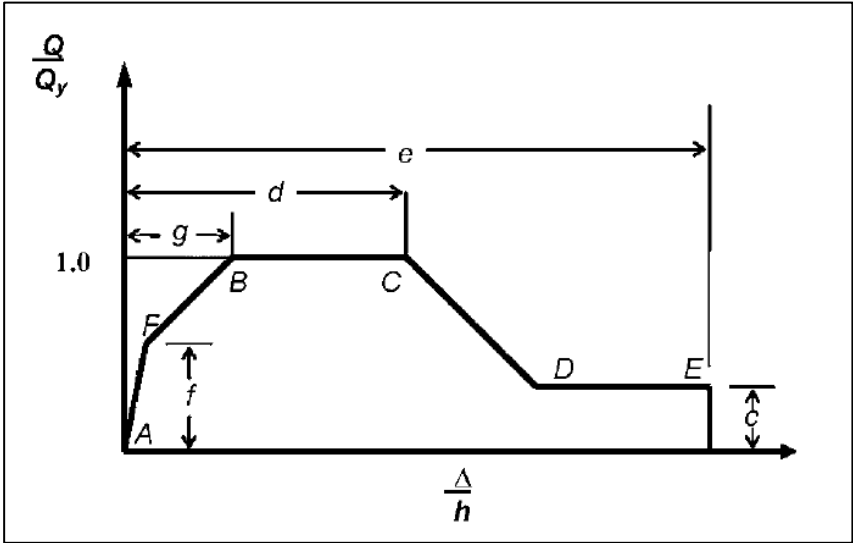


Figure 2.16. Shear force-deformation backbone curve bases on ASCE-41-13

2.4 Nonlinear Modeling of Reinforced Concrete Members

This part presents the proposed derivation of modeling parameters for nonlinear modeling of reinforced concrete structural members. First of all, general properties of

the inelastic components for reinforced concrete frame members are described. Afterwards, derivation of modeling parameters for frame members and inelastic component frame types are presented. Then modeling parameters for reinforced concrete shear walls are explained. Several parametric case studies have been carried out in order to calibrate shear walls for a reliable and effective nonlinear modeling. Finally, nonlinear modelling of coupling beams is explained.

2.4.1 Nonlinear Modeling Parameters for Reinforced Concrete Beam and Column Members

Efficient nonlinear component types are available in commercial and research computer software for modelling of reinforced concrete beams and columns, from three dimensional continuum finite element models to concentrated hinge (lumped plasticity) models. Inelastic structural moment frame systems are generally modelled by inelastic beam, column and beam-column joints. Concentrated hinge model has been utilized commonly for reinforced concrete beams and column. The reasons of this and shortcomings and advantages of inelastic components types were explained in the previous paragraphs. The part of beam-column joint is also modelled as either a group of rotational springs or stiff end zone in a proper manner.

Concentrated hinge model comprises of concentrated plastic hinges with quasi-elastic elements. Concentrated plastic hinge is based on the global force-deformation response of prismatic component, which is illustrated in Figure 2.3. It is essential to define correct force-deformation relationship of components for predicting members and global structure behavior accurately when subjected to different levels of ground motion intensity. Force-deformation action of components is changeable from a component type to another since it is depended on the expected controlling behavior of member under the expected loading. For example, if the governing behavior of component is bending, then this action is presented as either moment-rotation relationship or moment-curvature relationships, depending on demand and capacity measures.

The characteristic key parameters of concentrated hinges are obtained from idealized moment-curvature analysis under an expected specific axial load level. This is the boundary capacity curve of components under monotonic loading but under cycling loading both strength and stiffness degrade which is illustrated in Figure 2.17 (FEMA 440-A, 2009). Accordingly the effects of strength and stiffness degradation on seismic response must be considered for a reliable nonlinear modeling.

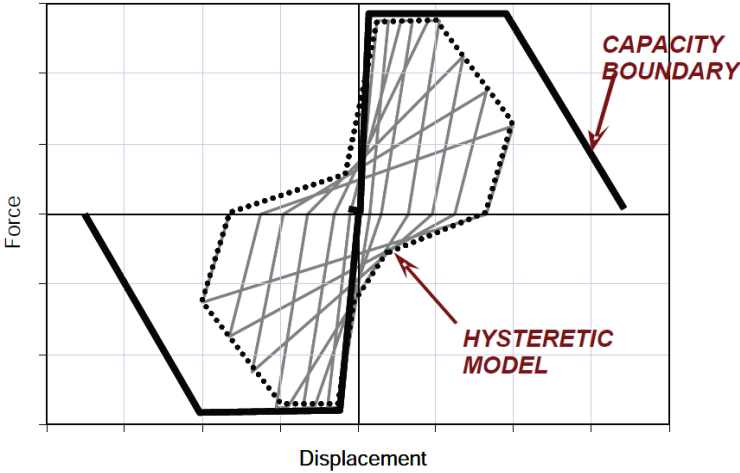


Figure 2.17. Monotonic capacity curve and hysteretic model (FEMA P440A, 2009)

PEER/ATC 72-1, which is one of the detailed guidelines about nonlinear modeling for seismic design and analysis of tall buildings suggest four options to consider cyclic deterioration appropriately, which is illustrated in Figure 2.18. In option 1, the effect of cyclic loading is incorporated explicitly in the model. The cyclic envelope curve of component depends on the loadings. In the second option, if the cyclic envelope curve is known from laboratory test, then the obtained cyclic envelope curve is used directly in the modeling but additional cyclic strength and stiffness deterioration is not incorporated in the model since this curve depends on the test loading protocol. In option 3, the effects of cyclic degradation are incorporated implicitly by using modification factors on the key parameters of initial monotonic backbone curve. Suggested modification factors are taken as;

- The initial yield strength and deformation remains same as the initial backbone curve values.

- The maximum strength of modified cyclic curve is taken as 0.9 times of the monotonic backbone curve ultimate strength but this cannot be less than the initial yield strength.
- The pre-capping deformation range of modified cyclic curve is taken as 0.7 times of the monotonic backbone curve pre-capping deformation range.
- The post-capping deformation range of modified cyclic curve taken as 0.5 times of the monotonic backbone curve post-capping deformation range.
- The residual strength of modified cyclic curve taken as 0.7 times the initial backbone residual strength
- The ultimate deformation of modified cyclic curve taken as 1.5 times the deformation related to maximum strength of initial backbone.

In the last option, effects of degradation and the range of strength degradation and residual part are not incorporated in the analytical model but with a small exception, the ultimate strength is taken as 0.8 times maximum strength of the backbone curve and the ultimate deformation point is obtained as the slope that is equal to that in options 2 or 3 from the maximum strength to 0.8 times of maximum strength.

Considering all models, option 1 is the most realistic but complicated model in practice. Option 2 and 3 is similar since it is not accepted any additional cyclic deterioration and cyclic degradation is considered implicitly. Option 4 is the most restrictive model. The implementation all of these models are accepted, which depends on the analysis tool and other available data.

The representation of force deformation relationship also changes from a seismic code (or guideline) to other as illustrated in Figure 2.19. As it can be seen, all types except TEC-2007 have the same key parameters until ultimate strength (force) point. After this point, the characteristic backbone curves differ from each other because of the uncertainties of inherent strength loss.

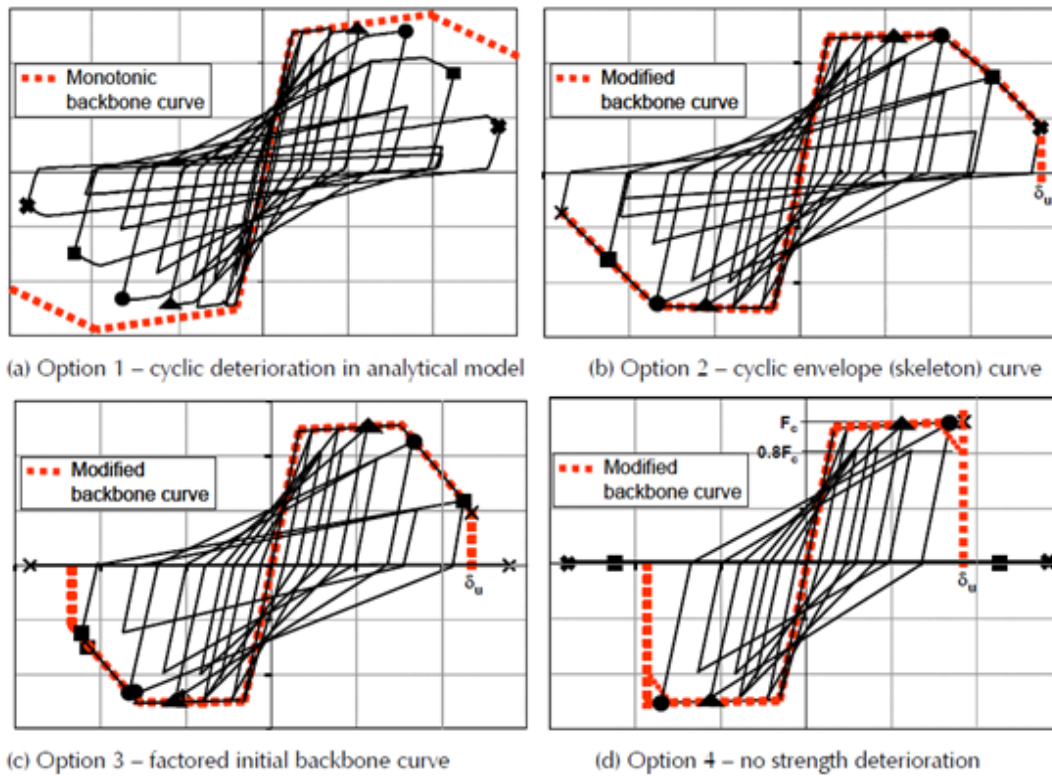


Figure 2.18. Options for component modelling (ATC-72, 2010)

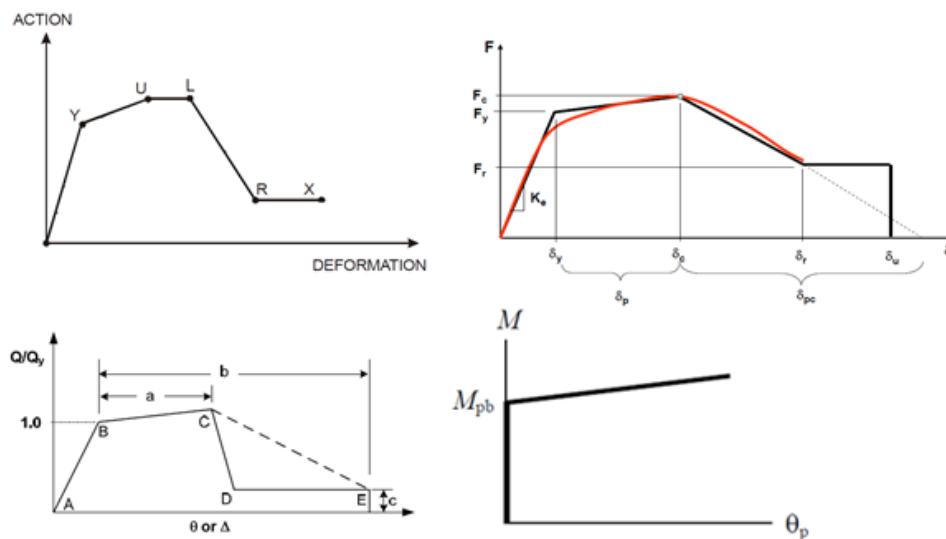


Figure 2.19. Comparison force-deformation relationship of Perform 3D, Ibarra-Krawinkler, ASCE/SEI 41-06, TEC-2007

As it can be seen, some specific points must be known to define a ductile backbone curve. These parameters are initial stiffness, post-yield stiffness, degrading stiffness,

yield strength, ultimate strength, residual strength and deformation parameters related to each key strength parameter. Some of guidelines such as ASCE/SEI 41-13, strength parameters are obtained from moment-curvature analysis and it gives deformation parameters and residual strength (a, b, c) by considering the effects of cyclic deterioration implicitly. Initial stiffness must be determined accordingly and post yield stiffness is proposed between zero and 10 % of the initial slope. In TEC-2007 and IMM, all parameters are obtained from moment curvature analysis by disregarding cyclic deterioration. On the other hand, PEER ATC-72-1 gives some analytical equations depending on the component properties to define the monotonic backbone curve. Cyclic degradation is suggested to apply explicitly or implicitly in the analytical model.

Effective stiffness of reinforced concrete beams and columns are employed to account for the effects of concrete cracking, bond slip, shear effects etc. when concentrated hinge models are utilized. Effective stiffness value which is derived from the calibration of load-deformation behavior of reinforced concrete member tests is the secant stiffness of member. Two common flexural effective stiffness values are described for different performance levels, lower-bound (larger) and upper-bound (smaller) stiffness respectively. The flexural effective stiffness values change these ranges but the lower-bound stiffness which corresponds to 0.4 times the yield point is used in service level evaluation, where deformation or damage of the structural members is expected to remain below the yield region. The upper-bound flexural stiffness which corresponds to yield point is utilized in collapse prevention level evaluation where deformation or damage of the structural members is expected to go beyond the elastic region [ATC-72, 2010]. For this purpose, seismic codes and alternative non prescriptive seismic guidelines propose some effective stiffness values for reinforced concrete members. Haselton et al. has improved and proposed an analytical equation which is presented below for upper and lower bound stiffness based on 255 experimental column data. These equations are based on the axial load level and component properties. These equations are also employed for beams by considering zero axial load level [ATC-72, 2010].

$$K_{stf} : \frac{EI_{stf}}{EI_g} = -0.02 + 0.98 * \left[\frac{P}{A_g * f'_c} \right] + 0.09 * \left[\frac{L_s}{H} \right] \text{ where}$$

$$0.35 \leq \frac{EI_{stf}}{EI_g} \leq 0.8 \quad (2.1)$$

$$K_y : \frac{EI_y}{EI_g} = -0.07 + 0.59 * \left[\frac{P}{A_g * f'_c} \right] + 0.07 * \left[\frac{L_s}{H} \right] \text{ where}$$

$$0.2 \leq \frac{EI_y}{EI_g} \leq 0.6 \quad (2.2)$$

Similar column tests data are calibrated by Elwood et al. (2007). He proposes effective stiffness values for reinforced concrete members which have been taken in ASCE/SEI 41-13, which is presented in Table 2.1. The comparison of Haselton et al. and Elwood et al. are illustrated in Figure 2.20.

Table 2.1. Effective stiffness values according to ASCE/SEI 41-06

Component	Flexural Rigidity	Shear Rigidity	Axial Rigidity
Beams-non prestressed	$0.3E_cI_g$	$0.4E_cA_w$	-
Beams-prestressed	E_cI_g	$0.4E_cA_w$	
Columns with compression due to design gravity loads $\geq 0.5A_gf'_c$	$0.7 * E_cI_g$	$0.4E_cA_w$	E_cA_g
Columns with compression due to design gravity loads $\geq 0.1A_gf'_c$ or with tension	$0.3E_cI_g$	$0.4E_cA_w$	E_cA_g
Walls-cracked	$0.5E_cI_g$	$0.4E_cA_w$	E_cA_g
Flat Slabs-non prestressed	See section 6.4.4.2	$0.4E_cA_g$	
Flat Slabs-prestressed	See section 6.4.4.2	$0.4E_cA_g$	

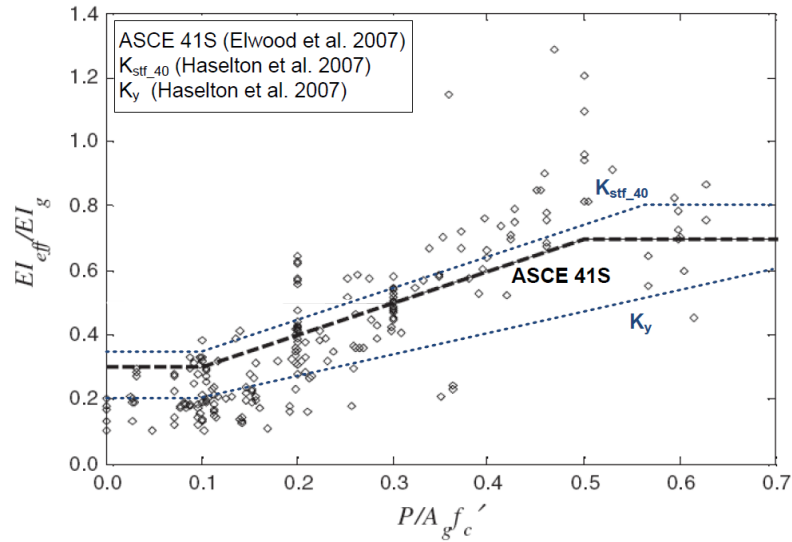


Figure 2.20. Comparison of proposed effective stiffness values by Haselton and Elwood (ATC-72, 2010)

LATBSTDC-2015 proposes similar effective stiffness values both service level and collapse prevention level for reinforced concrete member, which is illustrated in Table 2.2

Table 2.2. Reinforced concrete members stiffness properties (LATBSTDC, 2015)

Element	Serviceability and Wind linear or nonlinear models (flex. and she)	MCE-level Nonlinear models
Structural Walls	$0.75E_c I_g^*$ or $1.0 E_c I_g^{**}$ / $0.4E_c A_g$	$1.0 E_c I_g^{**}$ / $0.2E_c A_g$
Basement walls	$1.0 E_c I_g$ / $0.4E_c A_g$	$0.8 E_c I_g$ / $0.2E_c A_g$
Moment Frame Beams	$0.7 E_c I_g$ / $0.4E_c A_g$	$0.35 E_c I_g$ / $0.4E_c A_g$
Moment Frame Columns	$0.9 E_c I_g$ / $0.4E_c A_g$	$0.7 E_c I_g$ / $0.4E_c A_g$
Coupling Beams	$0.3 E_c I_g$ / $0.4E_c A_g$	$0.2 E_c I_g$ / $0.4E_c A_g$
Diaphragms (in-plane only)	$0.5 E_c I_g$ / $0.33E_c A_g$	$0.25 E_c I_g$ / $0.1E_c A_g$

* Frame models / ** Fiber model

$$E_c = 57000 * \sqrt{f'_c} \quad \text{for } f'_c \leq 6000 \text{ psi} \quad (2.3)$$

$$E_c = 40000 * \sqrt{f'_c} + 1 * 10^6 \quad \text{for } f'_c > 6000 \text{ psi} \quad (2.4)$$

TEC-2007 and IMM also proposes effective stiffness values which are presented below for reinforced concrete beams, columns and walls only but these values are very rough and very high for service level evaluation of tall buildings when compared to LATBSDC (2015) and ATC-72 (2010).

$$\text{for beams : } 0.4 E_c I_g \quad (2.5)$$

$$\text{for columns and shear walls : if, } \frac{N_D}{A_c * f_{cm}} \leq 0.10 \text{ then } 0.4 E_c I_g \quad (2.6)$$

$$\frac{N_D}{A_c * f_{cm}} \geq 0.40 \text{ then } 0.8 E_c I_g \quad (2.7)$$

$$0.1 \leq \frac{N_D}{A_c * f_{cm}} \leq 0.40 \quad (2.8) \text{ then linear entetpolasyon between } 0.4 E_c I_g \text{ and } 0.8 E_c I_g$$

2.4.2 Nonlinear Modeling of Beam Elements

As explained earlier, the monotonic F-D relationship of concentrated hinges are obtained from idealized moment-curvature analysis under an expected specific axial load level. In reinforced concrete beams, the axial load level is assumed as zero. Idealized bilinear moment-curvature which is proposed by Priestly et al. is widely employed to define monotonic backbone curve of the component, which is illustrated in Figure 2.21 [Priestly et al., 2007]. In this model, M_y is the first yielding strength point of the component when the outermost compression fiber of concrete from the neutral axis reaches the strain which is nearly 0.002, or when the outermost tension reinforcement from the neutral axis reaches yield stain, whichever develops first. The curvature at this point is yield curvature of the component and symbolized by ϕ_y' . Effective stiffness of the component which is denoted by $(EI)_e$ is acquired from the M- ϕ relationship directly, which is valid up to nominal moment capacity point when the outermost compression fiber of concrete from the neutral axis reaches the strain which is nearly 0.004 or when the outermost tension reinforcement from the neutral axis reaches nearly 0.015, whichever develops first. The curvature at this point is defined by nominal yield curvature of the component and symbolized by ϕ_y . After this point the slope of curve changes and plastic deformation becomes important without any significant strength gain until ultimate moment capacity point when strength loss starts because of correlation between the concrete crushing (causing

strength loss) and strain hardening or rupture of the reinforcement steel. The curvature and moment at this point is defined by ultimate curvature and ultimate moment of the component and symbolized by ϕ_u , M_u respectively.

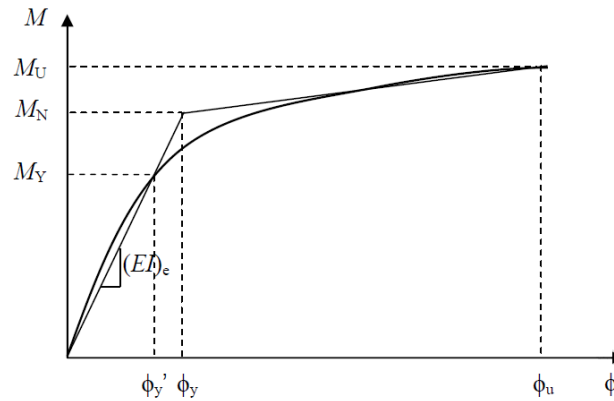


Figure 2.21. Inelastic and idealized moment curvature (Priestly et al., 2007)

There are four inelastic component frame types which depend on how and where plastic hinges (defining F-D relationship) are defined and which results are utilized to evaluate the performance of member [G. Powell seminar notes, 2012]. Inelastic frame beam components types are exact model, inelastic finite element model, plastic hinge model and plastic zone model which are explained separately below. All types except exact model are available in commercially available software.

The basic properties of these models for F-D relationship are mainly similar and obtained from moment curvature analysis, but there are several different aspects from each other. First, although bending moment is utilized as a strength measure for each method, either strain or rotation is employed as a deformation measure to assess the performance of members. However strain and rotation is related to each other by empirical equations, and there are two approaches among researchers and seismic guidelines about how members are assessed with respect to deformations. According to Powell [Powell seminar notes, 2012], obtaining curvature from the tests or/and analytical approaches is much more sensitive than obtaining rotation (or chord rotation) since it depends on plastic hinge length. When smaller hinge length is used and if the bending moment is measured at the maximum points of component

(usually at the beam ends) then the obtained curvature becomes high and localized with respect to inelastic beam theory. A trusted way to estimate curvature demand is not available accordingly. An applicable average strain or rotation may be a good choice for demand capacity measure. The other important difference among models is how a reliable analysis model is prepared in a simplest way since creating nonlinear model is a time consuming process. As considering nonlinear modeling of tall buildings, this is even more important. Creating a model with plastic zone model requires less time when considering commercially available software since the change of hinge length is a simple process. If plastic hinge model is employed and the hinge length is changed after model is generated, then nonlinear model must be regenerated since change of hinge length affects all rotation parameters to be needed for defining the backbone curve. On the other hand, ASCE-41-13 model depending on plastic rotation model gives the deformation capacity of components thus it is also a suitable method to apply.

2.4.2.1 Exact Model

“Exact” model is not a practical and easy model to employ in a nonlinear computer model since this approach utilizes the inelastic moment-curvature ($M-\phi$) relationship. Inelastic $M-\phi$ relationship comprises much more linear segments and stiffness at each step (Figure 2.22), and this results in complicated problems such as it is not compatible with the commercially available software and it causes a computationally expensive process due to comprising much more points and stiffness values (changing every analysis step). Instead of this, idealized bilinear or trilinear $M-\phi$ relationship is employed (Figure 2.22). Used deformation measure for demand capacity measure for exact model is average strain over plastic zone where significant plastic deformation is expected to occur.

2.4.2.2 Finite Element Model

Another model is the finite element model is illustrated in Figure 2.23. In this model, frame element is divided into a number of elements having a special hinge tributary length (mesh size) with quasi-elastic elements along the member length. Inelastic behavior of each element is concentrated at the center of each elements. Either

inelastic or idealized linear $M-\phi$ relationship is defined for each element. If inelastic $M-\phi$ relationship is described, the problems and complexities of the exact model are seen in this model similarly. However if idealized inelastic $M-\phi$ relationship is utilized with a well-defined mesh, it is expected that the results are even close to accurate. Although using a refined mesh size is a good approach in linear elastic analysis to capture the behavior of structure, this is not true for inelastic structural analysis. This is because when smaller mesh size is used, the localized maximum calculated strain grows increasingly and the general behavior of member loses sensitivity. The analysis also requires more computation time if many elements is used. Used deformation measure for demand capacity measure is curvature over plastic zone in this model.

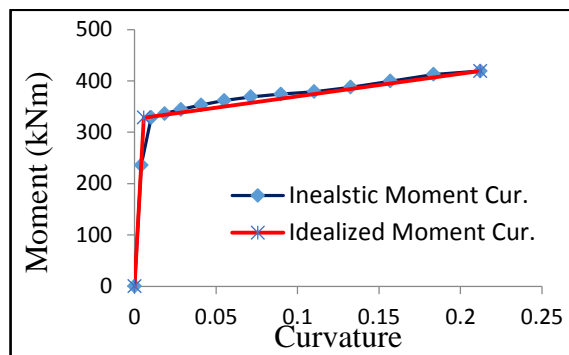


Figure 2.22. Comparison of inelastic and idealized moment curvature relationship

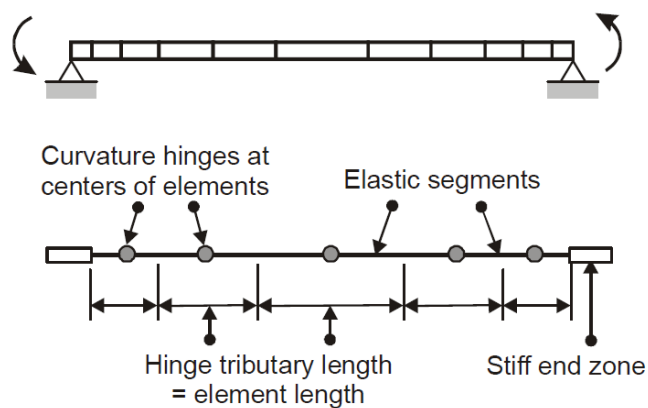


Figure 2.23. Finite element models (Perform 3D, 2011)

2.4.2.3 Plastic Hinge Model

The implementation of plastic hinge model is illustrated in Figure 2.24. In this model, all inelastic deformation (rotation) is assumed to concentrate in zero plastic hinge length. The properties of plastic hinges are obtained from section M- ϕ analysis. The strong aspect of this model is to give engineer assigning hinges wherever you want. For example this model is widely used in modelling reduced steel beam sections. The properties of hinges are assigned at the center of reduced beam section. Used deformation measure for demand capacity measure is rotation.

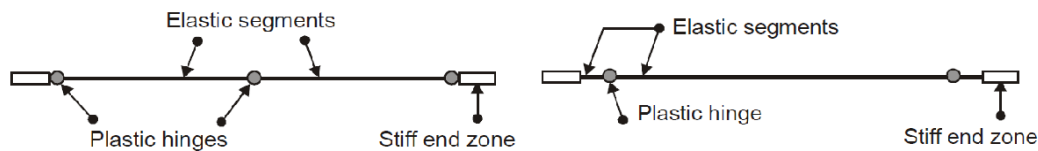


Figure 2.24. Plastic Hinge Model and its implementation to beam and reduced beam section

2.4.2.4 Plastic Zone Model

Unlike plastic hinge model, plastic zone model assume that all plastic deformation is gathered over a specific zone length but both models apply similar procedures to define the inelastic properties of components. However this model gives engineer a flexibility when describing the inelastic mathematical computer model. For example if engineer wants to change plastic hinge length and uses plastic hinge model, then he/she must change all nonlinear properties of the model since plastic rotations depend on plastic hinge length and plastic curvature ($\theta = l_p * \phi$). Instead of this, M- ϕ relationship is defined among the plastic hinge length which is assigned directly. One of the most important parameters is to choose a correct plastic zone (hinge) length. The actual plastic hinge length depends on the properties of the components and changes under the actual loading continually so it is not a practical application. There are several approaches to define plastic hinge length but it is taken as one-half of the section depth for frame members in practice. Used deformation measure for

demand capacity measure is average strain over plastic zone ($\theta = l_p * \phi$). This model is illustrated in Figure 2.25.

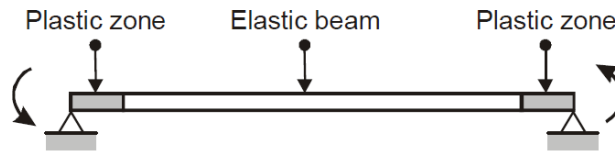


Figure 2.25. Plastic zone Model

2.4.3 Nonlinear Modeling of Reinforced Column Members

As reinforced concrete beams, reinforced concrete columns are also idealized frame elements consisting of inelastic lumped plasticity components at each end with quasi-elastic member. Its quasi elastic properties are also described in the previous section. The properties of concentrated plastic hinges of the column components are obtained with a similar process for reinforced concrete beams. The fundamental differences from the beam components are that columns can have significant axial forces and biaxial bending. Accordingly, P-M-M hinges with interaction surface must be defined to capture the inelastic behavior of columns rationally under the expected earthquake excitation. P-M-M hinges use plasticity theory [Perform 3D, component and element guidelines]. Bending properties of hinges are defined from moment-curvature analysis under a specific axial force level. For columns, axial load levels are taken as the expected factored gravity load ($G+nQ$) where n is a probabilistic value and taken as 0.2~0.3 for tall buildings.

2.4.4 Modeling of Reinforced Concrete Shear walls

As explained earlier, fiber models are generally used for shear wall elements for both collapse prevention level and service level evaluation if nonlinear time history is utilized. A shear wall member consists of a number of wall elements, which is illustrated in Figure 2.2. Each of the wall elements is comprised of a number of steel and concrete fibers, which is also illustrated in Figure 2.2. As explained earlier, most significant parameters in fiber model are using correct material stress-strain

relationship, choosing a convenient number of wall elements, fiber size and plastic hinge (element) length for a realistic nonlinear model. For this purpose, these parameters must be calibrated with respect to test results or parametric studies. The effect of material strain-stress relationship is explained elaborately in the material section part. Using a moderate strain hardening with a simplified trilinear model has also justified acceptable results when comparing test results. In this part, the effect of number of wall elements, fiber size and element length on the fiber model response is presented.

First of all, how the number of wall element numbers can affect analysis results are described to compare test results with two different analytical models. Thomsen and Wallace (2014) developed RW2 shear wall specimen was generated with respect to the geometry properties and the same cycling loading protocol. The first analytical model has comprised of six wall elements with four concrete fibers and twelve steel fibers, which is illustrated in Figure 2.26. Confined concrete models have been utilized for both of wall end regions (2 fibers) and unconfined concrete models have been employed for wall web (2 fibers). 1 % strain hardening has considered in the reinforcement steel material model. The wall elements length has taken as the estimated plastic hinge length which is one-half of the wall depth. The second analytical model is comprised of 48 wall elements (each of end region consists of two wall elements and web region also consists of two wall elements and elements length (height) taken as one-half the estimated plastic length) with eight concrete fibers and twelve steel fibers in total.

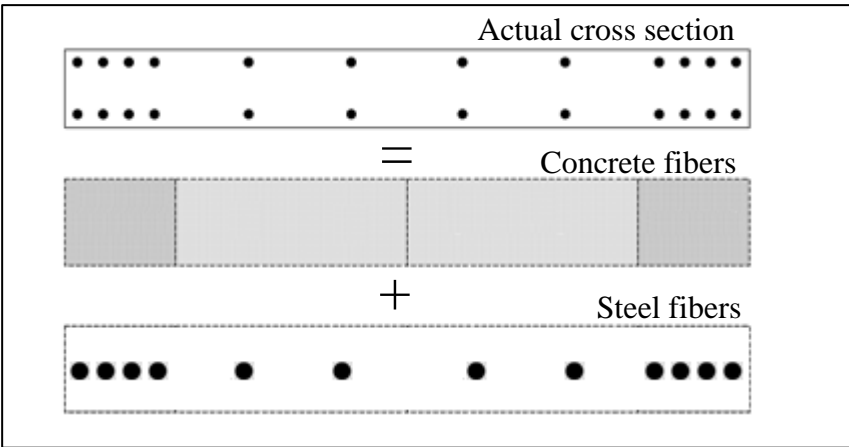


Figure 2.26. Comparison of actual and idealized section for fiber model

The analysis results compared with the experimental results at the base of the wall element are plotted in Figures 2.27 and 2.28. The results point out that using more wall elements has resulted in inaccurate results since inelastic deformations have gathered in a single element especially when drift ratio has increased. Instead of using too many elements, using an equal plastic hinge length with moderate wall elements gives more rational results but as the drift ratio increases, the discrepancies between the results of compression and tension end of wall region have grown. According to Wallace (2006), these differences might have occurred because of shear-flexural interaction.

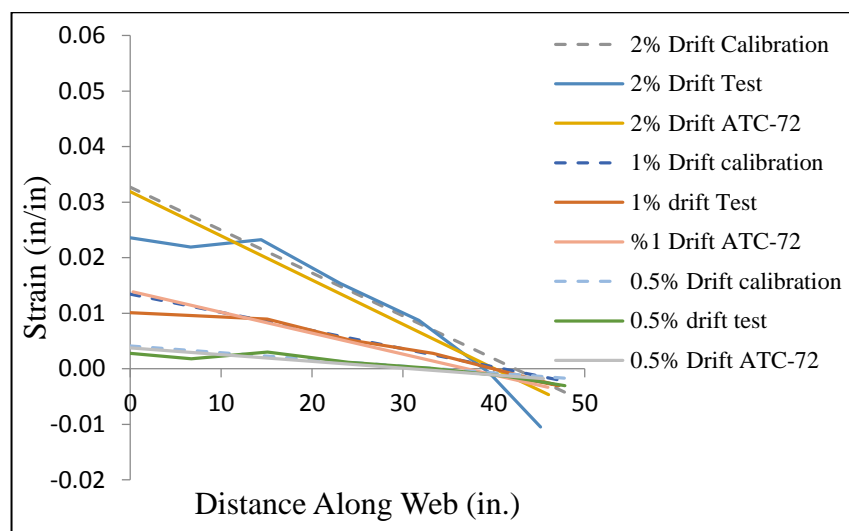


Figure 2.27. Strain distribution at the base of the wall for 6 elements

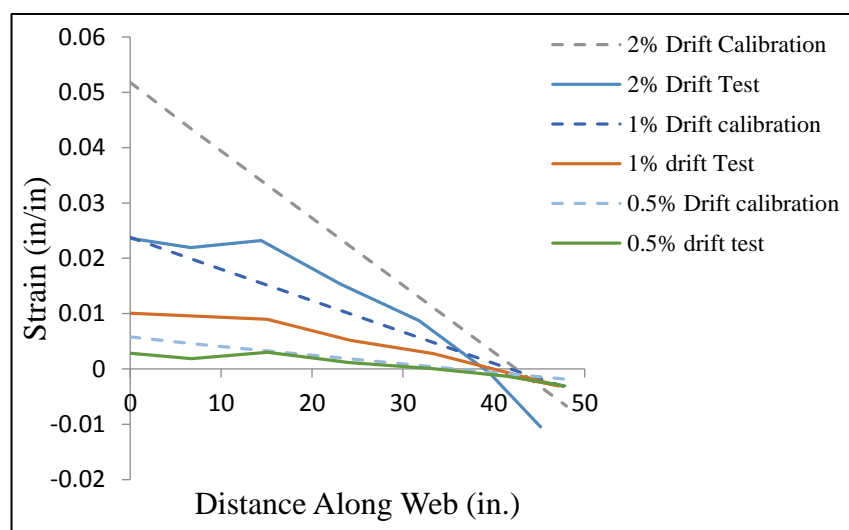


Figure 2.28. Strain distribution at the base of the wall for 48 elements

As we know, a tall building has much more components and connection so analysis and modeling stage is time consuming. Using many fibers can require much more time during analysis and modeling of tall buildings. In addition, it is generally not feasible using too many fibers in the nonlinear modeling of tall building by using commercially available software (Perform3D V5). In other words, number of fibers is limited in the analysis program. Accordingly, how the number of fiber can affect analysis results are examined by comparing detailed commercially available section analysis program XTRACT results with Perform 3D results to get the optimum number of fiber in modeling. For this purpose, a parametric study, four case studies with three different axial load levels (0, $0.15f_cA_c$ and $0.25f_cA_c$), has been done. A section having a 0.8 meter thickness and 22 meters in length designed according to TEC-2007 is employed. The detailed section properties are shown in the appendix part. These cases are explained below. For all cases, which are shown in the appendix part, confined concrete material model is utilized for the wall boundaries and unconfined concrete model is utilized for the wall web.

- Case 1: detailed model. Cross section is divided into 100*100 mm concrete fibers and each of the longitudinal reinforced steel is considered as a fiber in their exact location.
- Case 2: Cross section is divided into 800 mm length concrete fibers and longitudinal reinforced steel bars are idealized as fibers at the center of each concrete fiber.
- Case 3: Cross section is divided into 1600 mm length concrete fibers and longitudinal reinforced steel bars are idealized as fibers in the center of each concrete fiber.
- Case 4: The wall boundaries are divided into 600 mm length concrete fibers and the wall web is divided into 3200 mm length concrete fibers. Longitudinal reinforced steel bars are idealized as fibers in the center of each concrete fiber.

The comparative section analysis results for three different axial load levels have been plotted in Figure 2.29. The results point out that the influence of the number of fibers is very little in the predicted moment versus curvature relation in cases of zero

and $0.15f_cA_c$ axial load levels. Although there is a little difference in the predicted moment capacity, a significant difference is observed in ductility for Case 1 in comparison with the others when the axial load level increases to $0.25f_cA_c$. Case 1 is more brittle than others in this situation. The ductility is also reduced when axial load levels is $0.25f_cA_c$. It is generally limited to axial load level $0.25f_cA_c$ for reinforced concrete shear wall members for a ductile response for high rise structures in high seismicity regions [LATBSDC, 2015]. In addition, it can be seen that Case 4 results are more close to Case 1 than the others. As a result, instead of using too many fibers with more wall elements, using relatively more fibers in the wall boundaries with relatively less fibers in the wall web gives more realistic results for predicting the performance of structure.

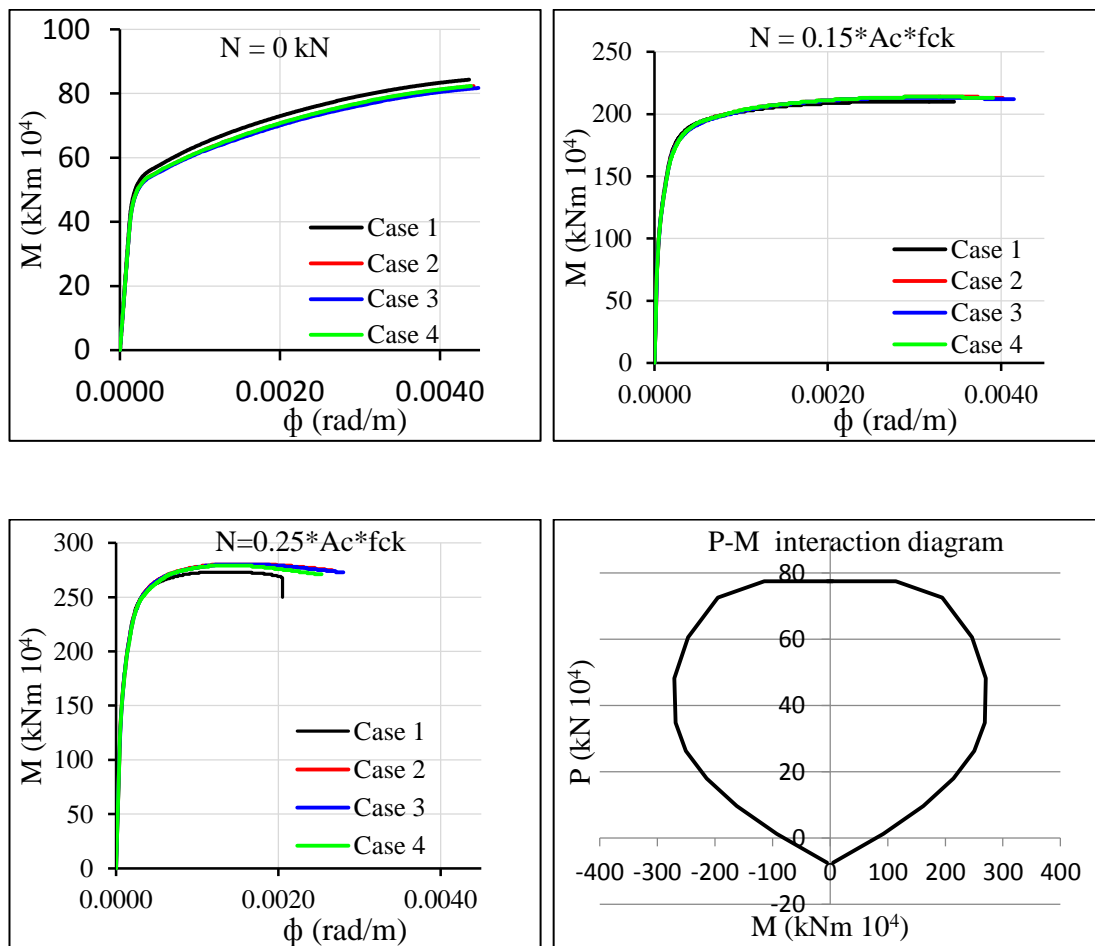


Figure 2.29. The effect of fiber size of the wall element for different axial load levels and interaction diagram

2.4.5 Nonlinear Modeling of Reinforced Concrete Coupling Beams

Coupling beams are designed as conventional coupling beams or diagonally reinforced concrete beams, which depend on the properties of (clear span to depth ratio) beams and loading on the beams. Diagonally reinforced concrete beams are utilized mostly in reinforced concrete wall buildings since use of diagonal coupling beams enhances the seismic performance of structure.

Reinforced concrete coupling beams can be modeled as either fiber model or lumped plasticity model (or slip extension) or shear displacement hinge model. Since current analytical models and acceptance criteria that are specified in codes for coupling beams are based on rigid plasticity model or shear displacement hinge model, which is illustrated in Figure 2.30. Accordingly, implementation of coupling beams by using these models is much easier and applicable in practice.

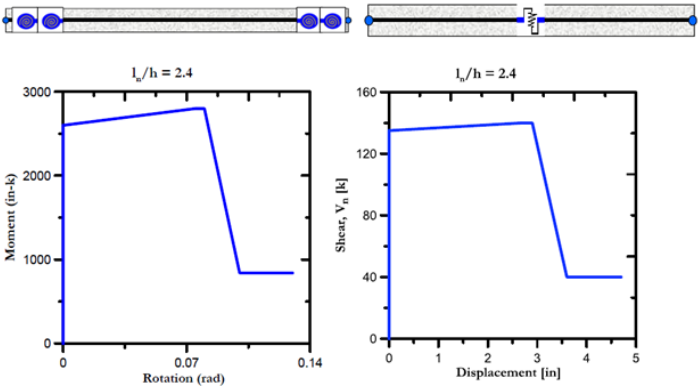


Figure 2.30. Rigid lumped plasticity and shear displacement hinge model with their backbone curves for coupling beams (ATC-72, 2010)

Similar to nonlinear beam modeling, the force deformation relationship of hinges and quasi elastic properties of frame member must be defined correctly to capture inelastic behavior of coupling beams under any earthquake excitations. For lumped plasticity hinge model, the force is moment force and the displacement is rotation across hinge. However for shear displacement hinge, the force is shear force and the displacement is shear displacement across the hinge. In practice, coupling beams are generally allowed to yield (flexural members) but it is not desired to fail due to shear.

Accordingly, the behavior of coupling beams is controlled by shear. Comparison of test results with analytical models by using both approaches show that both of these models are efficient to capture the overall load displacement behavior if hinge properties and proposed secant stiffness values are properly applied [ATC-72, 2010]. These models are rigid plastic models so there is no need of elastic stiffness for the hinge. Displacement or rotation and residual strength parameters are obtained from either experimental tests or reference seismic guidelines. For example ASCE SEI 41-13 gives displacement capacities and residual strength parameters. Nominal strength capacity must be calculated in accordance with ACI 318-08.

The effective stiffness values are generally defined in seismic codes which are shown in Tables 2.1 and 2.2. In addition to these reference effective stiffness values, in the light of current studies in PEER Review Initiative-ATC-72 (2010), it proposes to modify the effective stiffness values for diagonally coupling beams like this;

- If clear span to depth ratio is over 2.0, the behavior of coupling beams is controlled by flexure. Then;

$$\frac{l_n}{h} \geq 2 \rightarrow E_c I_{eff} = 0.15 E_c I_g \text{ and } G_c = 0.4 E_c \quad (2.9)$$

- If clear span to depth ratio is below 1.4, inelastic deformation is controlled by shear and flexural deformations because flexural and shear deformations are nearly equal.

$$\frac{l_n}{h} \leq 1.4 \rightarrow E_c I_{eff} = 0.15 E_c I_g \text{ and } G_c = 0.1 E_c \quad (2.10)$$

- If clear span to depth ratio is between these ranges, then linear interpolation is a feasible method to define effective stiffness values.

To define the nominal shear strength of coupling beams, some analytical equations are proposed depending on coupling beam types and properties. According to ACI 318-08 (similar to TEC 2007);

For conventional coupling beams, the nominal strength is the sum of concrete and steel:

$$V_n = A_{cv} (\alpha_c \lambda \sqrt{f'_c} + \rho_t f_y) \quad (2.11)$$

For diagonally coupling beams

$$V_n = 2A_{vd}f_y \sin \alpha \leq 0.83\sqrt{f'_c}A_{cw} \tag{2.12}$$

2.5 P-Delta Effects

One of the sources of nonlinear structural behavior is geometric nonlinearity since the effects of loads acting on the deformed shape of structure is considered. As a basis information, P-delta effects which are a type of geometric nonlinearity are caused by gravity loads acting on the displaced member joints, which results in adding an extra moment force on the members as it can be explained below. The theory of P-delta is based on two assumptions. First, the member shifts horizontally but axial extension of the member is ignored (infinitely axial rigidity). Small displacement rule is applied. The second assumption is that the equilibrium condition is satisfied at the displaced position of the member.

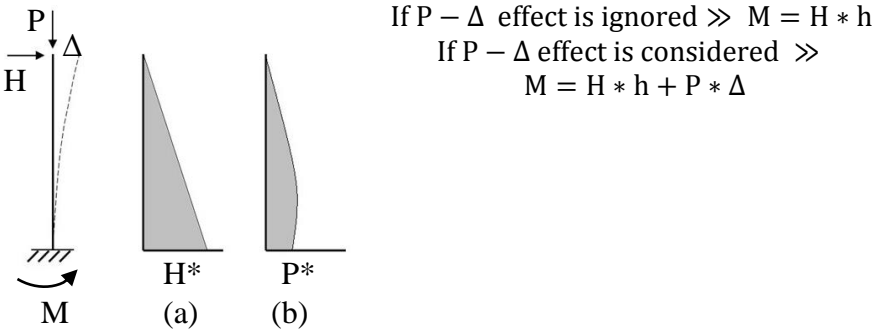


Figure 2.31. Cantilever columns and moment diagram for a) First-order effects only and, b) P-Δ effects only.

Considerable amount of studies has been carried to understand P-delta effects on the behavior of structure. The studies show that if the maximum displacement of the component goes beyond displacement corresponding to ultimate strength point (if the effective stiffness enters the range of negative part), P-Delta effects become more critical and trigger lateral drift increase. They may lead to lateral dynamic instability and collapse if the effects are sufficiently large. The studies also show that P-Delta affect the collapse capacity of moment-resisting frame systems more than the collapse capacity of shear wall structural systems. If the effective stiffness remains in

the positive effective stiffness range, the effects of P-Delta is generally under control but it does not give a guarantee [ATC-72, 2010].

As a result, the possible collapse of the structure is generally controlled by the combination of the effects of P-Delta and deterioration. P-Delta effects become more critical after where significant strength loss begins. In seismic performance of tall buildings, the axial load level of seismic force resisting systems and gravity column systems are very high and the structures move laterally under the seismic loading hence the P-Delta effects must be included in the analytical model both for service level and collapse prevention level.

2.6 Gravity Load Effects in Nonlinear Analysis

Unlike linear elastic analyses, the results of nonlinear analyses are influenced and depend on the gravity load effects directly; therefore the selection of appropriate expected gravity load is important. It is generally taken as dead load [D] and some portion of the design live load (L). Non-prescriptive consensus seismic design guidelines suggest the equations below to consider gravity loads in the NLTHA for tall buildings. (N: number of story)

$$1.0 * D + 0.20 * L \gg \text{(ATC - 72)} \quad (2.13)$$

$$1.0 * D + 0.25 * L \gg \text{(PEER - TBI)} \quad (2.14)$$

$$1.0 * D + n * L \gg \text{(IMM)} \quad (2.15)$$

$$n \leq 0.3$$

$$n = 0.01 * (50 - N) \quad N \leq 40 \quad (2.16)$$

$$n = 0.10 \quad N > 40 \quad (2.17)$$

2.7 Ground Motions Selection

The selection of ground motion records for nonlinear dynamic analysis is one of the most important steps in performance analysis. Selection of appropriate pairs of ground motion time series for a tall building from the recorded earthquake ground motions in the past are generally not available. Accordingly, a suite of ground motion time series (accelerograms) that were recorded during past earthquake are modified

in a way by considering the characteristic properties of structure, its site conditions and expected target seismic hazard and damping etc. The modifications employed for generating ground motion time series is a debatable issue, thus ground motions must be selected by a ground motion specialist from seismic hazard analysis carried out for special structures. As a basis, the algorithm of this procedure mainly consists of the following three steps:

1. Define target hazard spectrum with specified return periods by using either uniform hazard spectrum or conditional mean spectrum. Probabilistic seismic hazard analysis should consider the expected earthquakes on the faults that may affect the construction site.
2. Select a suite of ground motion pairs recorded during past earthquakes at stations that conform to site conditions which the building is to be built. Conformance of the employed earthquakes to the fault type and magnitude of the main events that dominate probabilistic seismic hazard analysis is also desirable.
3. Manipulate or modify the selected time series to match the target response spectrum by using either amplitude scaling or spectral matching procedures.

Uniform hazard spectrum is a method to define target hazard (response) spectrum by using various levels of ground motions. Uniform hazard spectrum consists of a set of acceleration spectral ordinates for different vibration periods which have the same probability of exceedance for a given exposure time [Sucuoğlu and Akkar, 2014]. Design response spectra defined in the current seismic codes (given a country map and corner period depending on soil condition) is based on this approach. Conditional mean spectrum is also a method to define target hazard spectrum based on condition on occurrence of an expected spectral acceleration value at the period of interest [Baker, 2011]. It is a site specific seismic hazard analysis by directly considering the fundamental period and higher mod periods of the building, and elongation of the fundamental period because of inelastic behavior of the structure.

The amplitude scaling procedure is a method that selected ground motion time series are amplified by a constant scale factor in order to match time series to target

response spectrum in specified a period range. For example in ASCE-SEI 7-10 for three dimensional analysis, if the scaling procedure is employed, the obtained average of the SRSS spectrum by using all of the scaled horizontal time series pairs must not fall below the corresponding ordinate of the selected target hazard spectrum in the period range between $0.2T$ and $1.5T$ where T is fundamental period of the building. On the contrary, spectral matching is a method based on modification of the frequency content of the selected ground motion time series so as to match the initial response spectrum by using selected time series with defined target hazard spectrum. According to report of NEHRP Seismic Design Technical Brief no: 4 and Moehle (2012), a tall building is a long-period structure, hence the effect of higher modes on the behavior of structure is important, thus using the scaling procedure by considering uniform hazard spectrum results in unexpected incorrect analysis results since using a high constant scaling factor causes unrealistic short period components in the scaled ground motions. Instead of this, using spectral matching procedure may be more appropriate to capture realistic results [Moehle, 2005]. Baker (2011) also has stated that uniform hazard spectrum is not a suitable target spectrum for matching ground motion time series and proposed to employ conditional mean spectrum for these problems. Tall buildings are special structures thus scaling procedure with conditional mean spectrum from site-specific seismic hazard analysis generally can be done by considering all of the properties of site conditions and the fundamental periods of the structure. This method is being widely employing for tall buildings.

2.8 Description of Performance Levels and Acceptance Criteria for Tall Buildings

Current seismic codes (especially seismic evaluation and retrofit of existing buildings) and alternative non-prescriptive consensus seismic design guidelines employ performance based design approach to understand building behavior under expected seismic hazard levels. Accordingly, two or more performance levels can be defined for a building when subjected to different levels of ground motion intensity since the effects of moderate earthquake on the structure and the consequent member damages are different from the effects of strong earthquakes. In addition, varied

performance levels can be implemented for different structures when subjected to the same earthquake excitation since the expected seismic performance of structures are related to structural types and the usage purpose of structure. On the other hand, current seismic codes and alternative non-prescriptive consensus seismic design guidelines use different performance parameters to describe acceptance criteria (limit states) for members and global behavior of structure to evaluate seismic performance. For example, whereas TEC-2007 utilizes strain limit values (states) to check the condition of damage of structural members (ductile members), ASCE-41-13 employs plastic rotation limit values to check the damage performance of structural members. In addition, while interstory drift ratio which is a building behavior limit for overall performance is not used for conventional regular buildings, it is a quite favorable measure for evaluating seismic performance of tall buildings when nonlinear analysis is utilized. In this part, firstly description of performance levels and acceptance criteria according to TEC-2007 and ASCE-41-13 are explained briefly. Then performance levels and acceptance criteria for tall buildings are described in accordance with non-prescriptive consensus seismic design guidelines for tall buildings.

2.8.1 Summary of Performance Levels and Acceptance Criteria According to TEC-2007

2.8.1.1 Description of Performance Levels

In the prescriptive provision about seismic evaluation and retrofit of existing buildings in TEC-2007 part 7, two steps have been made to evaluate seismic performance of a structure. Firstly, damage of each element under the expected earthquake excitation have been assessed to specify each member performance level in accordance with the condition of upper bound of concrete compressive strain and reinforcement tensile stain of the most critical section of member. TEC-2007 has described three limit states and four performance levels for a ductile member, which is illustrated in Figure 2.32. After that, the seismic performance level of buildings is specified with respect to the damage level of each member and distribution of shear force that come out under the expected earthquake excitation between members.

Four performance levels have been defined for buildings depending on building types, the usage purpose of the building and the probability of occurrence of earthquakes. These are immediate occupancy (IO), life safety (LS), pre-collapse (PC) and collapse (CL) performance level. Table 2.3 gives minimum building performance objectives under different expected earthquake levels.

Table 2.3. Minimum building performance objectives expected for different earthquake levels according to TEC-2007

The type of buildings and the usage purpose	Probability for the earthquake to be exceeded		
	50 % in 50 years	10 % in 50 years	2 % in 50 years
The buildings that should be used after earthquakes: Hospitals, health facilities, fire stations, communications and energy facilities, transportation stations, provincial or district administrative bodies, disaster management centers etc.	-	IO	LS
The buildings that people occupy for a long time period: Schools, accommodations, dormitories, pensions, military posts, prisons, museums...	-	IO	LS
The buildings that people visit densely and stay in for a short time period: cinema, theatre and concert halls, culture centers, sports facilities	IO	LS	-
Buildings containing hazardous materials: The buildings containing toxic, flammable and explosive materials and the buildings in which the mentioned materials are stored.	-	IO	PC
Other buildings: The buildings that does not fit the definitions given above (houses, offices, hotel, tourist facilities, industrial buildings, etc.)	-	LS	-

IO: Immediate occupancy, LS: Life safety, PC: Pre-collapse

2.8.1.2 *Damage Limits (acceptance criteria) for reinforced concrete members*

According to the procedure of TEC-2007, damage limit of the most critical section for each structural member must be defined in compliance with the prescriptive provision in Section 7.6. TEC-2007 have described three limit conditions and four performance levels for a ductile member depending on the upper bound of concrete compressive strain and reinforcement tensile stain of the most critical section that are anticipated to arisen from under the effect of the earthquakes. Limit states for concrete and tension steel are explained below if nonlinear analysis is employed:

- Minimum damage limit (MN): Minimum damage level is defined when the damage level of section is below or at the onset of plasticity. The upper bound strain level of concrete and reinforcement steel is described as below:

$$(\epsilon_{cu})_{MN} = 0.0035 \quad (\epsilon_s)_{MN} = 0.01 \quad (2.19)$$

- Safety damage Limit (GV): it is the limit if the damage level of section goes beyond the elastic limit but the section must have sufficient strength and deformation capacity to continue withstanding the effects of external force safely. The upper bound strain level of concrete and reinforcement steel is described as below:

$$(\epsilon_{cg})_{GV} = 0.0035 + 0.01 * (\rho_s / \rho_{sm}) \leq 0.0135 \quad (\epsilon_s)_{GV} = 0.04 \quad (2.20)$$

- Collapsing damage limit (GC): it is the limit if the damage level reaches incipient collapse or initiation of the significant strength loss. The upper bound strain level of concrete and reinforcement steel is described as below:

$$(\epsilon_{cg})_{GC} = 0.004 + 0.014 * (\rho_s / \rho_{sm}) \leq 0.018 \quad (\epsilon_s)_{GV} = 0.06 \quad (2.21)$$

Damage limits in a cross section which is defined above and section damage regions are illustrated in Figure 2.30. As it can be seen, if the damage level of the most critical section of the member does not reach MN, it is located in “Minimum

Damage Region”, if the damage level of the most critical section of the member is located between MN and GV, it is in the “Significant Damage Region”, if the damage level of the most critical section of the member is located between GV and GÇ it is in the “Severe Damage Region”, and if the damage level of the most critical section of the member goes beyond GÇ it is in the “Collapsing Region”.

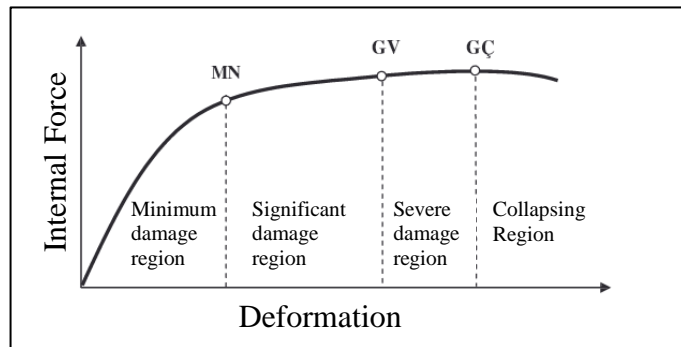


Figure 2.32. Damage limits and region for reinforced concrete section according to TEC-2007

2.8.2 Summary of Performance Levels and Acceptance Criteria According to ASCE-SEI 41-13

Unlike TEC-2007, ASCE-SEI 41-13 evaluates the seismic performance of structure only at the member level. Six different performance levels and two intermediate structural performance ranges have been defined for structure but three performance levels have been specified for structural ductile members which is illustrated in Figure 2.33. These are Collapse Prevention (CP), Life Safety (LS) and Immediate Occupancy (IQ) performance levels. In addition to key parameters (a, b and c) of the component to define backbone, ASCE-41-13 gives limit states of each performance level (IO, LS and CP) for each structural member (Table 2.4, 2.5 and 2.6). Here, a and b are plastic deformation capacity and c is residual strength of the component after sudden strength loss from C to D. These parameters are needed to define the backbone curve. a, b, and c can be also obtained from analytical procedures verified by experimental evidence. The detailed information about acceptance criteria for different members is available in the ASCE-41-13 documents. As a summary, to evaluate seismic performance of a structure, obtained damage (plastic rotation) of

each element under the expected earthquake excitation have been compared with specified performance levels. If each member satisfies the expected performance level, then the seismic performance level of the structure is acceptable.

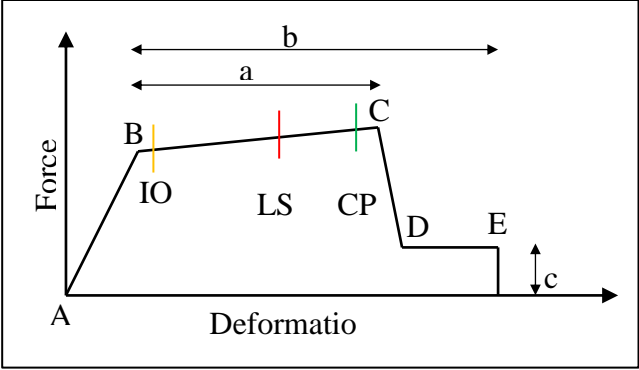


Figure 2.33. Generalized force-deformation relation for reinforced concrete flexural elements or components with performance levels

Table 2.4. Modeling Parameters and Numerical Acceptance Criteria for Nonlinear Procedures—Reinforced Concrete Beams According to ASCE 41-13

Conditions			Modeling Parameters ^a			Acceptance Criteria ^a		
			Plastic Rotations Angle (radians)		Residual Strength Ratio	Plastic Rotations Angle (radians)		
			a	b		Performance Level		
					IO	LS	CP	
Condition i. Beams controlled by flexure ^b								
$\rho - \rho'$	Transverse reinforcement ^c	$\frac{V}{b_w d \sqrt{f'_c}}$ ^d						
ρ_{min}								
≤ 0.0	C	≤ 3 (0.25)	0.025	0.05	0.2	0.010	0.025	0.05
≤ 0.0	C	≥ 6 (0.5)	0.02	0.04	0.2	0.005	0.02	0.04
≥ 0.5	C	≤ 3 (0.25)	0.02	0.03	0.2	0.005	0.02	0.03
≥ 0.5	C	≥ 6 (0.5)	0.015	0.02	0.2	0.005	0.015	0.02
≤ 0.0	NC	≤ 3 (0.25)	0.02	0.03	0.2	0.005	0.02	0.03
≤ 0.0	NC	≥ 6 (0.5)	0.01	0.015	0.2	0.0015	0.01	0.015
≥ 0.5	NC	≤ 3 (0.25)	0.01	0.015	0.2	0.005	0.01	0.015
≥ 0.5	NC	≥ 6 (0.5)	0.005	0.01	0.2	0.0015	0.005	0.01
Condition ii. Beams controlled by shear ^b								
Stirrup spacing $\leq d/2$			0.0030	0.02	0.2	0.0015	0.01	0.02
Stirrup spacing $> d/2$			0.0030	0.01	0.2	0.0015	0.005	0.01
Condition iii. Beams controlled by inadequate development or splicing along the span ^b								
Stirrup spacing $\leq d/2$			0.0030	0.02	0.0	0.0015	0.01	0.02
Stirrup spacing $> d/2$			0.0030	0.01	0.0	0.0015	0.005	0.01
Condition iv. Beams controlled by inadequate embedment into beam-column joint ^b			0.015	0.03	0.2	0.01	0.02	0.03

NOTE: f'_c in lb/in^2 (MPa) units.

^a Values between those listed in the table should be determined by linear interpolation.

^b Where more than one of conditions i, ii, iii, and iv occur for a given component, use the minimum appropriate numerical value from the table.

^c “C” and “NC” are abbreviations for conforming and nonconforming transverse reinforcement, respectively. Transverse reinforcement is conforming if, within the flexural plastic hinge region, hoops are spaced at $\leq d/3$, and if, for components of moderate and high ductility demand, the strength provided by the hoops (V_s) is at least 3/4 of the design shear. Otherwise, the transverse reinforcement is considered nonconforming.

^d V is the design shear force from NSP or NDP.

Table 2.5. Modeling Parameters and Numerical Acceptance Criteria for Nonlinear Procedures—Reinforced Concrete Columns According to ASCE 41-13

Conditions		Modeling Parameters ^a			Acceptance Criteria ^a			
		Plastic Rotations Angle (radians)		Residual Strength Ratio	Plastic Rotations Angle (radians)			
		a	b		Performance Level			
				IO	LS	CP		
Condition i. ^b								
$\frac{P}{A_g f_c'}$	$\rho = \frac{A_s}{b_w s}$							
≤ 0.1	≥ 0.006	0.035	0.060	0.2	0.005	0.045	0.060	
≥ 0.6	≥ 0.006	0.010	0.010	0.0	0.003	0.009	0.010	
≤ 0.1	$= 0.002$	0.027	0.034	0.2	0.005	0.027	0.034	
≥ 0.6	$= 0.002$	0.005	0.005	0.0	0.002	0.004	0.005	
Condition ii. ^b								
$\frac{P}{A_g f_c'}$	$\rho = \frac{A_s}{b_w s}$	$\frac{V}{b_w d \sqrt{f_c'}}$						
≤ 0.1	≥ 0.006	≤ 3 (0.25)	0.032	0.060	0.2	0.005	0.045	0.060
≤ 0.1	≥ 0.006	≥ 6 (0.5)	0.025	0.060	0.2	0.005	0.045	0.060
≥ 0.6	≥ 0.006	≤ 3 (0.25)	0.010	0.010	0.0	0.003	0.009	0.010
≥ 0.6	≥ 0.006	≥ 6 (0.5)	0.008	0.008	0.0	0.003	0.007	0.008
≤ 0.1	≤ 0.0005	≤ 3 (0.25)	0.012	0.012	0.2	0.005	0.010	0.012
≤ 0.1	≤ 0.0005	≥ 6 (0.5)	0.006	0.006	0.2	0.004	0.005	0.006
≥ 0.6	≤ 0.0005	≤ 3 (0.25)	0.004	0.004	0.0	0.002	0.003	0.004
≥ 0.6	≤ 0.0005	≥ 6 (0.5)	0.0	0.0	0.0	0.0	0.0	0.0
Condition iii. ^b								
$\frac{P}{A_g f_c'}$	$\rho = \frac{A_s}{b_w s}$							
≤ 0.1	≥ 0.006		0.0	0.060	0.0	0.0	0.045	0.060
≥ 0.6	≥ 0.006		0.0	0.008	0.0	0.0	0.007	0.008
≤ 0.1	≤ 0.0005		0.0	0.006	0.0	0.0	0.005	0.006
≥ 0.6	≤ 0.0005		0.0	0.0	0.0	0.0	0.0	0.0
Condition iv. Columns controlled by inadequate development or splicing along the clear height ^c								
$\frac{P}{A_g f_c'}$	$\rho = \frac{A_s}{b_w s}$							
≤ 0.1	≥ 0.006		0.0	0.060	0.4	0.0	0.045	0.060
≥ 0.6	≥ 0.006		0.0	0.008	0.4	0.0	0.007	0.008
≤ 0.1	≤ 0.0005		0.0	0.006	0.2	0.0	0.005	0.006
≥ 0.6	≤ 0.0005		0.0	0.0	0.0	0.0	0.0	0.0

NOTE: f_c' is in lb/in² (MPa) units.

^a Values between those listed in the table should be determined by linear interpolation.

^b Refer to Section 10.4.2.2.2 for definition of conditions i, ii, and iii. Columns are considered to be controlled by inadequate development or splices where the calculated steel stress at the splice exceeds the steel stress specified by Eq. (10-2). Where more than one of conditions i, ii, iii, and iv occurs for a given component, use the minimum appropriate numerical value from the table.

^c Where $P > 0.7A_g f_c'$, the plastic rotation angles should be taken as zero for all performance levels unless the column has transverse reinforcement consisting of hoops with 135-degree hooks spaced at $\leq d/3$ and the strength provided by the hoops (V_s) is at least 3/4 of the design shear. Axial load P should be based on the maximum expected axial loads caused by gravity and earthquake loads.

^d V is the design shear force from NSP or NDP.

Table 2.6. Modeling Parameters and Numerical Acceptance Criteria for Nonlinear Procedures—R/C Shear Walls and Associated Components Controlled by Flexure According to ASCE 41-13

Conditions			Plastic Hinge Rotation (radians)		Residual Strength Ratio	Acceptable Plastic Hinge Rotation* (radians)			
			a	b		Performance Level			
					c	IO	LS	CP	
i. Shear walls and wall segments			Confined Boundary ^b		0.015				
$\frac{(A_t - A_t')f_y + P}{t_w w f_c'}$	$\frac{V}{t_w w \sqrt{f_c'}}$								
≤0.1	≤4	Yes	0.010	0.020	0.75	0.005	0.015	0.020	
≤0.1	≥6	Yes	0.009	0.015	0.40	0.004	0.010	0.015	
≥0.25	≤4	Yes	0.005	0.012	0.60	0.003	0.009	0.012	
≥0.25	≥6	Yes	0.008	0.010	0.30	0.0015	0.005	0.010	
≤0.1	≤4	No	0.006	0.015	0.60	0.002	0.008	0.015	
≤0.1	≥6	No	0.003	0.010	0.30	0.002	0.006	0.010	
≥0.25	≤4	No	0.002	0.005	0.25	0.001	0.003	0.005	
≥0.25	≥6	No	0.002	0.004	0.20	0.001	0.002	0.004	
ii. Shear wall coupling beams ^c									
Longitudinal reinforcement and transverse reinforcement ^d			$\frac{V}{t_w w \sqrt{f_c'}}$	0.050					
Conventional longitudinal reinforcement with conforming transverse reinforcement			≤3	0.025	0.040	0.75	0.010	0.025	0.050
			≥6	0.020	0.035	0.50	0.005	0.020	0.040
Conventional longitudinal reinforcement with nonconforming transverse reinforcement			≤3	0.020	0.025	0.50	0.006	0.020	0.035
			≥6	0.010	0.050	0.25	0.005	0.010	0.025
Diagonal reinforcement			NA	0.030	0.050	0.80	0.006	0.030	0.050

^a Linear interpolation between values listed in the table shall be permitted.

^b A boundary element shall be considered confined where transverse reinforcement exceeds 75% of the requirements given in ACI 318 and spacing of transverse reinforcement does not exceed $8d_b$. It shall be permitted to take modeling parameters and acceptance criteria as 80% of confined values where boundary elements have at least 50% of the requirements given in ACI 318 and spacing of transverse reinforcement does not exceed $8d_b$. Otherwise, boundary elements shall be considered not confined.

^c For coupling beams spanning <8 ft 0in., with bottom reinforcement continuous into the supporting walls, acceptance criteria values shall be permitted to be doubled for LS and CP performance.

^d Conventional longitudinal reinforcement consists of top and bottom steel parallel to the longitudinal axis of the coupling beam. Conforming transverse reinforcement consists of (a) closed stirrups over the entire length of the coupling beam at a spacing $\leq d/3$, and (b) strength of closed stirrups $V_s \geq 3/4$ of required shear strength of the coupling beam.

2.8.3 Performance Levels and Acceptance Criteria for Tall Buildings

2.8.3.1 Performance Levels

Non-prescriptive seismic guidelines for tall buildings except IMM define two performance levels for tall buildings. These are service level and collapse prevention level respectively. Service level evaluation stage is to check the structure under high probability of occurrence (frequent) earthquakes with return periods of 43 years, (50% probability of exceedance in 30 years). At this stage, it is generally desirable that the tall buildings remain essentially elastic. It is allowed a small post-yield deformation for ductile members but a permanent damage is not appreciated. Collapse prevention evaluation stage is to check the structure under the low probability of occurrence earthquakes with return periods of 2475 years (50% probability of exceedance in 2 years). It is desired to maintain their stability under expected strong earthquakes, namely collapse of the structures is undesirable. Instead of these, limited damage in specified locations and up to a specific stress value is permitted for reasonable designs.

Table 2.7. Expected minimum performance regions for different earthquake levels

The usage purpose	Probability of being exceeded		
	50 % in 50 years	10 % in 50 years	2 % in 50 years
Ordinary tall buildings (residences, offices, hotels)	Minimum damage region (IO)	Significant damage region (LS)	Severe damage region (CP)
Special tall buildings (Schools, Hospitals, health facilities)	-	Minimum damage region (IO)	Significant damage region (LS)

IMM has been defined three performance levels (IO, LS and CP) depending on usage purpose. Similar damage limit states for ductile member in TEC-2007, which is explained in the previous part, are used to evaluate seismic performance of tall

buildings. Expected minimum performance regions for different earthquake level are presented in Table 2.7.

2.8.3.2 Acceptance Criteria at the Component Level

As explained above, alternative non-prescriptive seismic guidelines for tall buildings may be used as the acceptance criteria in ASCE 41-13 and IMM but these acceptance criteria are inadequate for seismic performance of tall buildings since the seismic demands of tall buildings is different from conventional regular buildings. Accordingly, some additional acceptance criteria have been described for tall buildings in alternative non-prescriptive seismic guidelines for tall buildings. For example, there is not any provision about maximum transient drift ratio and residual drift ratio limit when nonlinear analysis is employed to evaluate the seismic performance of a structure according to TEC-2007 and ASCE-41-13. In addition, seismic performance of tall buildings is based on expected material properties. Accordingly, limit states of some components (force controlled members) need revision.

Table 2.8. Typical Classification of Component Actions According to LATBSDC 2015

Component	Seismic Action	Classification	Criticality
Below grade perimeter walls	Flexure	Force controlled	Non-Critical
	Shear	Force controlled	Critical
Parking ramp walls	Flexure	Deformation Controlled	N/A
	Shear	Force controlled	Critical
Podium walls	Flexure	Deformation Controlled	N/A
	Shear	Force controlled	Critical
Tower core walls (over their entire height)	Flexure	Deformation Controlled	N/A
	Shear	Force controlled	Critical
Core wall coupling beams	Shear /Flexure	Deformation Controlled	N/A
Floor slabs	Out of plane flexure around supports	Deformation Controlled	N/A
Diaphragms with major shear forces	Flexure	Force controlled	Non-Critical
	Shear	Force controlled	Critical
Gravity columns	Flexure	Force controlled	Critical
Foundation	Flexure	Force controlled	Non-Critical
	Shear	Force controlled	Critical

Before starting analysis and assessment, all structural element actions can be categorized as either force-controlled or deformation-controlled and if expected action of component is force-controlled, then the action can be categorized as either critical or non-critical action for a good representation. LATBSDC (2015) gives a table to classify action of components, which is shown in Table 2.8. PEER and LATBSDC (using a similar approach) define acceptance criteria at the components for collapse prevention level.

2.8.3.2.1 Force-Controlled Actions

If expected governing and controlling type of action to be captured during analysis for components is force and if a structure loses its structural stability under lateral and gravity loads because of this force, then these types of component are defined as force-controlled components. Heavy damage of these components results in failure of the structure. Accordingly, these types of component must be controlled by their strength capacity. Critical force controlled components are shown in Table 2.8. For this purpose, PEER and LATBSDC suggest following acceptance criteria for components.

$$F_{uc} \leq \kappa_i * \phi * F_{n,e} \quad (2.22)$$

F_{uc} = 1.3~1.5 times the mean value of demand from analyses (minimum suite of seven ground motions). PEER proposes to use 1.3 if the standard deviation of obtained response results is less than 1.2 times the mean value, otherwise, 1.5 is suggested. LATBSDC propose to use 1.5. Here,

$F_{n,e}$ = nominal strength should be calculated from applicable codes or guidelines by using expected material properties.

ϕ = strength reduction factor

κ_i = 0.8~1.0 risk reduction factor depending on seismic risk category (given Table in LATBSDC 2015)

A ductile shear wall or column design is achieved when tension reinforcement yields before concrete reaches the capacity of compressive strain. As it can be illustrated in the parametric study for shear walls in Figure 2.29, as the axial load on the shear wall increases, ductility reduces. Accordingly, axial load on the shear walls and columns remain below the balance point for a ductile response of high rise structures in regions of high seismicity. The proposed limit states for shear walls and columns are:

- Whereas LATBSDC suggests limiting the axial load demand with $0.25 * f'_{ex}A_g$ on the shear wall under applicable load combinations when subjected to design earthquake level (DE), PEER-TBI suggests $0.3 * f'_{ex}A_g$ but under the maximum considered earthquake (MCE_R).

$$\frac{N_d}{f'_{ex}A_g} \leq 0.25 \quad (\text{under DE})$$

$$\frac{N_d}{f'_{ex}A_g} \leq 0.3 \quad (\text{under } MCE_R)$$

- LATBSDC suggests limiting the axial load demand on columns with $0.4 * f'_{ex}A_g$ under applicable load combinations when subjected to maximum considered earthquake (MCE_R)

$$\frac{N_d}{f'_{ex}A_g} \leq 0.4 \quad (\text{under } MCE_R)$$

Seismic shear demand on the shear wall is also limited for a good design. Hence;

- PEER-TBI proposes propose these upper limits for shear strength of shear walls

$$0.166\sqrt{f'_{ex}} \leq \tau \leq 0.25\sqrt{f'_{ex}} \quad (\text{under service level earthquake})$$

- PEER-TBI, LATBSDC and ACI318 propose these upper limits for shear strength of shear walls under any earthquake excitation.

$$\tau \leq 0.664\sqrt{f'_{ex}} \quad \text{for walls sharing lateral load}$$

$$\tau \leq 0.83\sqrt{f'_{ex}} \quad \text{for single wall}$$

N_d : The mean value of axial force demand from analyses (N)

f'_{ex} : Expected compressive strength of concrete (MPa)

τ : The mean value of shear strength demand from analyses (MPa)

A_g : Gross area of concrete section (mm^2)

2.8.3.2.2 Non – Critical Force Controlled Actions

If expected governing and controlling type of action to be captured during analysis for components is force and if a structure does not lose its structural stability under lateral and gravity loads because of this force, then these types of component are defined as non-critical force-controlled components. These types of components must be also controlled by their strength capacity. For this purpose PEER-TBI and LATBSDC propose the approach below.

$$F_u \leq \kappa_i * \phi * F_{n,e} \tag{2.23}$$

F_u = the mean value of demand from analyses (minimum suite seven ground motions).

$F_{n,e}$ = nominal strength should be calculated from applicable codes or guidelines by using expected material properties.

ϕ = strength reduction factor

κ_i = 0.8~1.0 risk reduction factor depending on seismic risk category (given Table in LATBSDC 2015)

2.8.3.2.3 Deformation controlled Actions

The seismic performance of each deformation controlled action should be compared with the demand of components which are taken as the mean values of analysis results with limit states of the components. As explained above, the limit states given by ASCE-41-13 or TEC-2007 can be used.

ASCE-SEI 41-13 (2013), PEER-TBI (2010) and ATC-72 (2010) also suggests maximum suitable strain limits for concrete and reinforcement steel, which are given below:

Compressive strain of unconfined concrete under the pure compression ≤ 0.002

Compressive strain of other concrete conditions ≤ 0.005

Compressive strain of reinforcement steel ≤ 0.02

Tensile strain of reinforcement steel ≤ 0.05

2.8.3.3 Acceptance Criteria for the Overall Building Behavior

According to PEER-TBI and LATBSDC, overall building acceptance criteria for tall buildings involve maximum transient drift, residual drift and loss of story strength. Although maximum transient drift is employed both for service level evaluation and collapse prevention levels, residual drift and loss of story strength is only employed for collapse prevention level. As explained earlier, if NLTHA is employed for service level evaluation, it is generally proposed to use minimum three suite pairs of ground motion time series. If less than seven suite pairs are used, then the maximum response values should be employed for assessment, otherwise, the average of maximum values of each analysis should be employed for the evaluation of structure. On the other hand, if NLTHA is employed for collapse prevention level, it is proposed to use minimum seven pairs of ground motion time series. The average and maximum interstory transient drift ratio values of each analysis should be employed for assessment of collapse prevention level. The following limit states for overall building behavior are proposed in order to check the performance of structure with respect to determined performance levels:

For service level evaluation stage:

- If less than seven pairs of ground motion are used, $\delta_{\max} \leq 0.5 \%$
- If seven or more than seven pairs of ground motion are used, $\delta_{\text{ave}} \leq 0.5 \%$

For collapse prevention level evaluation stage

- It is not proposed to use less than seven pairs of ground motions
- If seven or more than seven pairs of ground motion are used, $\delta_{\text{ave}} \leq 3.0 \%$
- If seven or more than seven pairs of ground motion are used, $\delta_{\max} \leq 4.5 \%$
- If seven or more than seven pairs of ground motion are used, $\delta_{\text{res/ave}} \leq 1.0\%$

- If seven or more than seven pairs of ground motion are used, $\delta_{\text{res}/\text{max}} \leq 1.5 \%$
- $\Sigma X_{\text{fi}} \geq 0.8 * \Sigma X_{\text{in}}$

δ_{max} : the absolute value of the maximum transient drift ratio in each story from the suite pairs of ground motion

δ_{ave} : the absolute value of the average transient drift ratio in each story from the suite pairs of ground motion

$\delta_{\text{res}/\text{ave}}$: the absolute value of the average residual drift ratio in each story from the suite pairs of ground motion

$\delta_{\text{res}/\text{max}}$: the absolute value of the max residual drift ratio in each story from the suite pairs of ground motion

ΣX_{in} : initial total story strength

ΣX_{fi} : final total story strength

CHAPTER 3

CASE STUDY

3.1 Introduction

Performance based seismic design of tall buildings is widely carried out by using nonlinear dynamic analysis of a three dimensional analytical (computer) model of the buildings subjected to two horizontal earthquake components (vertical component is rarely used) simultaneously in order to simulate the seismic behavior of buildings rationally. Nonlinear mathematical model of the structure incorporates a number of assumptions, from the selection of idealized inelastic component types for each structural member to the estimation of gravity and seismic loads in order to capture the expected dynamic behavior of structures. All of these effects on the behavior of tall buildings have been explained elaborately in the previous Chapters. In this part, a reinforced concrete unsymmetrical-plan tall building is designed according to the Turkish Seismic Code under the design earthquake, followed by two performance levels (service level and collapse prevention level). NLTHA is employed by using pairs of ground motion suites and checking the results in compliance with the determined target performance levels. Several performance targets have not been satisfied, hence preliminary design has been revised. The case study is re-analyzed and evaluated to achieve the particular objectives of performance evaluation levels. The results for both of the initial and revised design cases are presented separately.

3.2 General Properties of the Case Study Building

The case study is a reinforced concrete unsymmetrical-plan tall building with 34 stories and 115 meter height. There are no basement ground levels, and story levels start from the ground level but the first two stories has a larger floor plan area but there are no additional shear walls in the first two stories. Typical floor plan, which is 19 m by 48.25 m, and 3D view of the building, is shown in Figure 3.1. As it can be seen, the shape of the buildings changes and becomes smaller in the upper stories.

The story heights are 4 m for the first two stories and the top two stories, and 3.3 m for all other stories. This building is a real residential project which was built in Ankara located in seismic zone 4 but it is redesigned as if it is located in seismic zone 1 for this study.

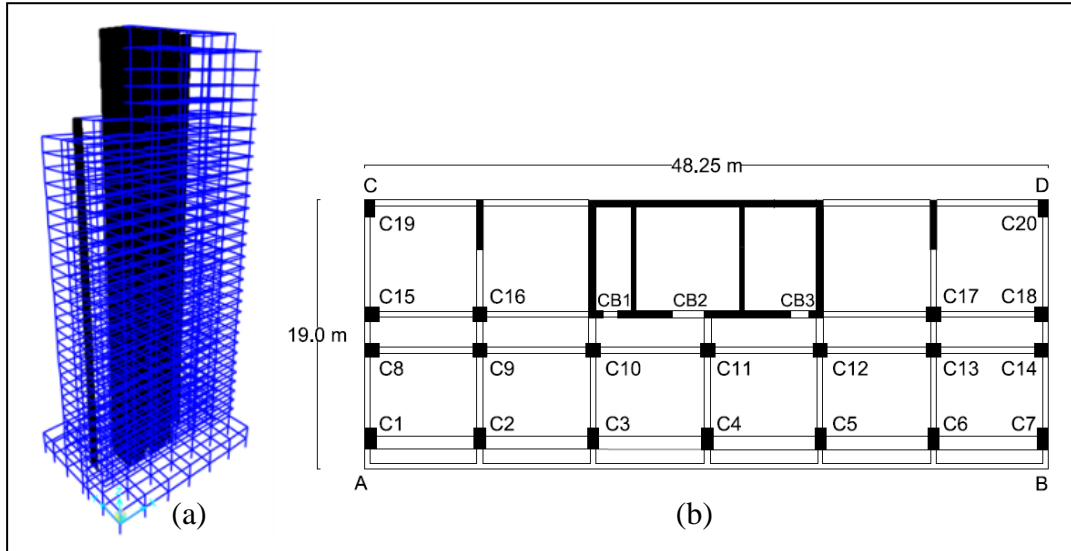


Figure 3.1. (a) 3-D view and (b) typical floor plan of the building

The properties selected at the design stage are listed below. The linear elastic spectrum and inelastic design spectrum for design per TEC-2007 is presented in Figure 3.2

Seismic Zone 1: $A_0 = 0.4$

Building importance factor: $I = 1$

Earthquake response reduction factor: $R_x = R_y = 6$

Soil Type: Z2, $T_a = 0.15$ sec and $T_b = 0.4$ sec

Live load participation factor: $n = 0.3$

Characteristic strength of concrete (C45): $f_{ck} = 45$ MPa

Characteristic strength of reinforcement steel (S420): $f_{yk} = 420$ MPa

Then linear spectrum analysis has been employed by SAP-2000 V15 software and internal forces are obtained for critical sections. Finally the selected critical sections have been designed according to TS 500-2000 and TEC-2007 by considering

capacity design principles. The design approach of the critical sections has not been mentioned there but all of the critical section design details have been presented in the appendix part.

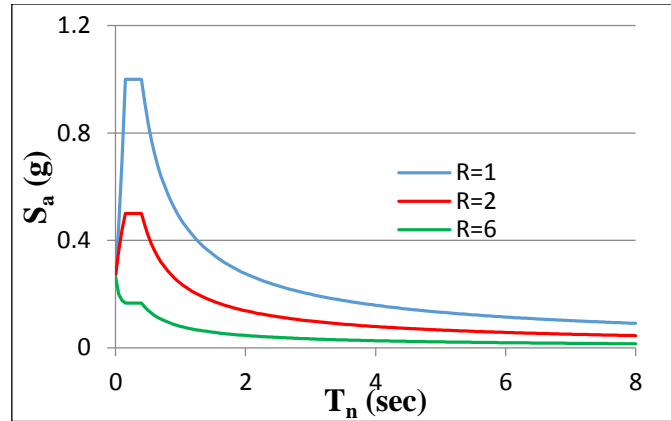


Figure 3.2. TEC-2007 design and elastic spectrum

The slab is selected to be composed of joists. The direction of joist beams is extended along the longitudinal direction of structure.

Member dimensions for beams are $400 \times 600 \text{ mm}^2$ for all stories except A-B axis beams which are $1000 \times 320 \text{ mm}^2$. In spite of using similar section size for beams, a number of different beams which have different longitudinal reinforcement and shear details have been employed over the buildings. Design detail of selected beam sections are given in the appendix part. The columns are labelled from C1 to C19 which are presented in Figure 3.1. The corner column dimensions (C1, C7, C19 and C20) are $800 \times 1500 \text{ mm}^2$ throughout the entire height of the building. The dimensions of interior columns (from C7 to C17) are $1000 \times 1000 \text{ mm}^2$ throughout the height of building. The dimensions of columns from C2 to C7 are $800 \times 1500 \text{ mm}^2$ in the first six floors. After that the dimensions of the columns have reduced to $700 \times 1400 \text{ mm}^2$ until the 29 floor and to $700 \times 1200 \text{ mm}^2$ expect C2 for the four upper stories. The minimum longitudinal reinforcement provision and/or the axial force level control the behavior of all columns. Design details of selected columns are presented in the appendix part.

The diagonally reinforced concrete coupling beams of the building are labeled CB1, CB2 and CB3 respectively. The dimension of coupling beams is presented in Table 3.1.

Table 3.1. Section properties of the coupling beams (l_v/h)

CB1 (cm)	CB2 (cm)	CB3(cm)
120*50	260*50	120*50

Shear walls of building are labeled from SW1 to SW9 which are presented in Figure 3.3. The dimensions of shear walls are presented in Table 3.2. A design detail of selected shear walls is presented in the appendix.

Table 3.2. The section dimensions of shear walls (centimeters)

SW1/SW7	SW2/SW6	SW3	SW4	SW5	SW8/SW9
50*350	50*800	50*1600	50*500	50*600	30*800

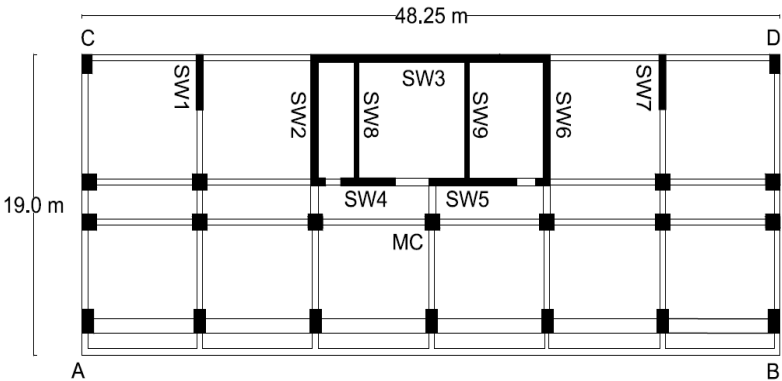


Figure 3.3. Labels of shear walls

3.2.1 Eigenvalue (Free Vibration) Analysis

Free vibration properties of the building are obtained from the elastic model using un-cracked section properties. Eigenvalue analysis results and the effective modal mass results for the first twelve modes are presented in Table 3.3. Figures 3.4 to 3.7 illustrate the first four modal vectors of the building with respect to normalized mass.

Table 3.3. Free vibration properties of the building for the first twelve modes

Mode	T_n (sn)	M_x^* (ton)	M_y^* (ton)	$M_x^*/\sum M_x$	$\sum M_x$	$M_y^*/\sum M_y$	$\sum M_y$
1	3.08	359.3	22746.3	0.010	0.010	0.602	0.602
2	2.73	16125.5	1099.1	0.426	0.436	0.029	0.631
3	1.43	8271.8	237.8	0.219	0.655	0.006	0.637
4	0.86	1977.4	1734.4	0.052	0.707	0.046	0.683
5	0.66	1195.4	4581.1	0.032	0.739	0.121	0.804
6	0.48	2.5	77.7	0.000	0.739	0.002	0.806
7	0.35	4017.3	377.4	0.106	0.845	0.010	0.816
8	0.31	542.2	1509.5	0.014	0.859	0.040	0.856
9	0.28	1.9	470.7	0.000	0.859	0.012	0.868
10	0.21	393.6	103.8	0.010	0.870	0.003	0.871
11	0.18	472.5	1032.4	0.012	0.882	0.027	0.898
12	0.16	686.8	159.7	0.018	0.900	0.004	0.903

T_n : Natural Period

M_x^* , M_y^* : Effective modal mass for x (the long side of structure) and y (the short side of structure) direction respectively.

$M_x^*/\sum M_x$, $M_y^*/\sum M_y$: Effective modal mass ratio for x and y directions respectively.

$\sum M_x$, $\sum M_y$: total effective modal mass ratio for x and y directions respectively.

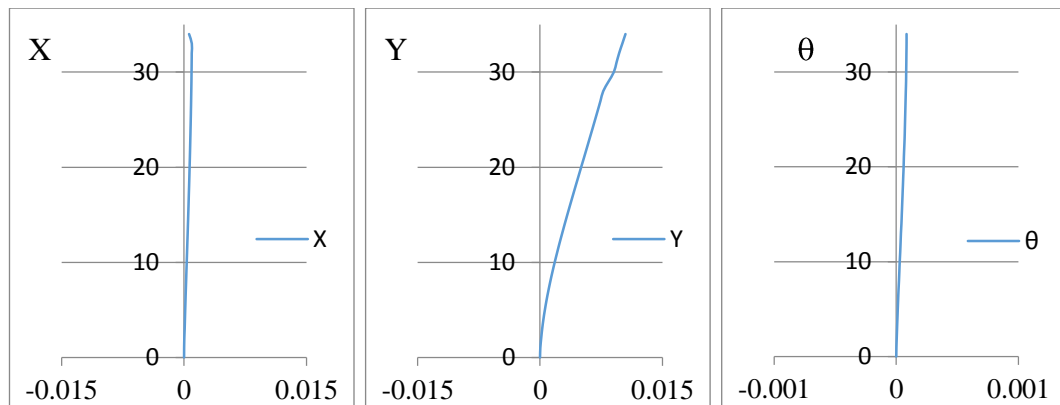


Figure 3.4. The first mode shape ($T_1=3.08$ sec)

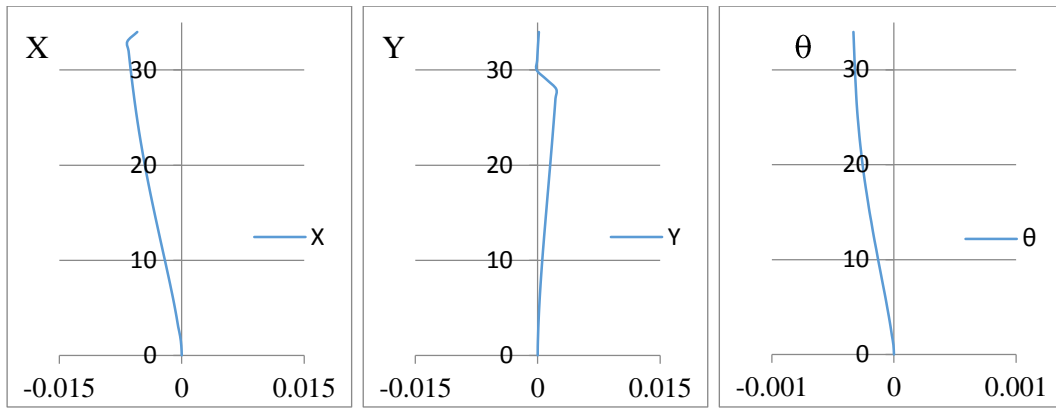


Figure 3.5. The second mode shape ($T_2=2.73$ sec)

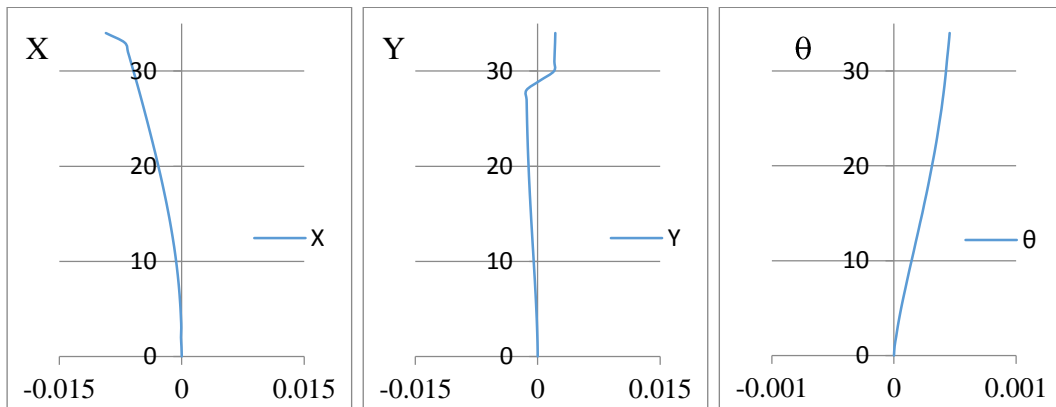


Figure 3.6. The third mode shape ($T_3=1.43$ sec)

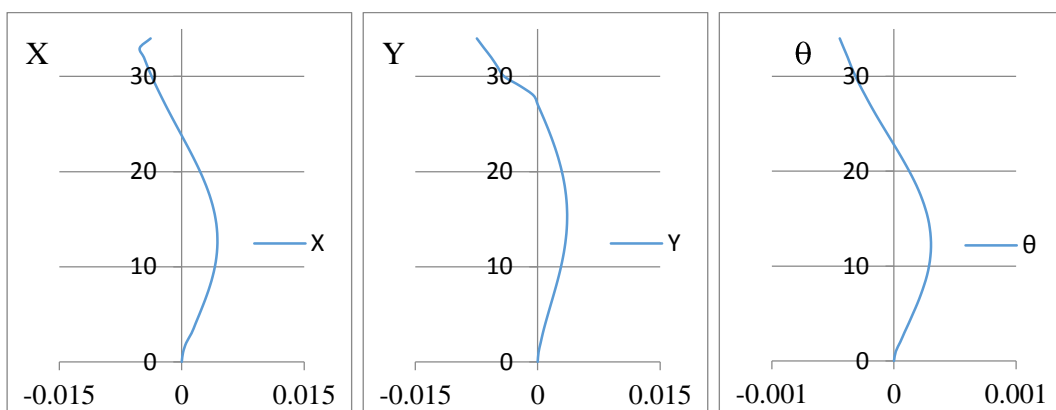


Figure 3.7. The fourth mode shape ($T_4=0.86$ sec)

3.3 Nonlinear Modeling of the Case Study Building

Nonlinear analytical model of the case study building is generated by using the Perform-3D V5 (2011). This is the only available commercially available software which offers a number of nonlinear modeling options for structural members from finite element model (only frames) to fiber model to concentrated plasticity model in order to generate nonlinear modeling by considering cyclic loading effects on response either directly or indirectly. Perform-3D V5 utilizes the event-to-event (load or displacement control) strategy which is accepted as a reliable method for nonlinear analysis. These assumptions explained below are made during nonlinear modeling of the case study.

- Three-stage approach was employed for this case study. In the preliminary stage, the building is designed according to TEC-2007. Then nonlinear time history analysis is employed both for service level evaluation under a suite set of seven service level earthquake (SLE) shakings with a return period of 43 years, and collapse prevention level under a suite set of seven maximum considered earthquake (MCE) ground shakings with a return period of 2475 years. Finally the results have been evaluated in compliance with the pre-determined target performance levels.
- Nonlinear dynamic analysis is based on the expected material properties. For this purpose, expected strengths are taken as $1.17f_y$ for the yield strength of reinforcement steel and $1.3f_c$ for the compressive strength of concrete where f_y and f_c are the characteristic strengths of steel and concrete respectively. The elastic modulus (E) is taken as $5000\sqrt{f'_{exp}}$.
- In the case study, beam frame members are modeled with “plastic zone model” element. No strength deterioration model is utilized. In this regard, plastic hinge lengths which are assumed as one half of the section depth are defined at both ends of all beams. For inelastic beam component properties, bi-linear moment curvature relationships are defined along the hinge lengths by considering the designed section properties of each beam component type,

both for positive and negative actions. For calculating the effective flexural stiffness of quasi-elastic sections, section moment of inertia (I_g) for each beam is reduced by multiplying the gross inertias of beams with 0.7 for service level evaluation and 0.35 for collapse prevention levels. Shear rigidity is taken as GA and G is taken as $0.4E$.

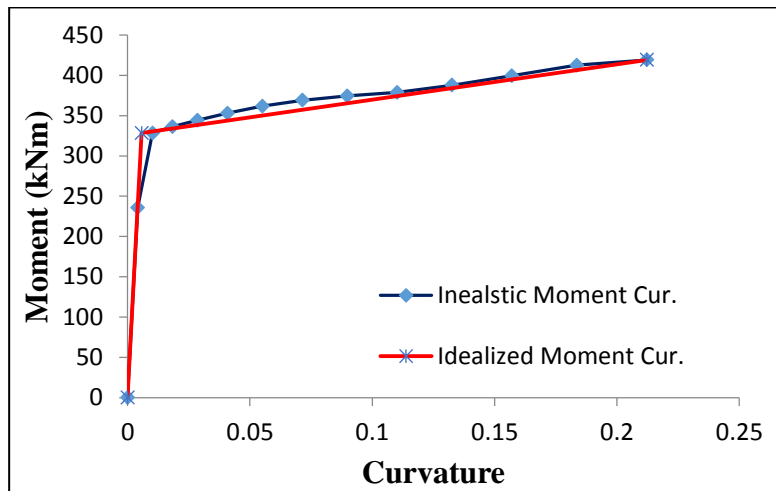


Figure 3.8. Comparison of inelastic and idealized (used) moment curvature relationship

- Column frame members are modeled with P-M-M hinges with interaction surface (considering bi-axial bending and axial force). No strength deterioration model is utilized. In this regard, plastic hinge lengths which are assumed as one half of the section depth are defined at both ends of all columns. For inelastic column component properties, bi-linear moment curvature relationships are defined along the hinge lengths by considering the designed section properties of each column component type. Interaction surface of the each component are also defined. For calculating the effective flexural stiffness of quasi-elastic sections, section moment of inertia (I_g) for each column is reduced by multiplying the gross inertias of beams with 0.9 for service level evaluation and 0.7 for collapse prevention levels. Shear rigidity is taken as GA and G is taken as $0.4E$.

- Reinforced concrete shear wall members are modeled by using inelastic fiber sections over the entire height. As explained in Chapter 2, several important issues must be considered when fiber elements are used for shear walls. These are using a reliable concrete and reinforcement steel material model, choosing a correct number of wall elements, a reliable fiber size for each wall elements section and a plastic hinge (element) length. The effect of these parameters on the behavior of structure and how these parameters should be selected and calibrated was explained elaborately in chapter 2. Accordingly, each shear wall elements is modelled by considering this philosophy in the case study. For this purpose, the following parameters are selected:
 - Saatcioglu-Razvi confined concrete material model (idealized by tri-linear forms) is utilized for the wall boundaries and Saatcioglu-Razvi unconfined concrete model (idealized by tri-linear forms) is utilized for the wall web.
 - 1% strain hardening with a simplified trilinear model by considering cyclic degradation and unloading stiffness coefficients which is shown in Figure 2.4 is employed for reinforcement steel model.
 - The number of wall elements used for core shear wall is presented in Figure 3.9.

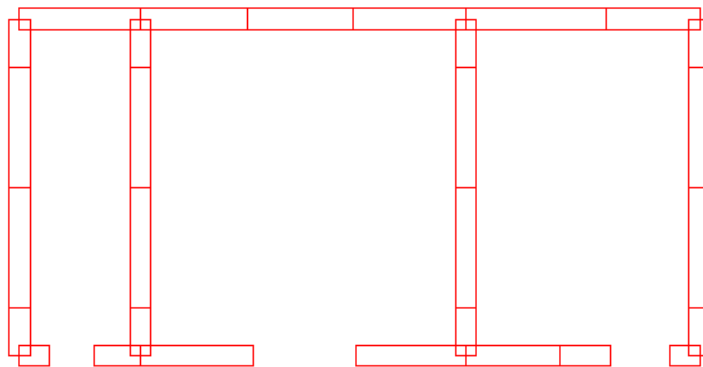


Figure 3.9. Number of wall elements for core shear wall

- Each wall element generally consists of four concrete fibers and twelve steel fibers. Relatively more steel fibers in the wall boundaries with relatively less steel fibers in the wall web is utilized for each shear wall elements.

- Wall element length (wall height) is taken nearly equal to the estimated plastic length, which is taken as the smaller value of one-half of the wall length (depth, l_n) or story height.
- Shear behavior of shear walls are modelled according to ASCE SEI 41-13.
- Reinforced concrete diagonal coupling beams are modeled by utilizing shear displacement hinge model. The properties of shear displacement hinges are obtained from ASCE-SEI 41-13 and ACI 318-8 by considering the designed properties of each coupling beam, but rigid plastic shear hinge is not employed. Instead, post cracking effects are also considered in the analytical model. Cracking strength is assumed to occur at minimum values of $0.415\sqrt{f'_{exp}}$ or 0.60 % of the nominal shear strength (ACI 318-8). The corresponding shear displacement at point U is assumed as an average shear strain of 0.004 over the beam length. Other key parameters are obtained from ASCE SEI 41-13.

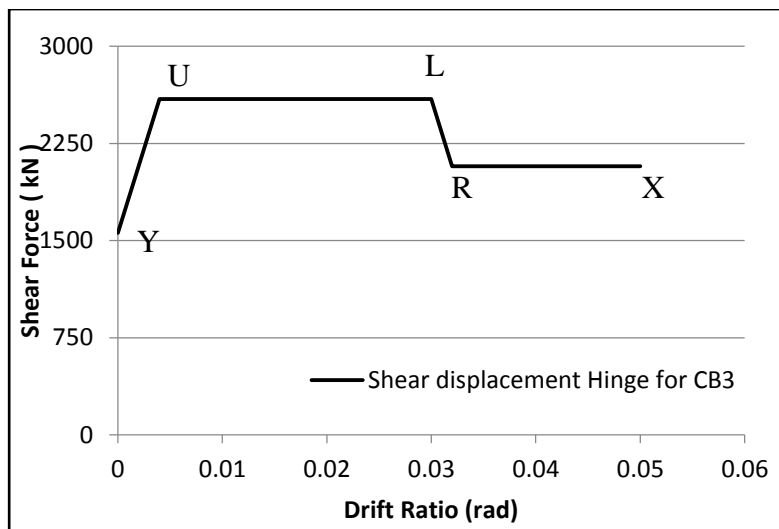


Figure 3.10. The characteristic backbone curve of coupling beams (CB3)

- Quasi-elastic properties of coupling beams are selected from ATC-72. Effective flexural stiffness and shear stiffness are taken as:

$$E_c I_{eff} = 0.15 E_c I_g \text{ and } G_c = 0.1 E_c$$

- Rigid diaphragms are assigned to each story level.
- P-Delta effects are considered in the model for both service level evaluation and collapse prevention level.
- Rayleigh damping is computed by considering 2.5 % damping in the T/T1 range of 0.2 and 1.25 for both performance levels.
- Earthquake load combinations in nonlinear dynamic analyses are selected as $1.0 D + 0.25 L + 1.0 E$.
- Accidental eccentricity is not considered for both performance level analyses.
- The effect of joist slab is ignored.

3.4 Ground Motion Selection

The set of ground motions which is used in the case study for service level evaluation and collapse prevention levels include seven different horizontal component pairs of ground motions. Table 3.4 presents several important properties of the selected reference ground motions. Two of the ground motions are ordinary type and others are pulse type. Spectral matching method is employed in order to generate suitable ground motions time series in accordance with the defined target spectrum by manipulating selected reference ground motions. These selected reference ground motions time series, which are presented in the appendix, were downloaded from PEER strong motion database.

The derivation of generated ground motions were carried out by using SeismoMatch v2.1 (2013) software program which utilizes the wavelets algorithm proposed by Abrahamson [1992] and Hancock et al. [2006]. According to Hancock and Bommer (2007), the properties of generated ground motions is similar to the selected reference ground motion properties since the derivation stage depends on modifying the frequency contents of the selected reference ground motions so as to match the initial response spectrum with the given target response spectrum. Accordingly, the manipulated ground motion properties do not show significant different properties from the selected reference ground motions.

The process consists of three steps. First step is the definition of target response spectrum for both performance levels in accordance with the expected earthquake, damping and vibration properties. For service level evaluation, target spectrum is defined as an earthquake with 30% probability of being exceeded in 50 years (return period of 43 years) with a damping ratio of 2.5 %. In TEC-2007, there is no analytical equation or approach in order to modify a reference target spectrum from the desired target spectrum by considering the effect of expected earthquake return period and damping value. Accordingly, some analytical equations are proposed.

- For this study, linear elastic design spectrum for the selected properties at the design stage is multiplied by an importance factor (I) in order to consider the effect of expected earthquake return period [Sucuoğlu and Akkar, 2014].

$$I = \left(\frac{T_{LR}}{T_L} \right)^{-1/k} \quad (3.1)$$

I : Importance factor

T_{LR} : Reference return period

T_L : Target return period

k : a coefficient depending on seismicity, (Eurocode proposes 3)

- For this study, to consider the damping effects on linear elastic design spectrum, two equations below are adjusted at the spectral ordinates of linear spectrum.

$$S_a(\xi) = \frac{1}{\eta} S_a(\xi = 5\%) \quad (3.2)$$

$$\eta = \sqrt{\frac{5 + \xi}{10}} \quad (3.3)$$

$S_a(\xi)$ Spectral acceleration ordinate with target damping value ξ .

$S_a(\xi = 5\%)$: elastic design spectral ordinate

η : damping scaling factor

For the collapse prevention level, similar to service level evaluation, target spectrum is defined as an earthquake with 2% probability of being exceeded in 50 years (return period of 2475 years) with a damping ratio of 2.5 %. After defining the target

spectrum, spectrum matching is employed by using Seismo Match software. Figures 3.10 and 3.11 show the acceleration spectra of generated ground motions, their mean spectrum and TEC (2007) design spectrum for both performance levels.

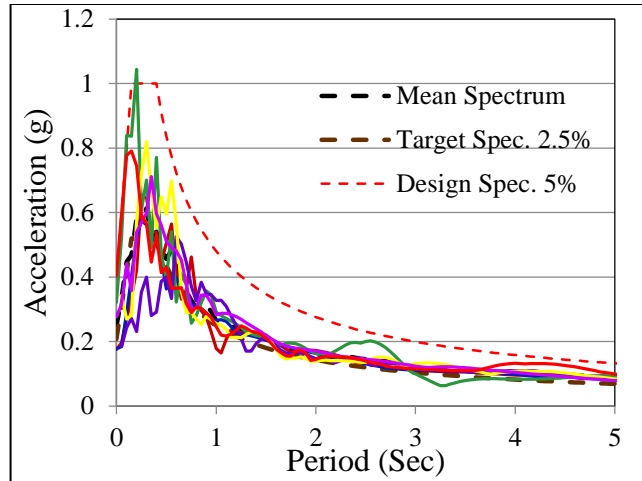


Figure 3.11. Acceleration response spectra of generated ground motions, mean acceleration spectrum, target spectrum and TEC2007 design spectrum for SLE

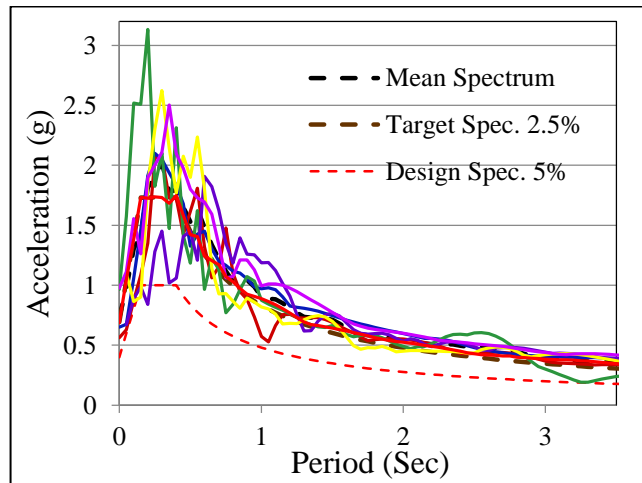


Figure 3.12. Acceleration response spectra of generated ground motions, mean acceleration spectrum, target spectrum and TEC2007 design spectrum for MCE

Table 3.4 Reference ground motion properties

#	GM Code/Component	Earthquake (Mw)	CD (km)	Site Geol.	GM Type	PGA (g)	PGV (cm/s)	PGD (cm)
1	CLS000/Corralitos 00	Loma Prieta 10/18/89 (7)	5.1	B	Pulse	0.644	52.2	10.88
	CLS090/Corralitos 90					0.479	45.2	11.37
2	LOMAP/LEX 00	Los Gat. -Lex Dam 10/18/89 (7)	5	A	Pulse	0.42	73.5	20
	LOMAP/LEX 90					0.445	62.18	16.63
3	SFERN/PCD164	San Fer. / Pac. Dam 02/09/71 (6.6)	2.8	B	Pulse	1.226	112.5	35.5
	SFERN/PCD254					1.16	54.3	11.73
4	CHICHI/CHY006-E	Chi Chi 20/09/99 (7.6)	14.93	C	Pulse	0.364	55.4	25.59
	CHICHI/CHY006-N					0.345	42.8	15.18
5	DUZCE/DZC180	Duzce 11/12/99 (7.1)	8.2	D	Ordinary	0.348	60.9	42.09
	DUZCE/DZC270					0.535	83.5	51.59
6	IMPVALL/H-E04140	Imperial Valley 15/10/79 (6.9)	4.2	C	Ordinary	0.485	3.4	20.2
	IMPVALL/H-E04230					0.36	76.6	59.01
7	ERZIKAN/ERZ-EW	Erzincan 13/03/92 (6.9)	2	D	Pulse	0.515	83.9	27.35
	ERZIKAN/ERZ-NS					0.496	64.3	22.78

3.5 Presentation of Results for the Case Study

In this part, maximum average transient interstory drift ratios of each corner and mass center of structure, maximum average shear stress and axial load level on SW2, SW3 and SW3 in a story, maximum average axial strain of SW2, SW3 and SW3 throughout the entire height of the walls and maximum average axial load level of each column group have been presented. Since the pre-determined acceptance criteria for shear walls and columns have not been satisfied, preliminary design has been revised. The results of maximum average curvatures of beams and displacements of coupling beams has been presented only for the revised design which is presented in Part 3.7

3.5.1 Interstory Drift Ratios

Maximum interstory transient drift ratio at each story is calculated at the mass center and at the each corner of that story because of unsymmetrical-plan of the case study building. Each corner and mass center of a story is labelled as A, B, C, D and MC, which is illustrated in Figure 3.1.

Performance levels of maximum average transient interstory drift ratios are taken as 0.5% and 3% for service level and collapse prevention level evaluations, respectively. In addition, the limit state of the maximum drift ratio in each story for each ground motion is taken as 4.5% for collapse prevention level. The average transient interstory drift ratio obtained from the set of ground motions with the maximum transient interstory drift ratio obtained from each ground motion series are presented in Figures 3.12 to 3.15 for both performance levels and for both X and Y directions. As it can be seen in these figures, the obtained results satisfy target performance levels. However, because of unsymmetrical plan about X direction, which is shown in Figure 3.49, the building rotates about strong axis where SW3 is located in. In addition, results show that, higher modes add substantially to the global response of the structure.

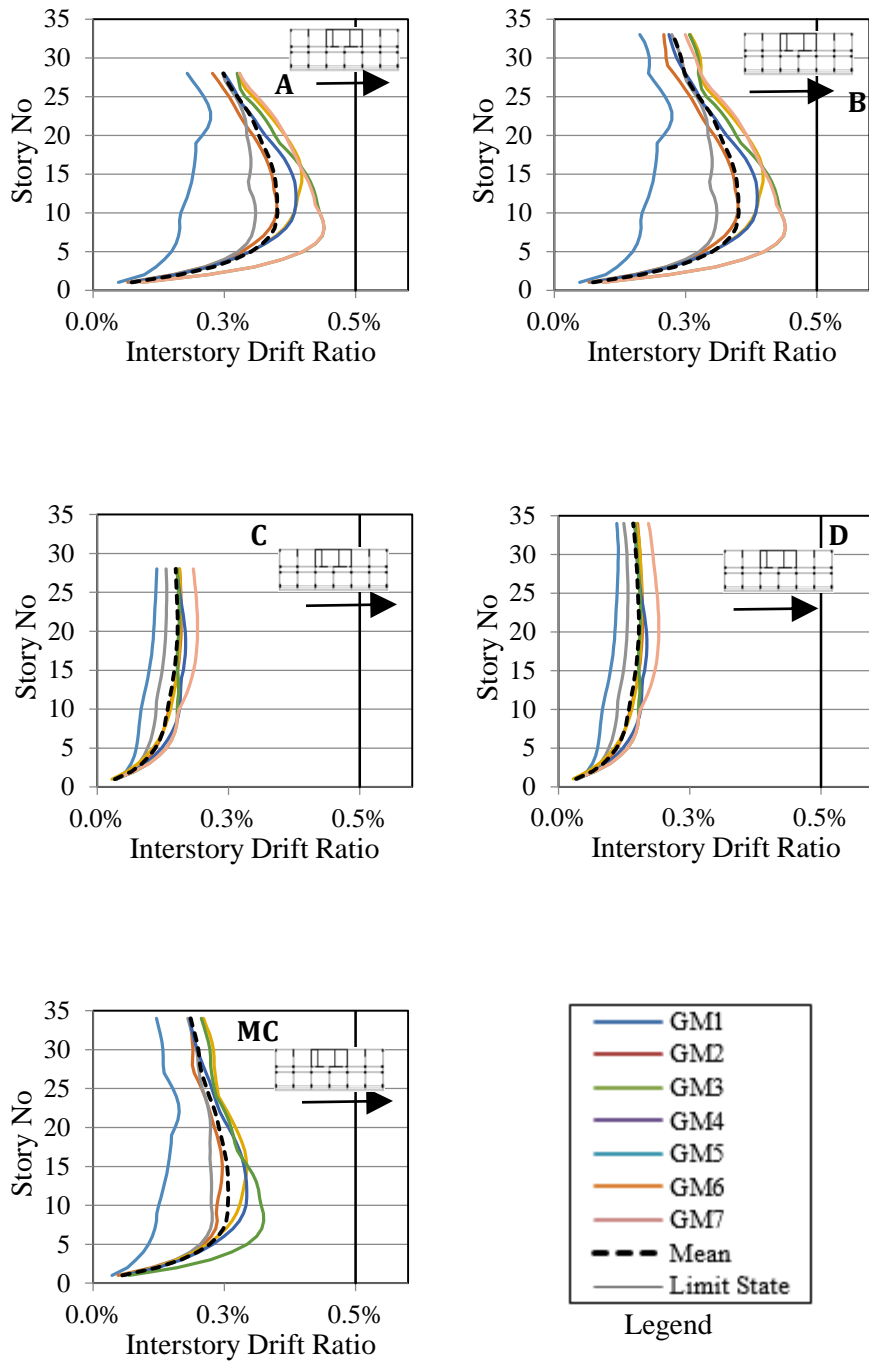


Figure 3.13. Maximum transient interstory drift ratios for each ground motion with maximum average transient interstory drift ratios obtained from a set of SLE shaking in X direction

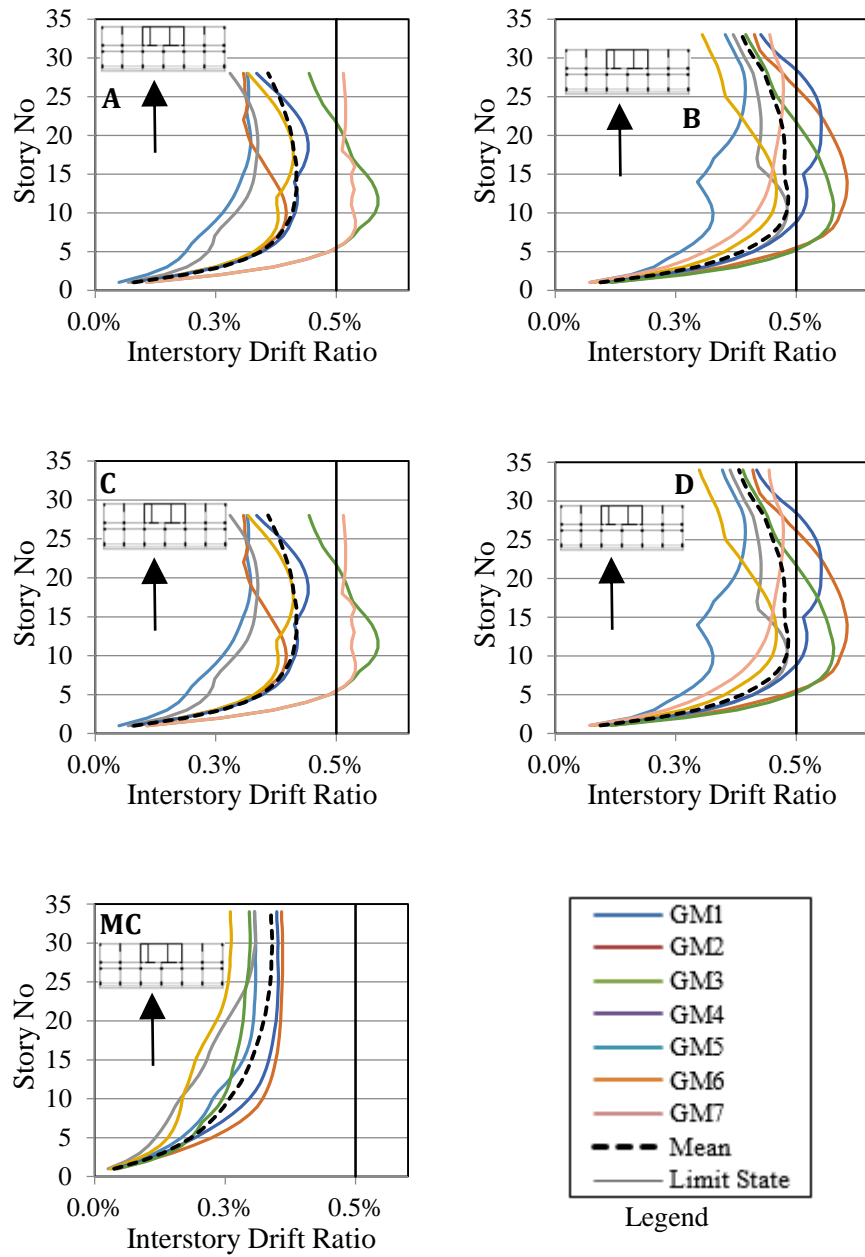


Figure 3.14. Maximum transient interstory drift ratios for each ground motion with maximum average transient interstory drift ratios obtained from a set of SLE shaking in Y direction

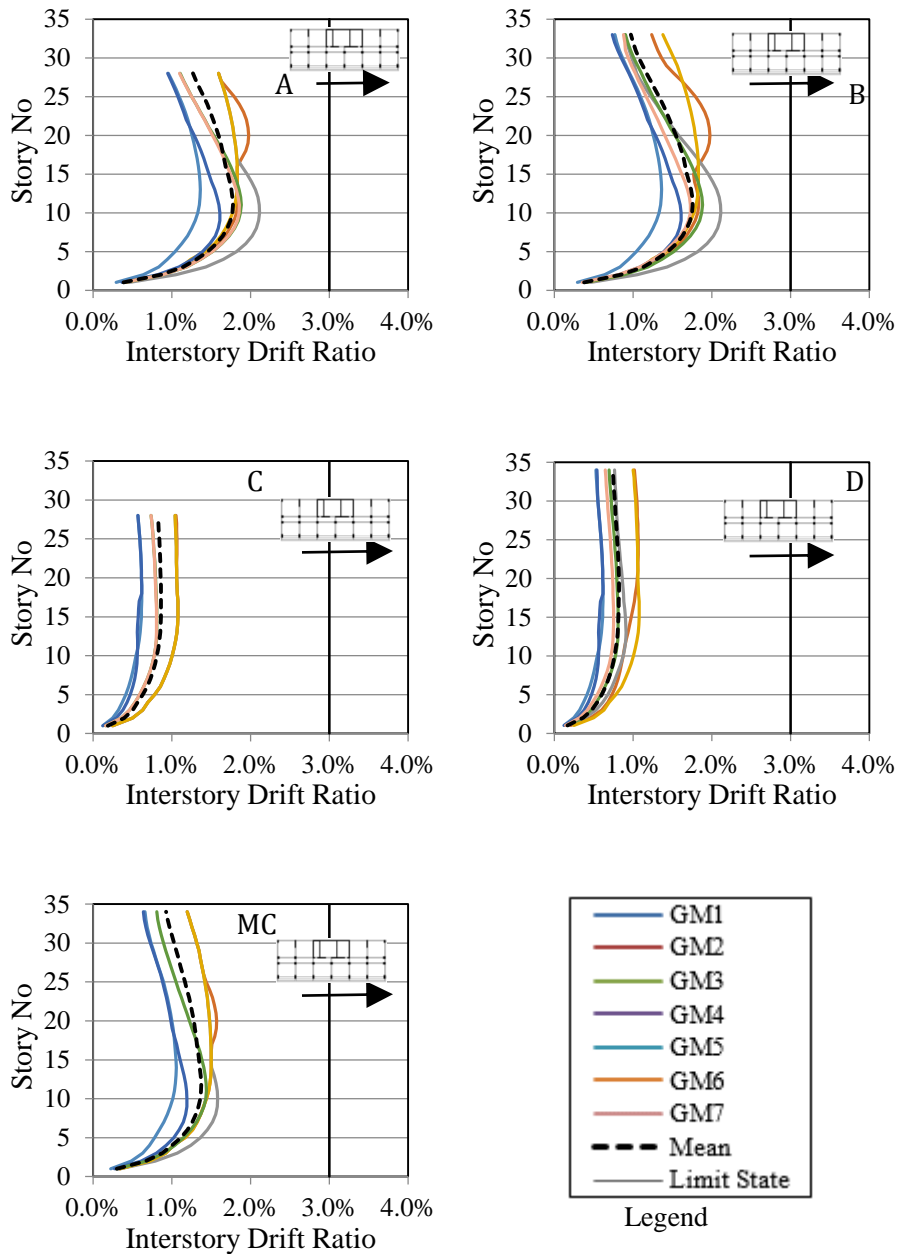


Figure 3.15. Maximum transient interstory drift ratios for each ground motion with maximum average transient interstory drift ratios obtained from a set of MCE shaking in X direction

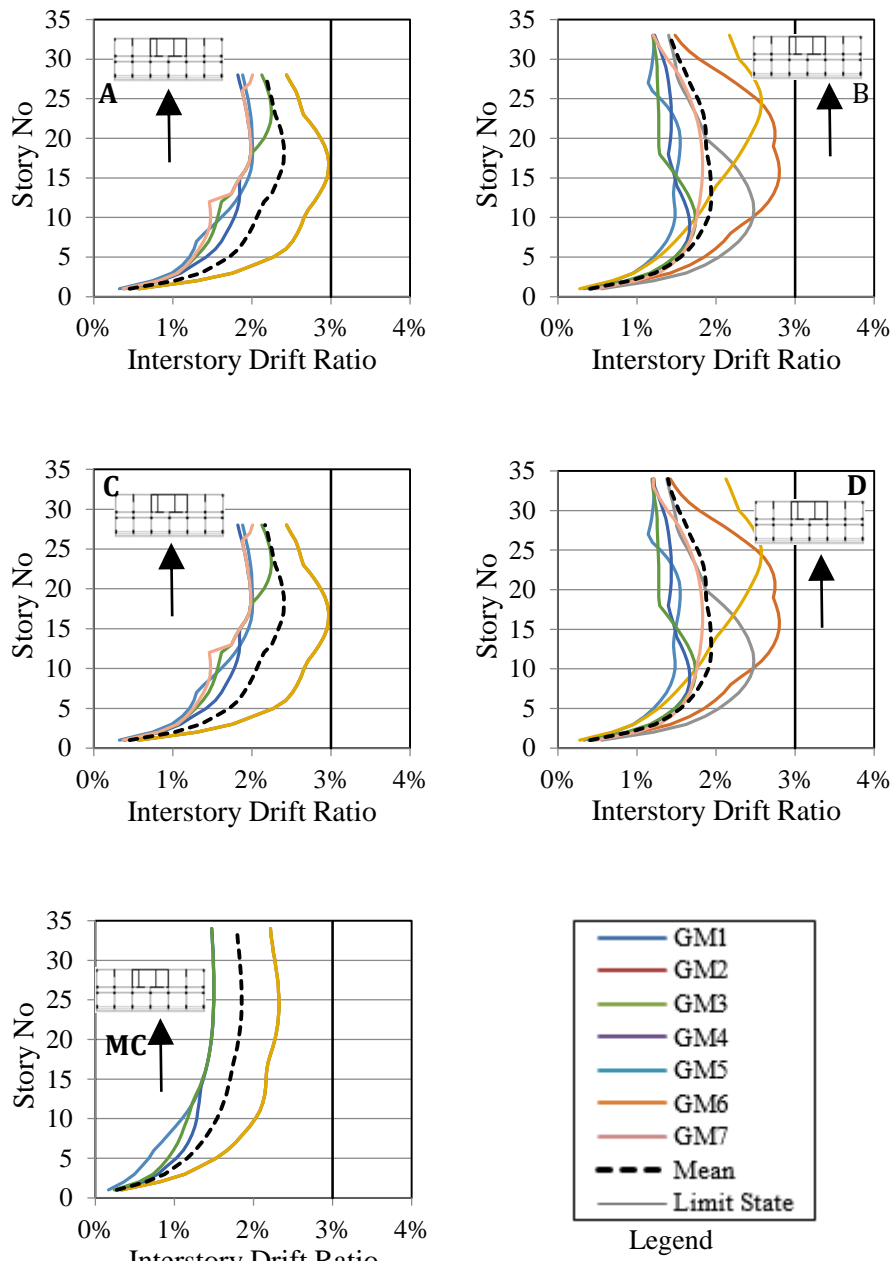


Figure 3.16. Maximum transient interstory drift ratios for each ground motion with maximum average transient interstory drift ratios obtained from a set of MCE shaking in Y direction

3.5.2 Average Shear Stress and Axial Load Level of Shear Walls

In seismic design of tall buildings, shear walls (especially core shear walls) are the preliminary seismic force resisting members thus they are desired to withstand not only all of the lateral forces (seismic and wind) but also a considerable amount of

gravity forces due to having less redundant structural systems. The expected governing and controlling type of action to be captured during analysis for the tower core walls is force. Accordingly, these forces must be limited for a ductile design. In other words, shear failure of structural members are generally not desired. In addition to these effects, nonlinear analysis is based on some rational assumptions and quite a few uncertainties are available for nonlinear modeling. For this purpose, seismic codes and non-prescriptive guidelines bring some limitations on axial loads and shear stresses on shear walls. In this case study, the average shear stress of shear walls is limited by the ACI-318-8 provisions. PEER-TBI and LATBSDC suggest also these limitations to check the shear stresses of shear wall members. The following limitations are employed:

- Upper limits for shear strength of shear walls under any earthquake excitation:

$$\tau_u \leq 0.664\sqrt{f'_{ex}} \text{ for walls sharing lateral load}$$

$$\tau_u \leq 0.83\sqrt{f'_{ex}} \text{ for single walls}$$

- Cracking of shear wall may not be a desirable behavior under service level earthquake (SLE) shaking. Accordingly, the provisions below which are given in ACI-318 in order to determine shear strength limit are used in this case study.

$$\tau_{cr} = \min(0.415\sqrt{f'_{ex}}, 0.6 V_n/A_{cw})$$

V_n : Nominal shear strength,

A_{cw} : Shear area

τ_{cr} : The cracking shear stress,

τ_u : Ultimate shear stress

τ_{ave} The average shear stress of a shear wall obtained from the average of maximum values of each analysis (for both negative and positive action).

Similarly, the axial load on shear walls is also limited for a ductile design. In this case study, the axial load level is limited by $\frac{N_d}{f'_{ex}A_g} \leq 0.30$ when subjected to MCE level shakings. This limit proposes by PEER-TBI (2010). Figure 3.17 to 3.22 illustrate the results of average shear stress and axial load levels for SW2, SW3 and SW6 (the main components of core shear walls) under SLE and MCE level shakings.

Results show that the axial load level at the bottom story level exceeds the pre-determined limit state for collapse prevention level, under SLE shaking also they are exceeded unexpectedly. In addition, the results show that the contribution of higher modes to total shear stress is significant under MCE shakings because the shear stresses of walls decrease from the second story to the 15th story, but increase from 15th story to 25th this story. After this story, the shear stresses decrease. The results also indicate that shear stresses reach their maximum value at the second story due to the presence of a podium level. High shear forces are transferred between the podium level and the tower. Moreover, SW3 shear wall also exceeds the limit of shear cracking stress under SLE shaking and the limit of ultimate strength capacity under MCE shaking. According to these results, the preliminary design is revised by increasing the dimension of shear walls instead of using higher strength material.

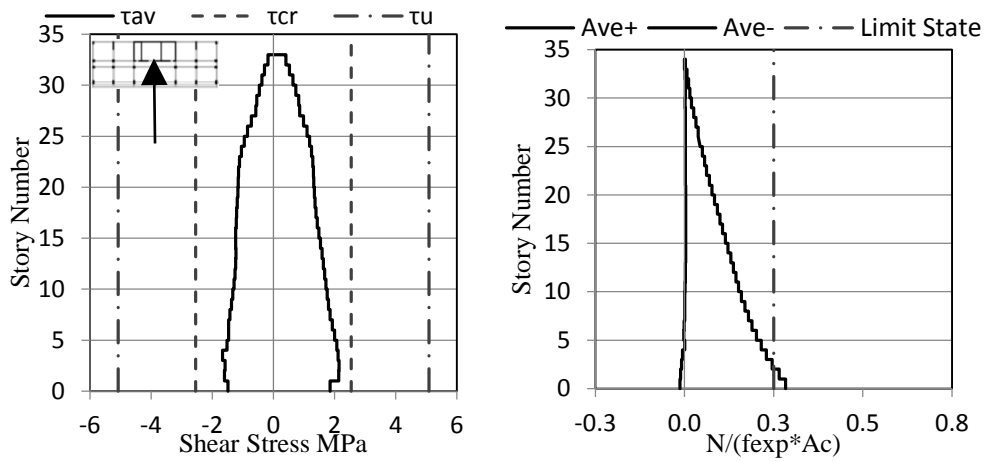


Figure 3.17. Max average shear stress and axial load on shear wall SW2 under SLE shaking

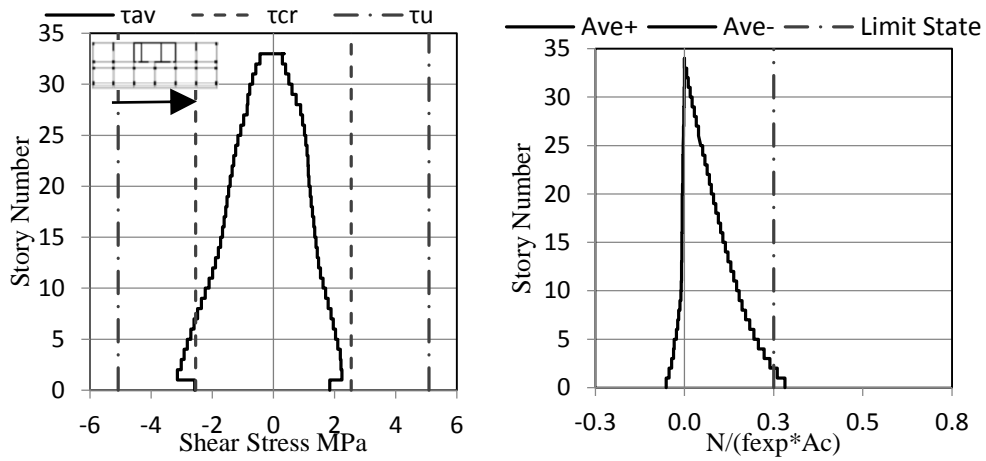


Figure 3.18. Max average shear stress and axial load on shear wall SW3 under SLE shaking

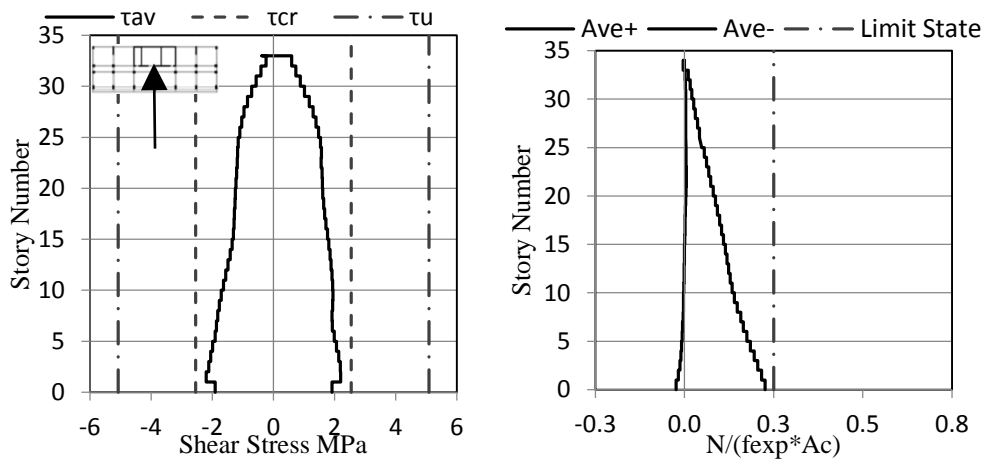


Figure 3.19. Max average shear stress and axial load on shear wall SW6 under SLE shaking

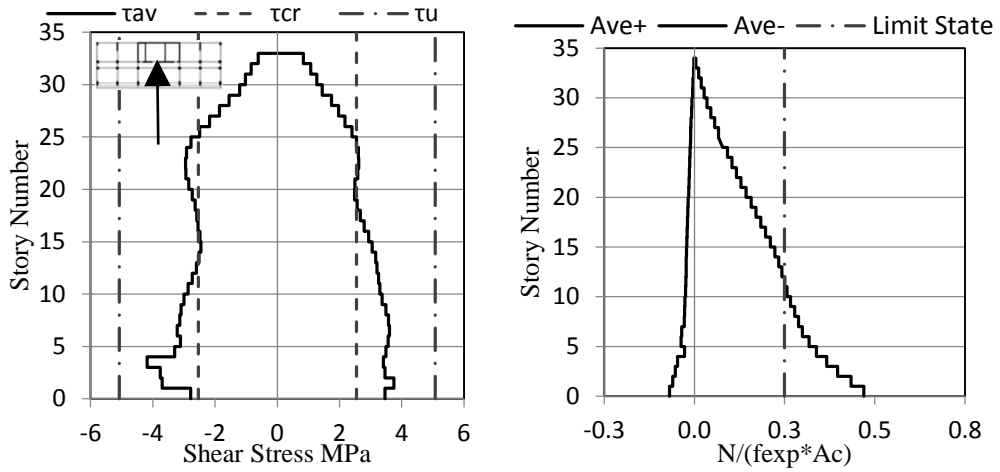


Figure 3.20. Max average shear stress and axial load on shear wall SW2 under MCE shaking

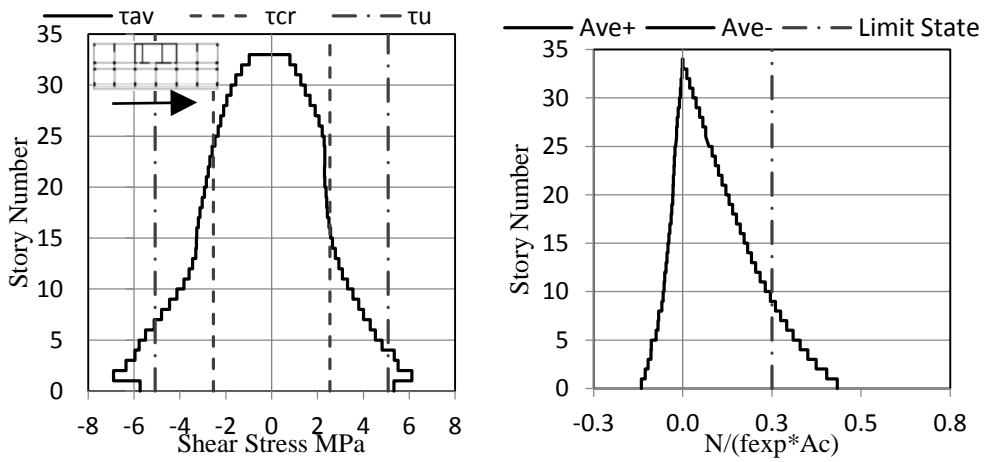


Figure 3.21. Max average shear stress and axial load on shear wall SW3 under MCE shaking

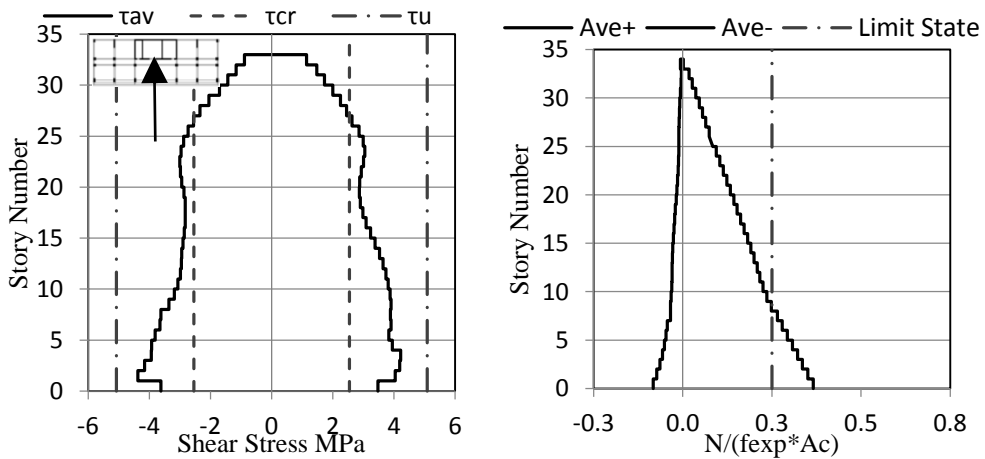


Figure 3.22. Max average shear stress and axial load on shear wall SW6 under MCE shaking

3.5.3 Axial Forces in Columns

The axial internal force on the reinforced columns should be limited because of similar reasons related to ductility which are explained for shear walls. In this case study, axial force in column is limited by $\frac{N_d}{f_{ex}A_g} \leq 0.40$ under MCE shaking. Figures 3.24 to 3.27 illustrate the axial force in each identical column group. As it can be observed in Figure 3.25, some columns of this group exceed the force limit state. Some of most critical columns in this group are presented in Figure 3.23 and labelled C10, C11 and C12 through all story levels. Especially C10 and C12 near the boundary of the core shear wall work as a boundary of the shear walls. Shear force which will be transferred between the shear walls to the columns by linking beams develop high axial force in the columns. The core shear wall withstands a considerable amount of seismic load when subjected to an earthquake excitation, thus load transfer between core walls and the relating beams and columns is high. Accordingly, these members are exposed to much higher effects compared to other members. Accordingly, columns which do not satisfy the required performance level are re-designed by increasing their dimension to satisfy the expected performance level.

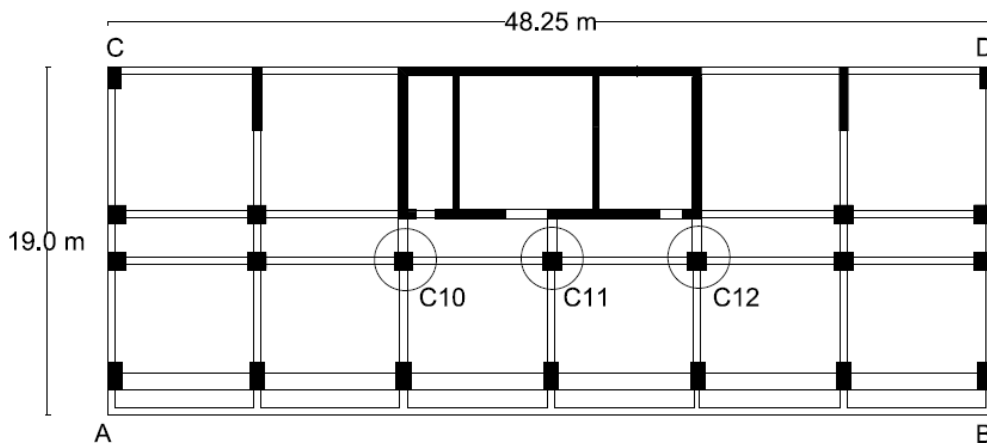
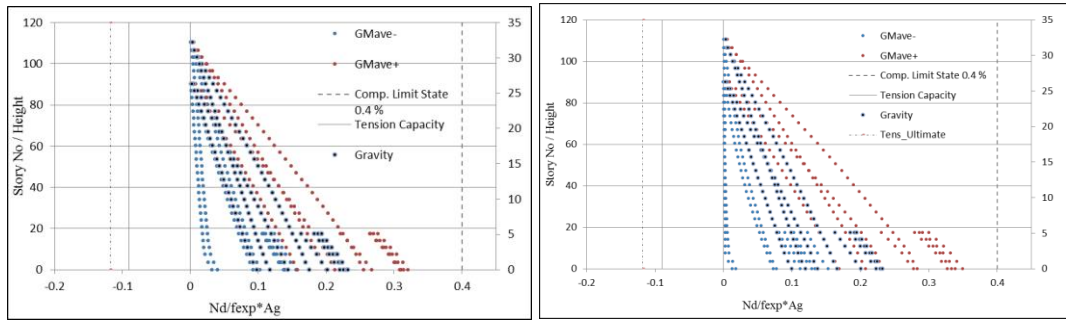


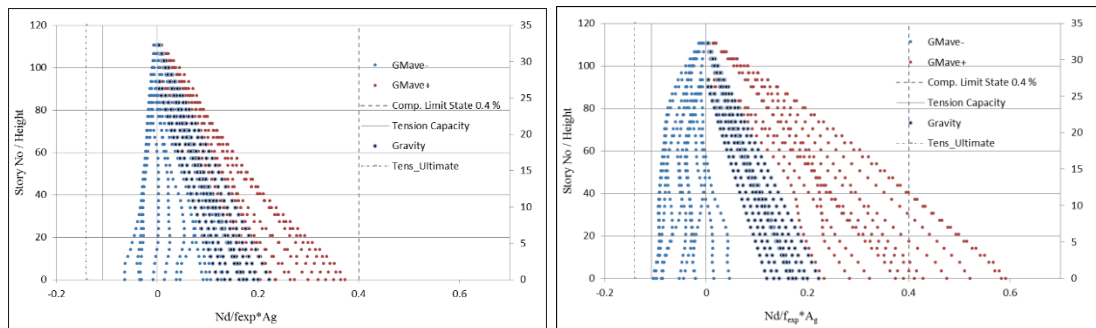
Figure 3.23. C10, C11 and C12 columns



(a)

(b)

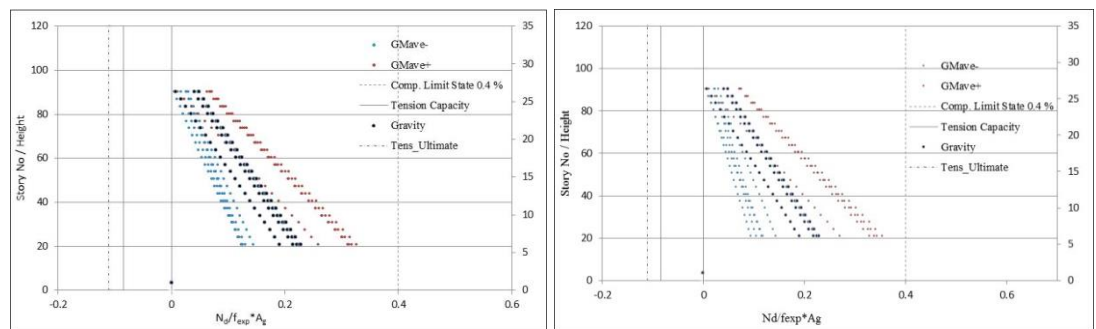
Figure 3.24. Average axial load level on C800*1500 columns (C1, C7, C19, C20 and the first six floors of C2 to C6) under (a) SLE, and (b) MCE shakings



(a)

(b)

Figure 3.25. Average axial load level on C1000*1000 columns (from C8 to C18) under (a) SLE and (b) MCE shakings



(a)

(b)

Figure 3.26. Average axial load level on C700*1400 columns (from C2 to C6 between 7th and 29th floor) under (a) SLE and (b) MCE shakings

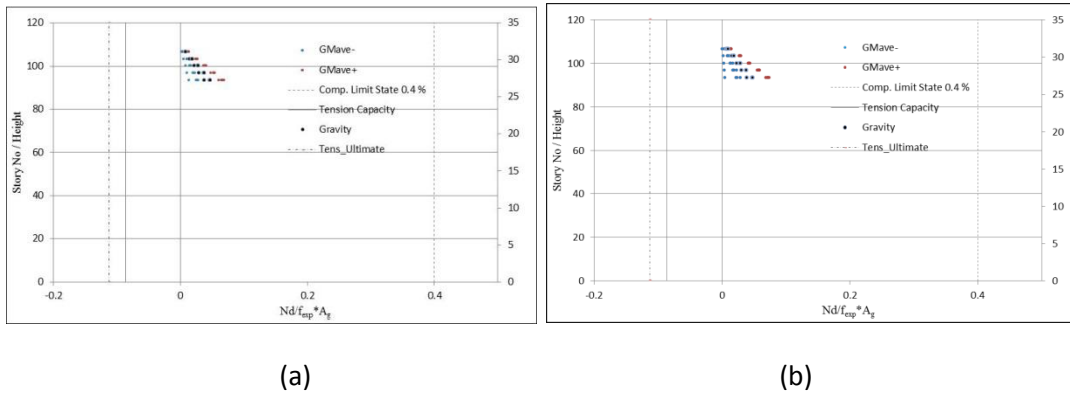


Figure 3.27. Average axial load level on C700*1200 columns (the four upper stories of C3, C4, C5 and C6) under (a) SLE and (b) MCE shakings

3.5.4 Axial Strain of Shear Walls

One of the performance parameters to anticipate the damage of shear walls under an earthquake excitation is axial strain. “Strain gauges” are used to determine the amount of tension and compression strains in the shear wall elements. The distribution of maximum average strain values for concrete in compression and reinforcement in tension over the height for SW2, SW3 and SW6 shear walls are presented in Figure from 3.27 to 2.32 for each performance level. These shear walls remain elastic under SLE shaking. However, a plastic zone which is nearly equal to 15% of building height has been developed at the base of each shear wall under the MCE excitation. Each shear wall has yielded but the amount of yielding of each shear wall is acceptable for collapse prevention performance. According to TEC-2007, SW2 member is in the minimum damage region ($\epsilon < 0.01$) and SW3 and SW6 are in significant damage region ($0.01 < \epsilon < 0.004$). According to ASCE 41-13, these tensile strain values are also acceptable ($\epsilon < 0.05$) for collapse prevention level. In addition, the amount of strain in compression at each story level and performance level is acceptable. The following symbols are used in presenting the axial strain results.

ACS: Mean axial compressive strain

ATS: Mean axial tensile strain

ϵ_{sy} : Yield strain

ϵ_{sy} : the strain corresponding maximum compressive strength of concrete

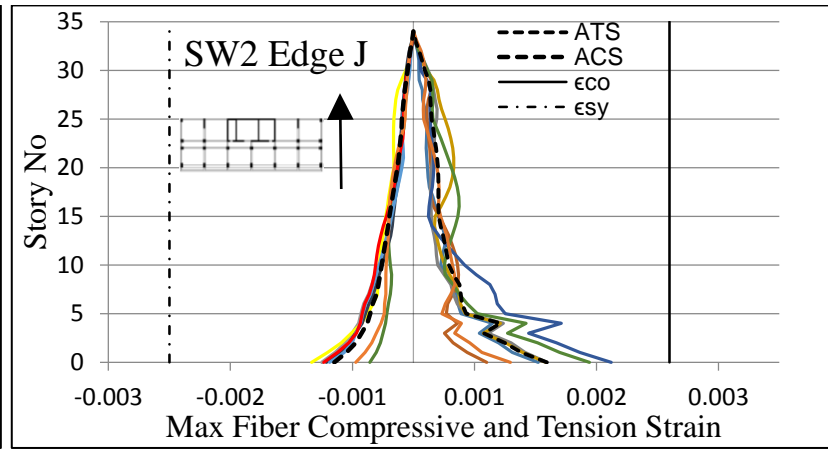
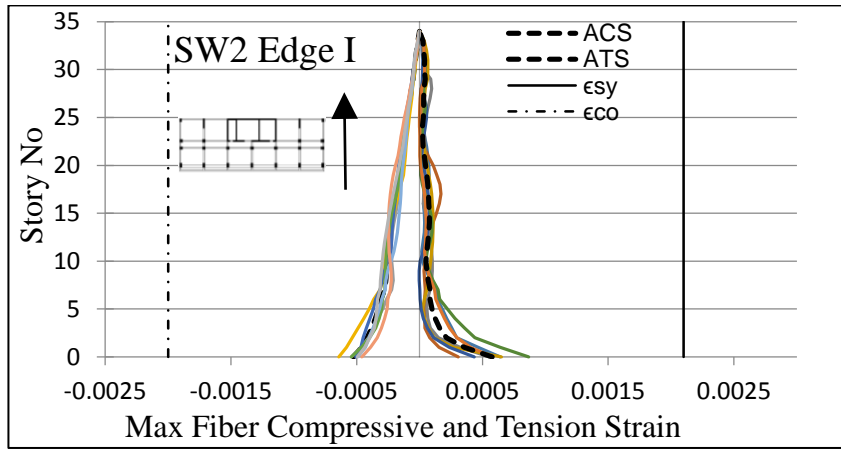


Figure 3.28. Axial strain at edge I (internal edge) and edge J (external edge) of shear wall SW2 under SLE shaking

96

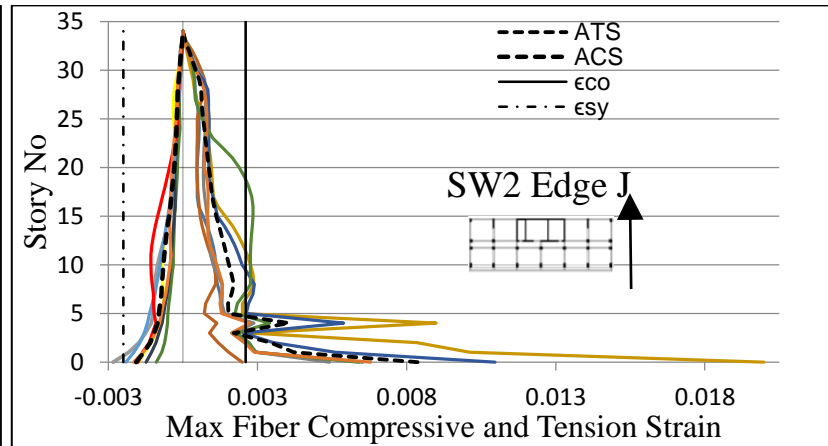
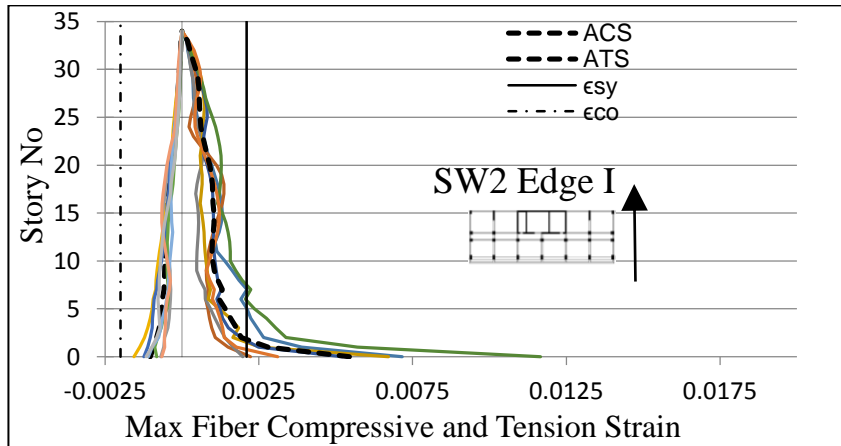


Figure 3.29. Axial strain at edge I (internal edge) and edge J (external edge) of shear wall SW2 under MCE shaking

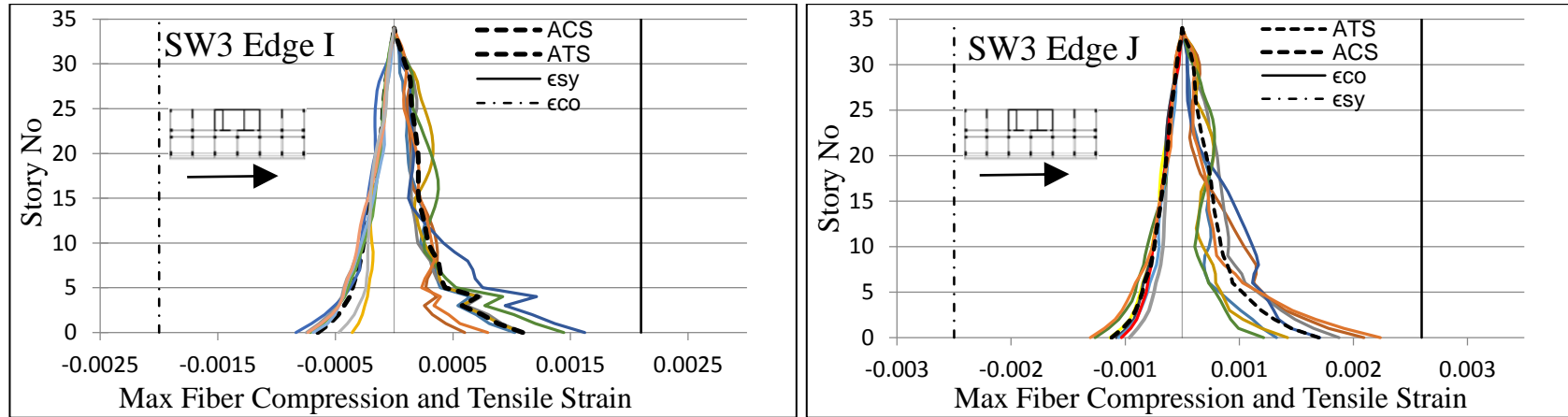


Figure 3.30. Axial strain at edge I (internal edge) and edge J (external edge) of shear wall SW3 under SLE shaking

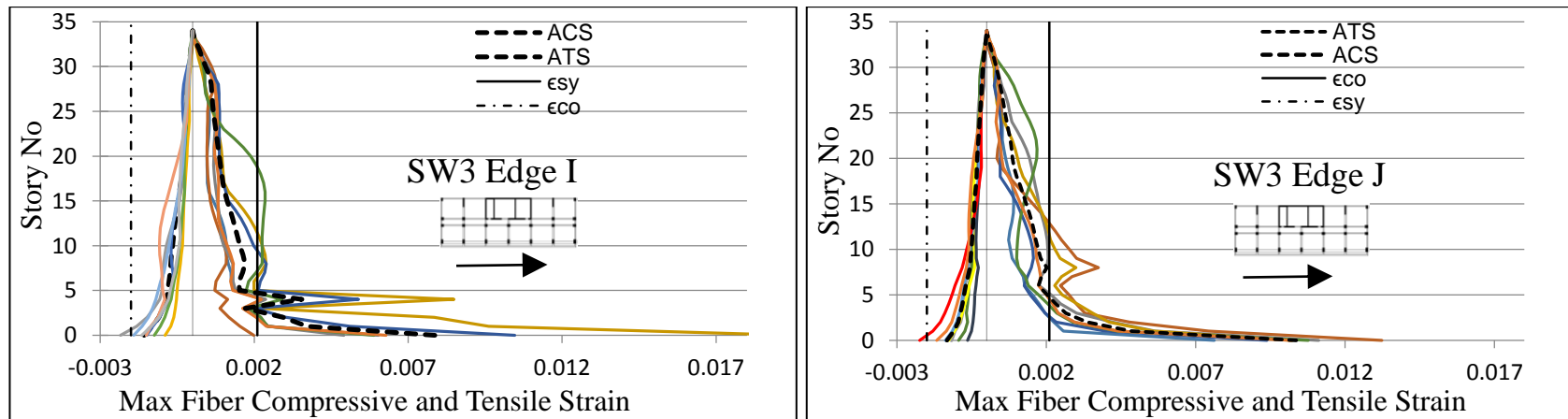


Figure 3.31. Axial strain at edge I (internal edge) and edge J (external edge) of shear wall SW3 under MCE shaking

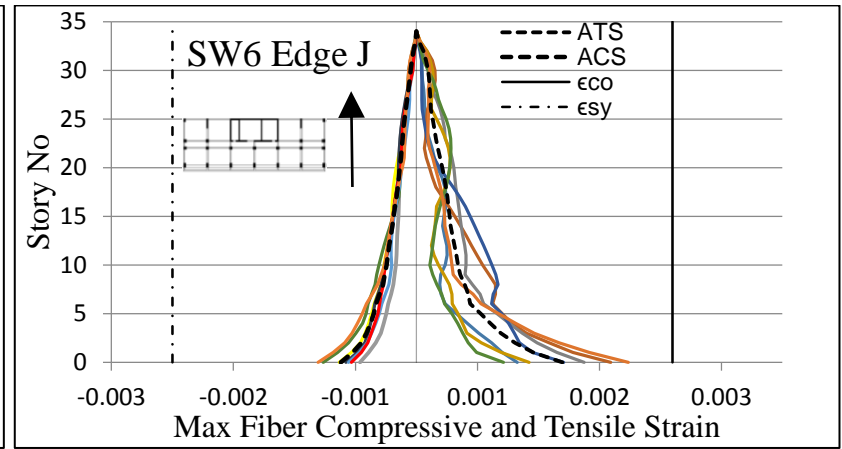
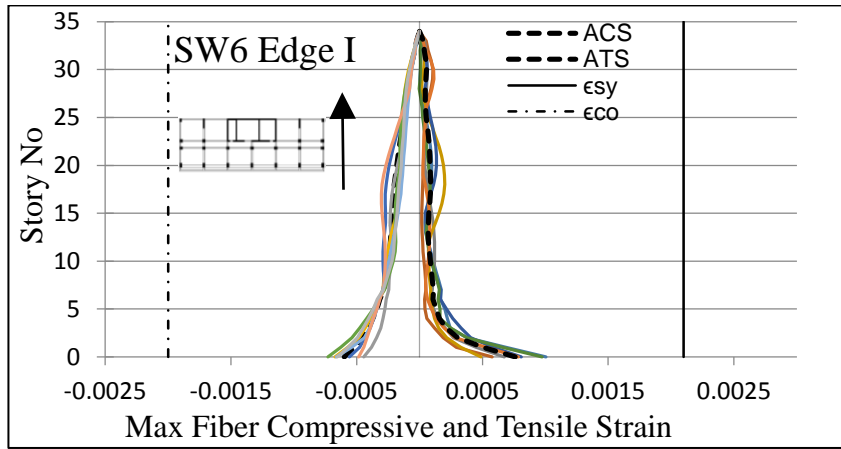


Figure 3.32. Axial strain at edge I (internal edge) and edge J (external edge) of shear wall SW6 under SLE shaking

97

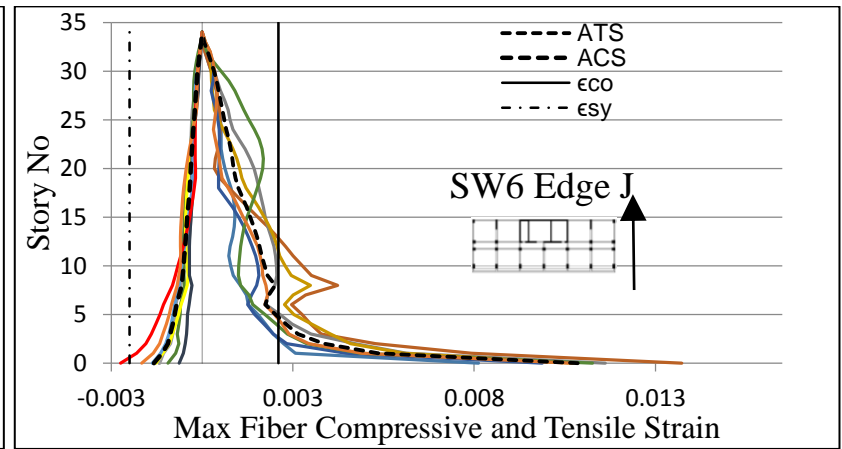
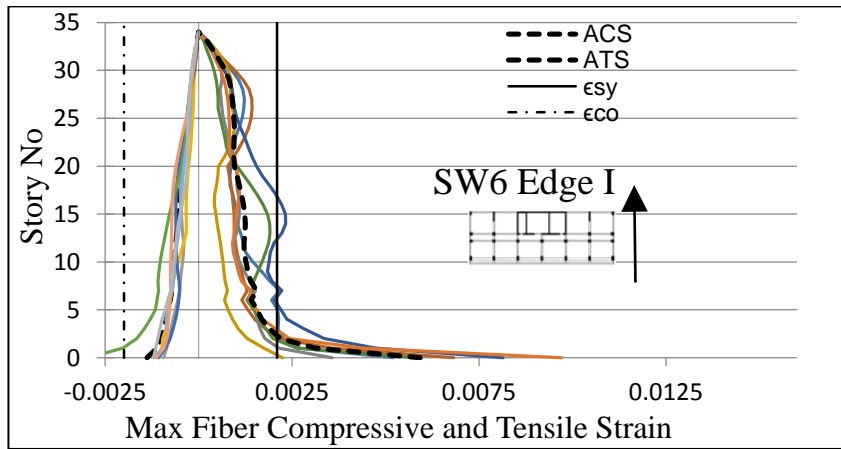


Figure 3.33. Axial strain at edge I (internal edge) and edge J (external edge) of shear wall SW6 under MCE shaking

3.6 Presentation of Results for the Revised Case Study

NLTHA is conducted for the original case study building by employing a suite of seven ground motion pairs and checking the results in compliance with the target performance levels determined for service level and collapse prevention level. A number of performance targets have not been satisfied in the case study building, hence the preliminary design is revised. Instead of changing the material strengths, section dimensions for members that do not satisfy required performance are increased to evaluate the dimension effects on anticipated building behavior. For this purpose, the section dimensions have changed such that:

- Thickness of SW2, SW3, SW4 SW5 and SW6 have been increased from 500 mm to 700 mm
- The dimensions of C8, C14, C15, C16 and C17 have increased from 100*100 cm² to 120*120 cm² in the first three stories,
- The dimensions of C9 and C13 have increased from 100*100 cm² to 120*120 cm² in the first six stories,
- The dimensions of C10, C11 and C12 have increased from 100*100 cm² to 120*120 cm² in the first twelve stories.
- The width of coupling beams has increased from 500 to 700 mm.

Free vibration properties of the revised building are obtained from the elastic model using un-cracked section properties. Eigenvalue analysis results and the effective modal mass results for the first twelve modes are presented in Table 3.5.

After the sections dimensions have changed, the case study is re-analyzed and evaluated in order to achieve the performance objectives. In addition to the selected results for case study, maximum average curvature of selected beams and maximum average displacement of selected coupling beams have been also presented for the revised case study. The obtained results are given below parts.

Table 3.5. Free vibration properties of the revised case study for the first twelve modes

Mode	Tn (sn)	Mx* (ton)	My* (ton)	Mx*/M	$\sum M_x$	$M_y^*/\sum M$	$\sum M_y$
1.00	2.87	11849.3	5299.4	0.313	0.313	0.140	0.140
2.00	2.56	4628.4	18360.2	0.122	0.436	0.486	0.626
3.00	1.30	6381.1	201.7	0.169	0.604	0.005	0.631
4.00	0.82	4425.0	531.9	0.117	0.721	0.014	0.645
5.00	0.61	514.7	6159.4	0.014	0.735	0.163	0.808
6.00	0.44	99.9	129.6	0.003	0.738	0.003	0.811
7.00	0.31	4282.4	290.7	0.113	0.851	0.008	0.819
8.00	0.29	262.7	662.7	0.007	0.858	0.018	0.837
9.00	0.26	111.5	1377.0	0.003	0.861	0.036	0.873
10.00	0.2	465.9	74.4	0.012	0.873	0.002	0.875
11.00	0.16	244.3	1208.6	0.006	0.880	0.032	0.907
12.00	0.15	69.3	11.0	0.002	0.881	0.000	0.907

3.6.1 Interstory Drift Ratios

As it can be seen the following inter story drift ratio results of revised case study (Figure 3.34-3.37), the targeted limit states are satisfied for both performance levels.

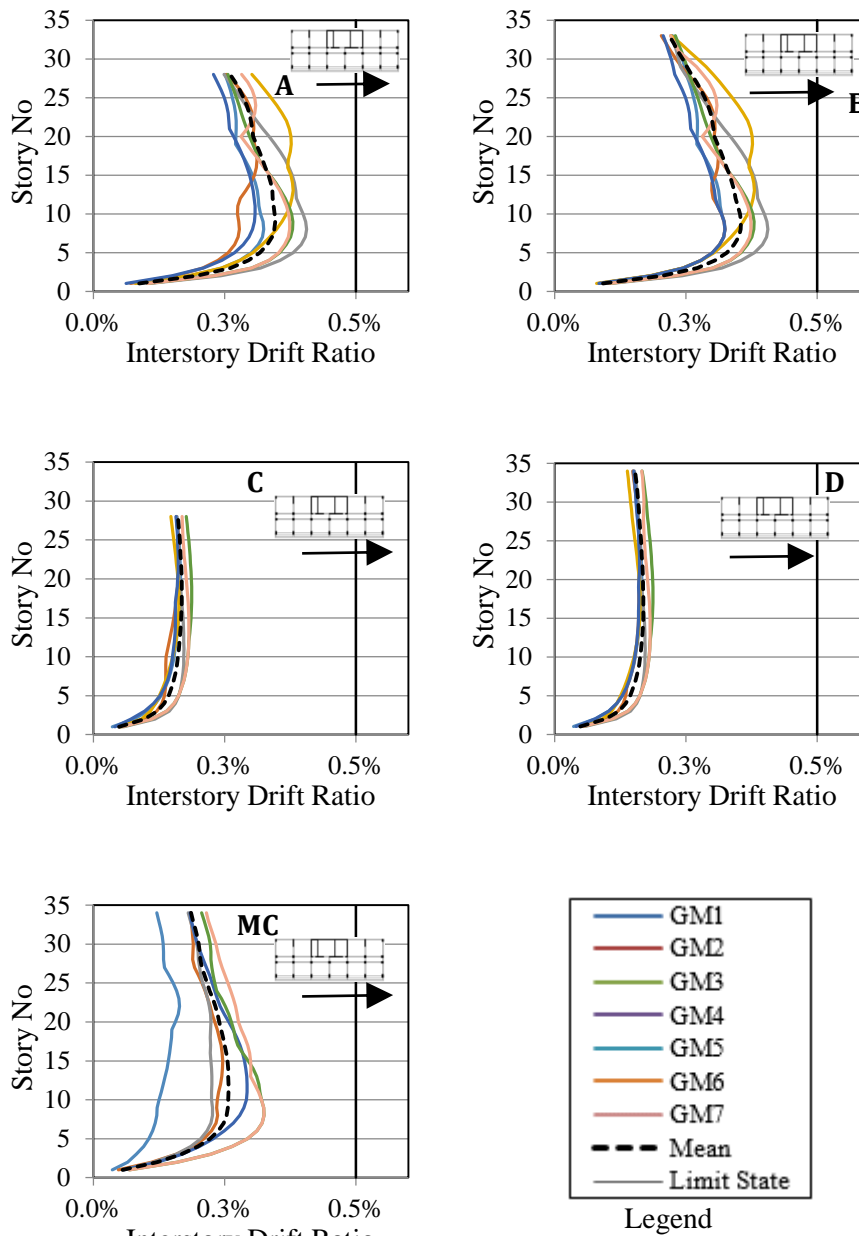


Figure 3.34. Maximum transient interstory drift ratios for each ground motion with maximum average transient interstory drift ratios obtained from a set of SLE shaking in X direction.

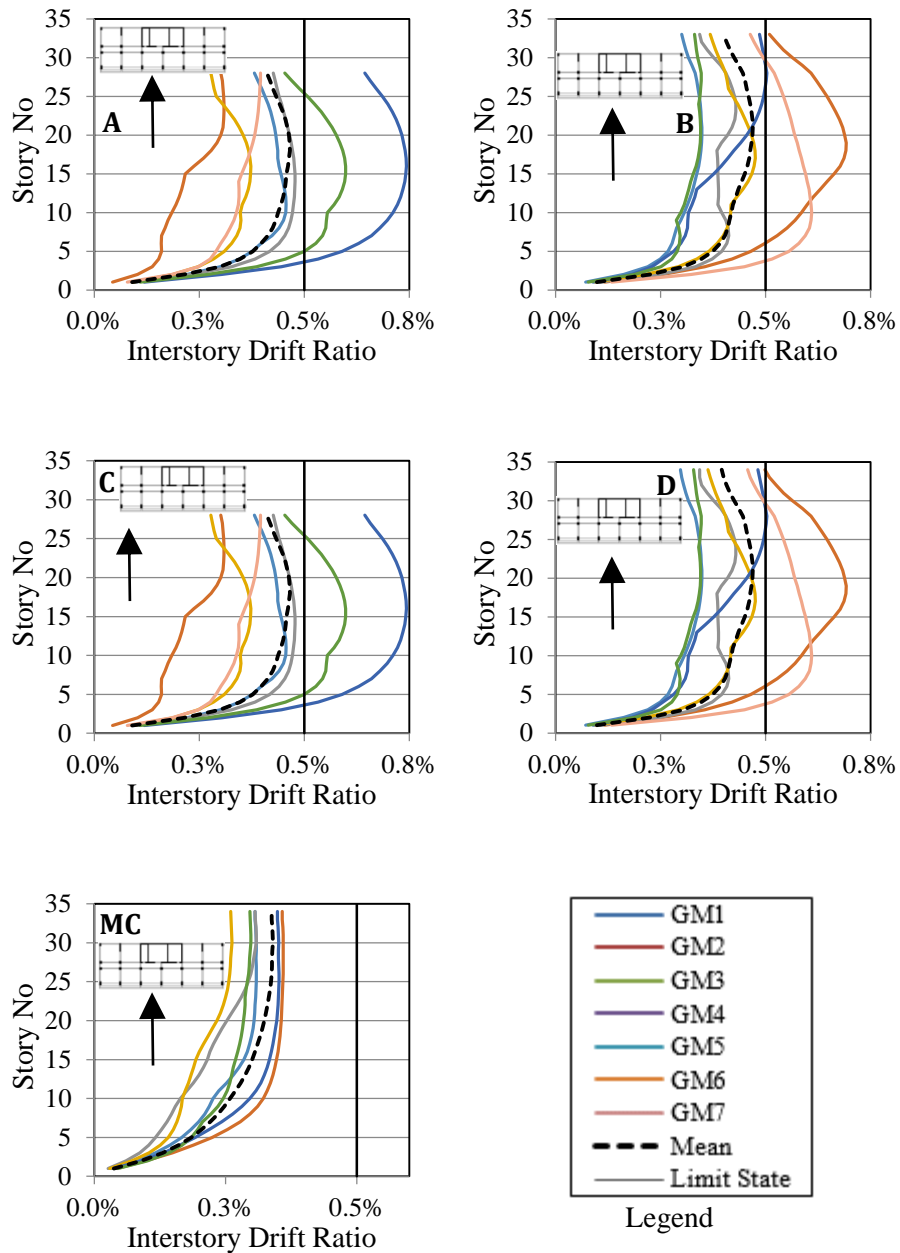


Figure 3.35. Maximum transient interstory drift ratios for each ground motion with maximum average transient interstory drift ratios obtained from a set of SLE shaking in Y direction

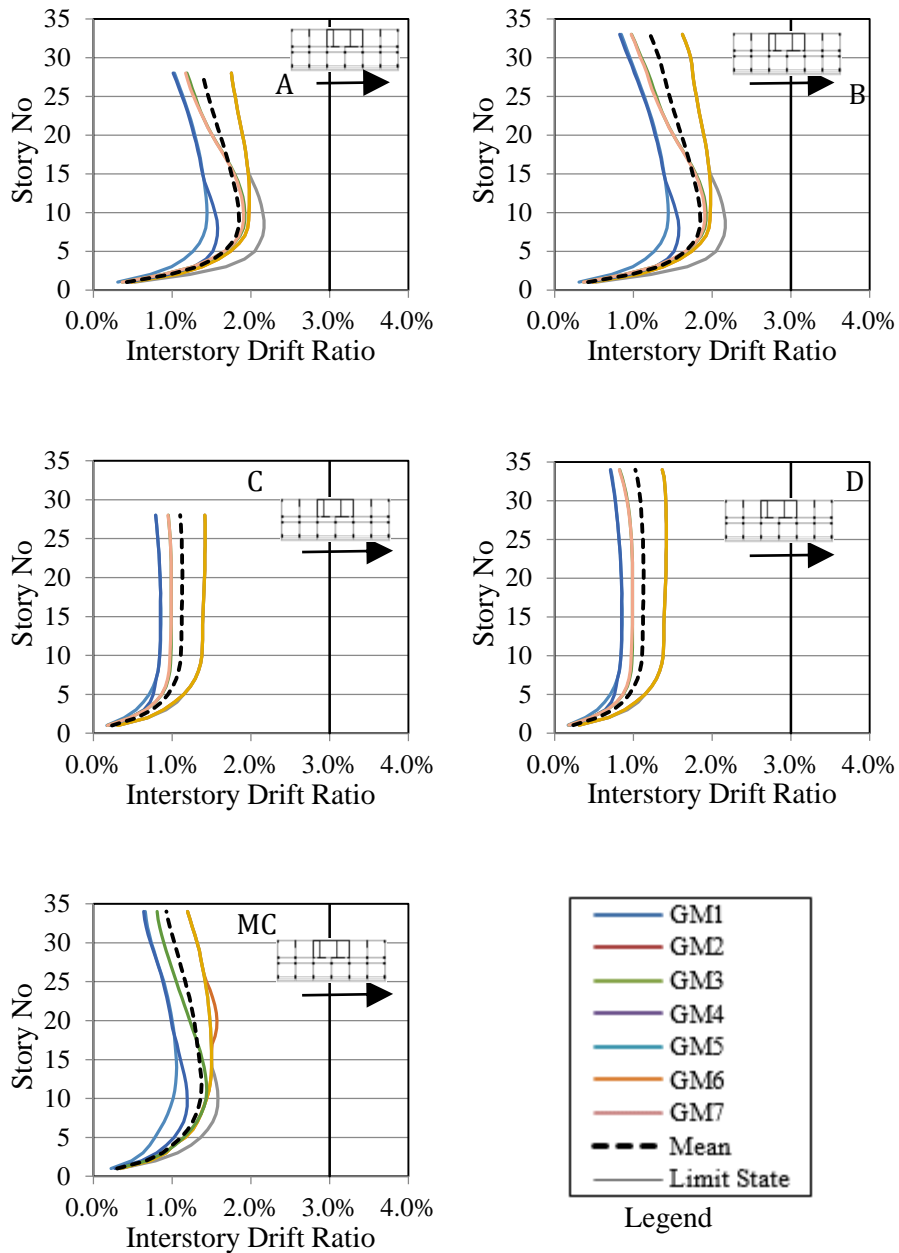


Figure 3.36. Maximum transient interstory drift ratios for each ground motion and maximum average transient interstory drift ratios obtained from a set of MCE shaking in X direction

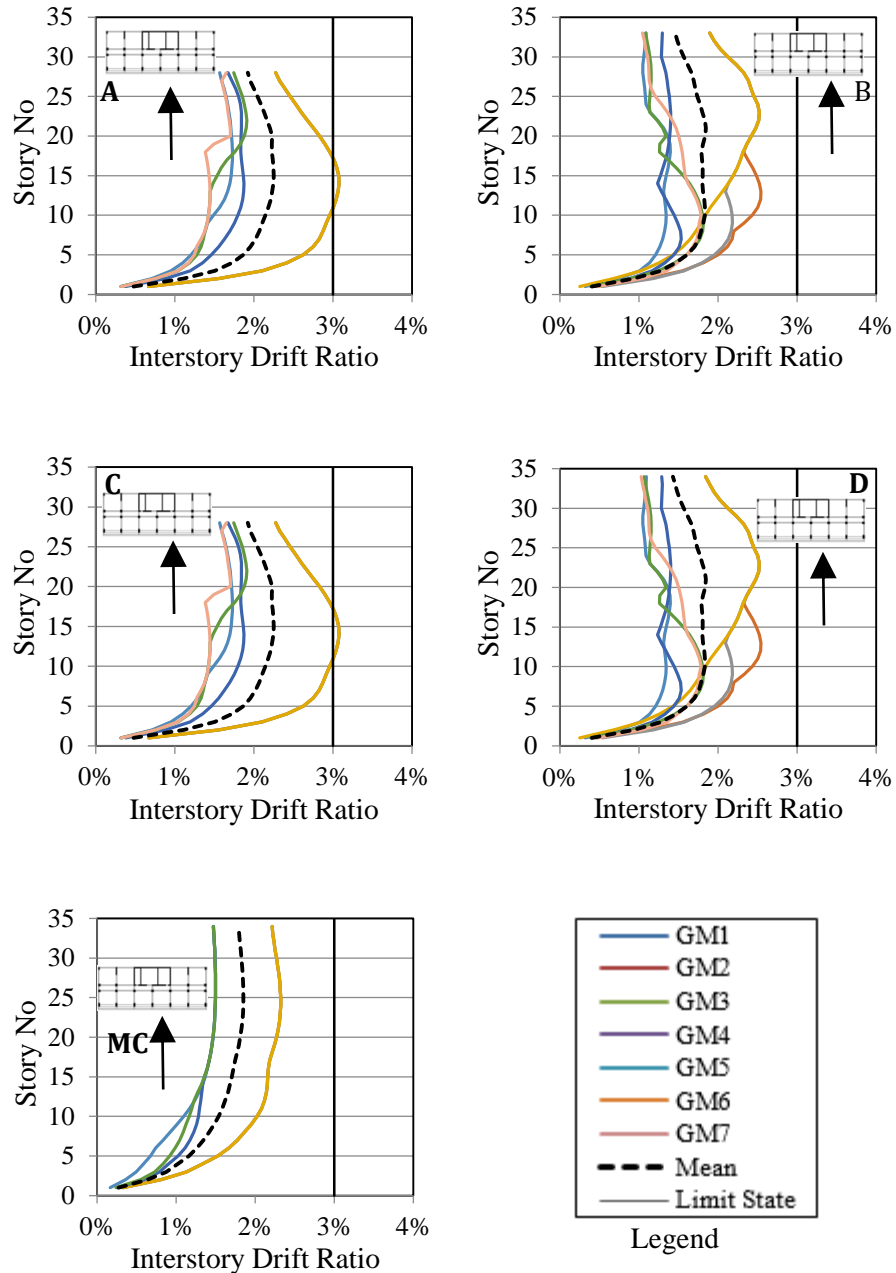


Figure 3.37. Maximum transient interstory drift ratios for each ground motion with maximum average transient interstory drift ratios obtained from a set of MCE shaking in Y direction.

3.6.2 Average Shear Stress and Axial Load Level of Shear Walls

As it can be seen the following maximum average shear stress and axial load level on shear walls SW2, SW3 and SW6 results of the revised case study (Figure 3.38- 3.43), nearly all targeted limit state is satisfied for both performance levels.

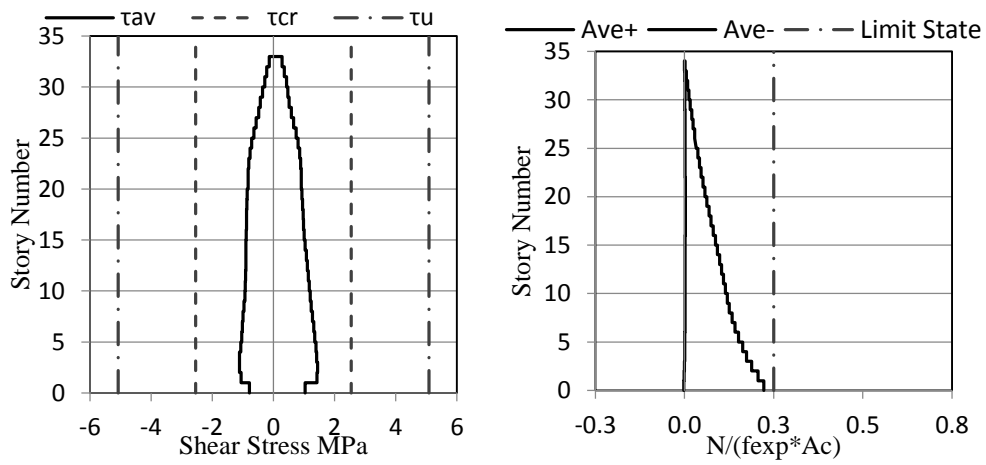


Figure 3.38. Average shear stress and axial load on shear wall SW2 under SLE shaking

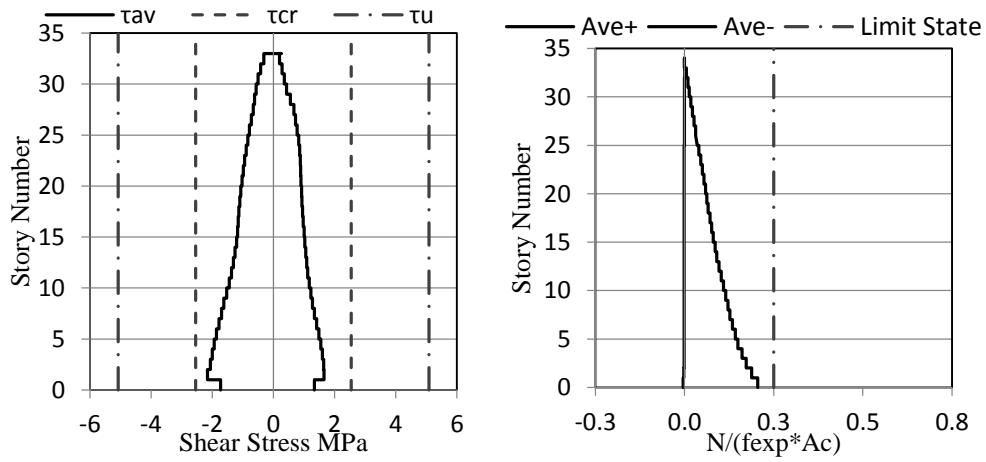


Figure 3.39. Average shear stress and axial load on shear wall SW3 under SLE shaking

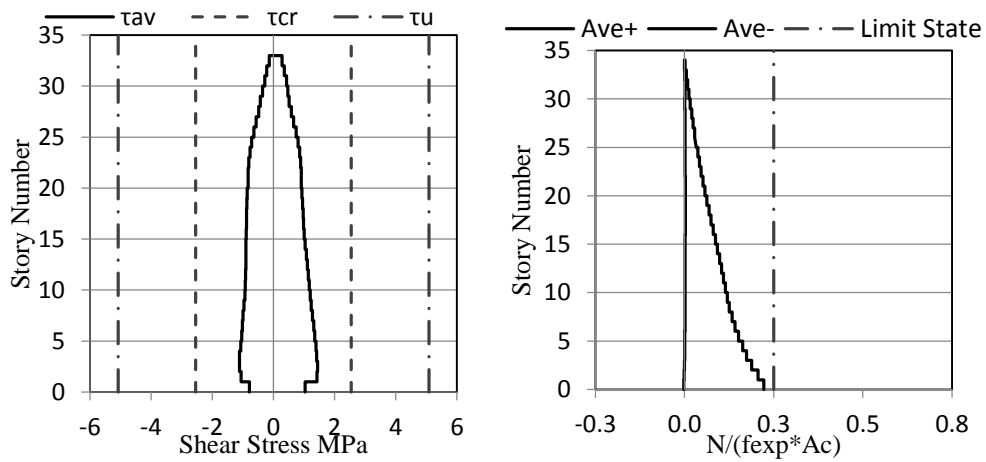


Figure 3.40. Average shear stress and axial load level on shear wall SW6 under SLE shaking

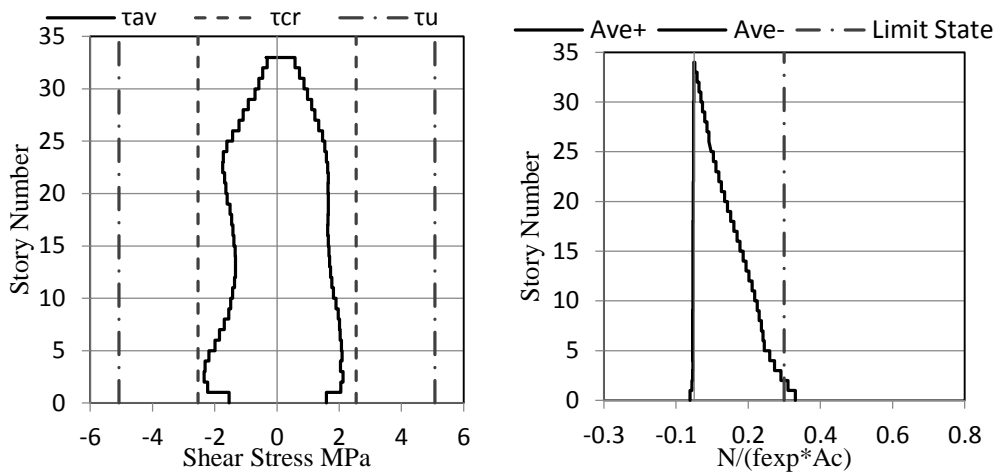


Figure 3.41. Average shear stress and axial load on shear wall SW2 under MCE shaking

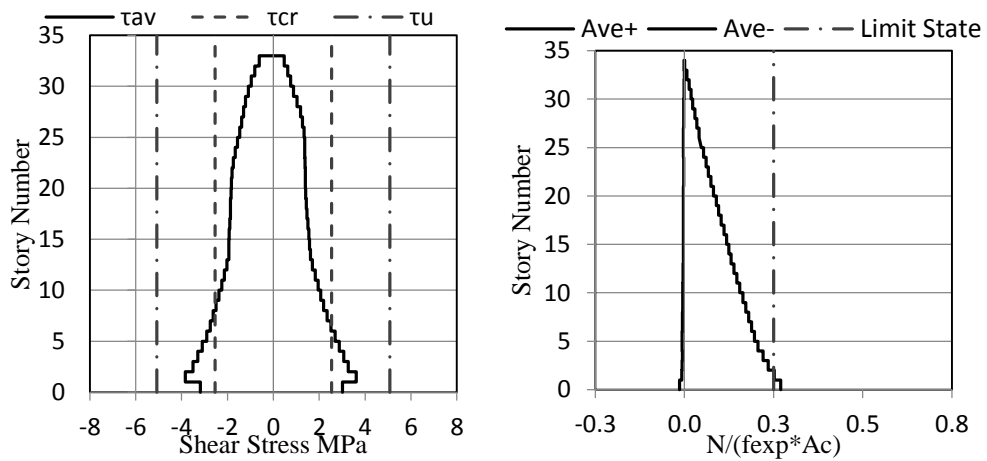


Figure 3.42. Average shear stress and axial load on shear wall SW3 under MCE shaking

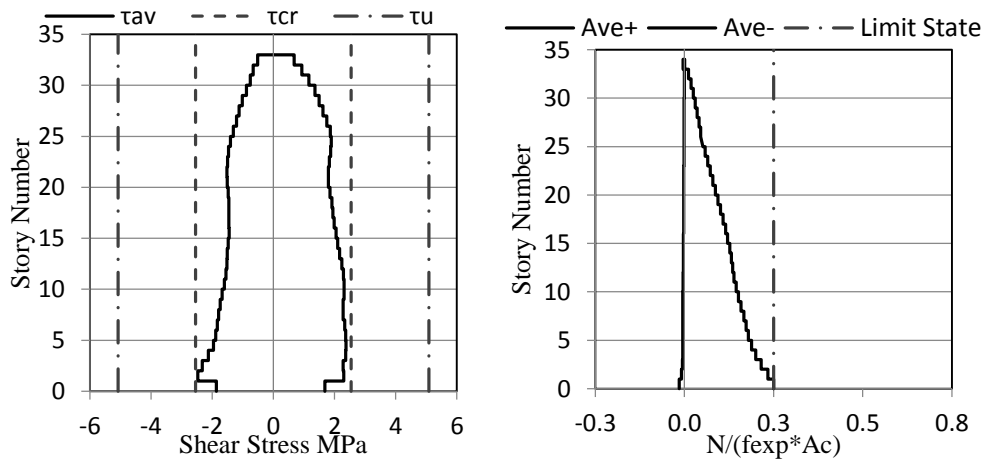


Figure 3.43. Average shear stress and axial load on shear wall SW6 under
MCE shaking

3.6.3 Axial Forces in Columns

Axial load level in all columns under SLE and MCE shaking is presented in Figure 3.44 and Figure 3.45 respectively. Axial load level in nearly all columns except R1, R2 and R3 under MCE shaking satisfies targeted performance levels. The columns which do not satisfy the required performance level should re-designed by increasing their dimension to satisfy the expected performance level. However, there is no need to re-analysis the structure after these revisions since these revisions are expected to have negligible effect on the lateral stiffness of the structure.

R1^{*}, R2^{*} and R3^{*} : Revision1, Revision2 and Revision3 respectively.

- R1^{*}: In revising the case study buildings column and shearwall dimensions, columns sizes of C10 and C12 should have been increased from 100x100cm to 120x120cm till the story number 15, not 12 to prevent the violation of the axial load ratio limit.
- R2^{*}: The dimensions of columns C16 and C17 should be revised again to obey the axial load ratio limits. This time, the dimensions of C16 and C17 should be increased till story number 5.
- R3^{*}: For the shown columns (C10 and C12), the dimensions should be revised to include the first three stories.

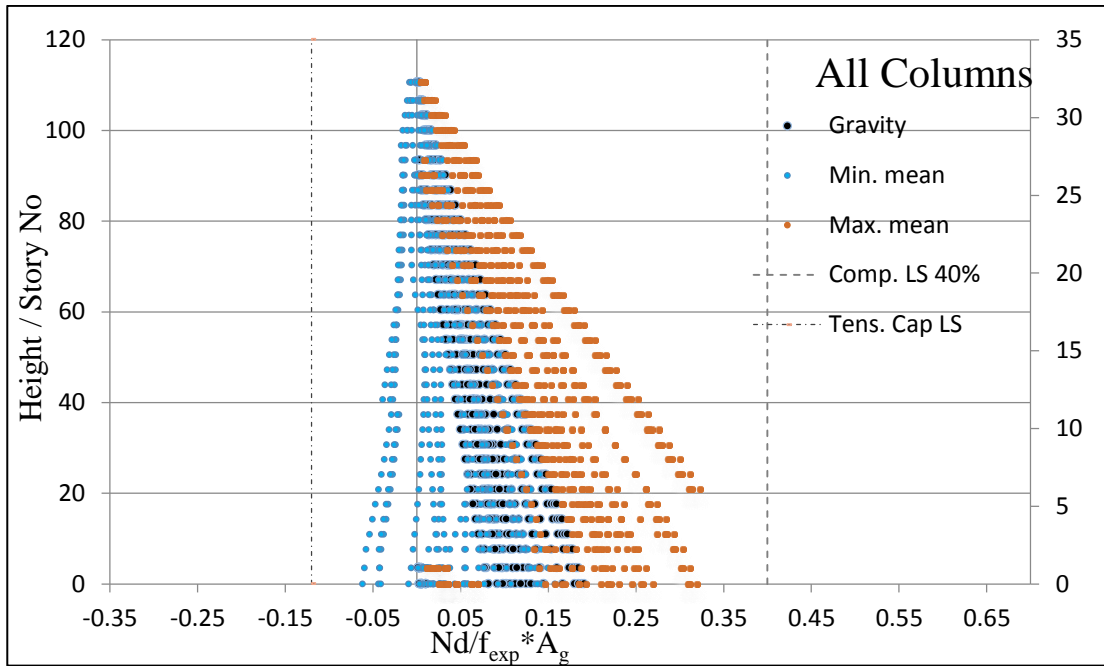


Figure 3.44. Average axial load level on all columns under SLE shaking

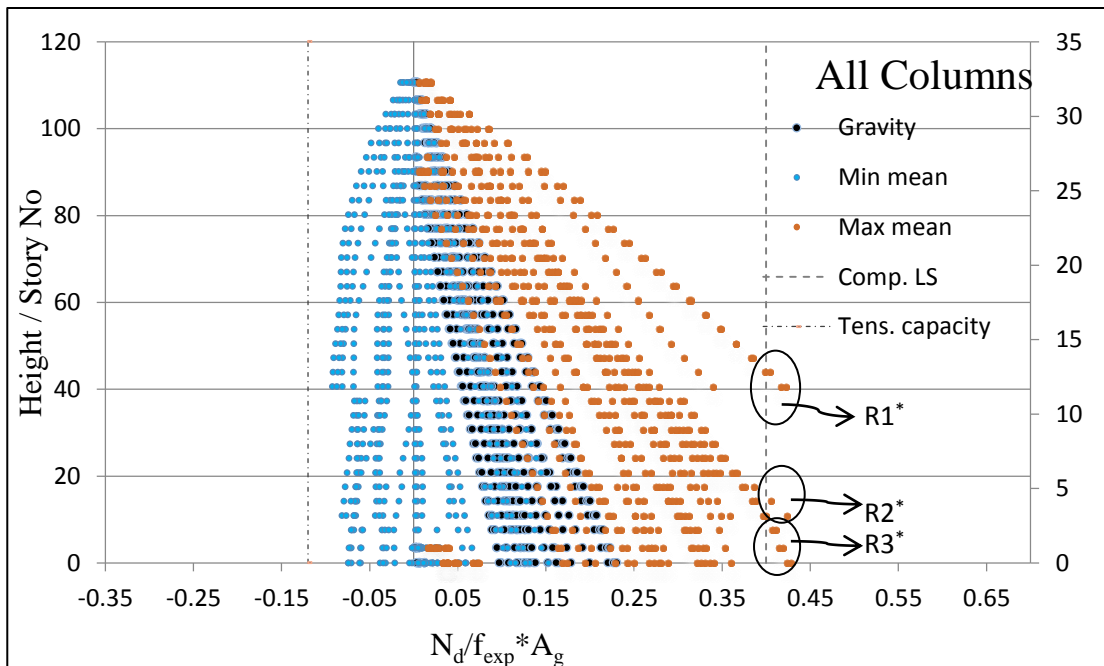


Figure 3.45. Average axial load level on all columns under MCE shaking

3.6.4 Axial Strain of Shear Walls

It can be observed in the axial strain results of shear walls (Figure 43 – 48) that, although the section dimension have been increased, axial tensile strain of core shear

wall segments (SW2, SW3 and SW6) has also been increased especially at the bottom of each shear walls and the upper stories of SW2 and SW6 under MCE shaking. While the upper stories of SW2 and SW6 have not yielded in the original case study, they have yielded in the revised case study due to the increasing demand under MCE excitation. Another reason that might trigger yielding at the upper story of shear walls is the reduction in the plan area of the structure after the roof level. The comparison and evaluation of the results of the original and revised case study are explained in Part 3.7. In the revised case study, each shear wall has yielded but the amount of yielding is under acceptable limits for collapse prevention performance level although the yielding at the upper story of shear walls are not a desired behavior

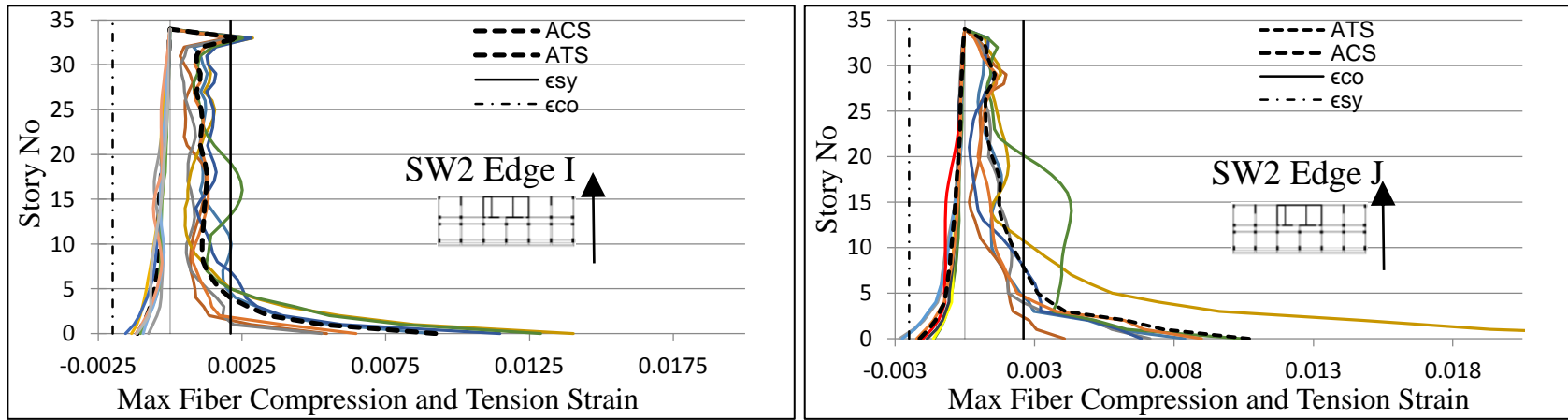


Figure 3.46. Axial strain at edge I (internal edge) and edge J (external edge) of shear wall SW2 under SLE shaking

601

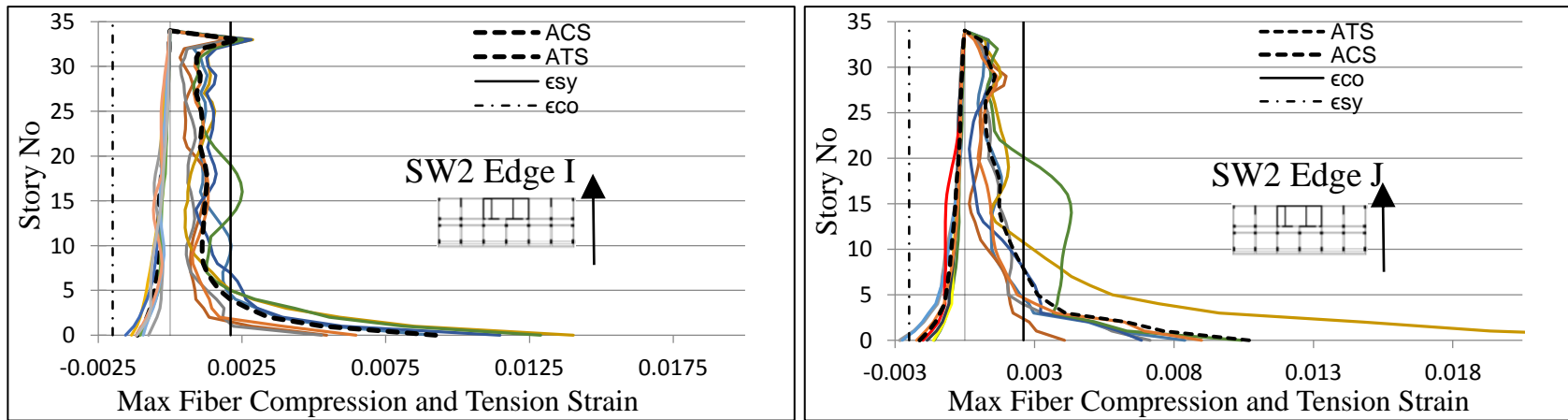


Figure 3.47. Axial strain at edge I (internal edge) and edge J (external edge) of shear wall SW2 under MCE shaking

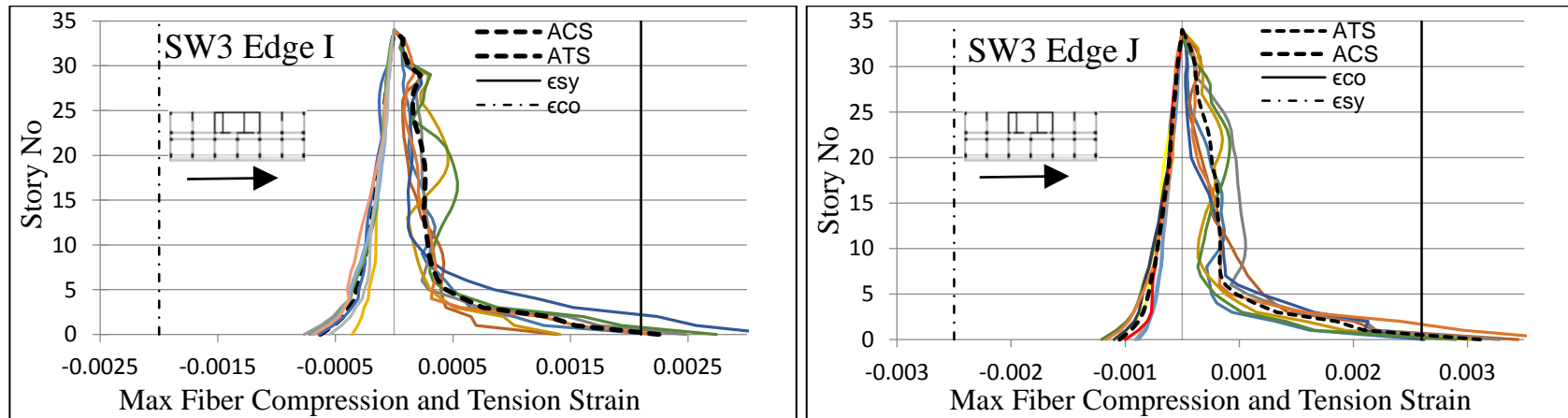


Figure 3.48. Axial strain at edge I (internal edge) and edge J (external edge) of shear wall SW3 under SLE shaking

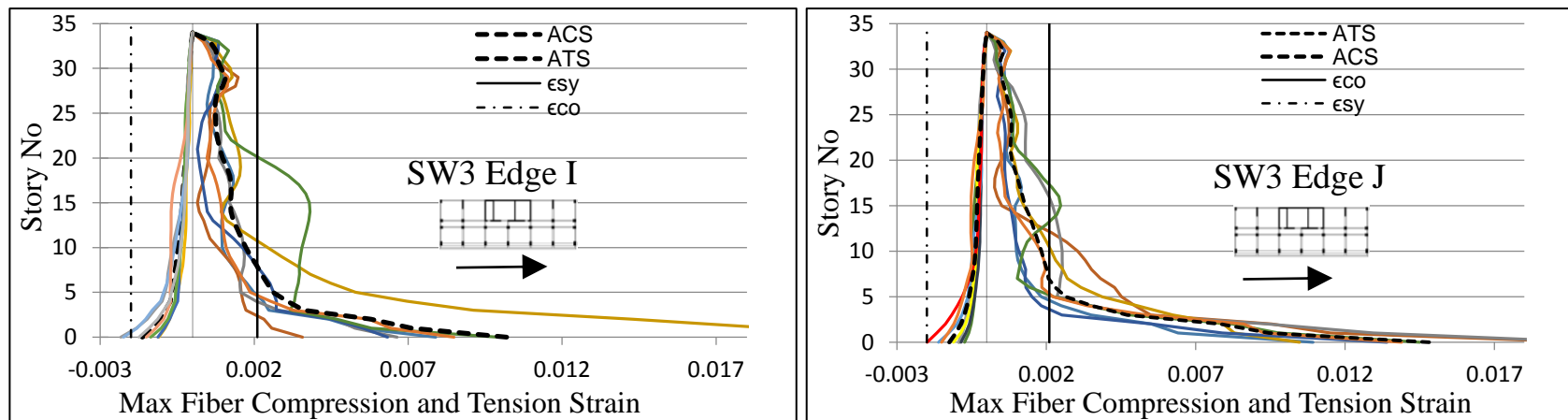


Figure 3.49. Axial strain at edge I (internal edge) and edge J (external edge) of shear wall SW3 under MCE shaking

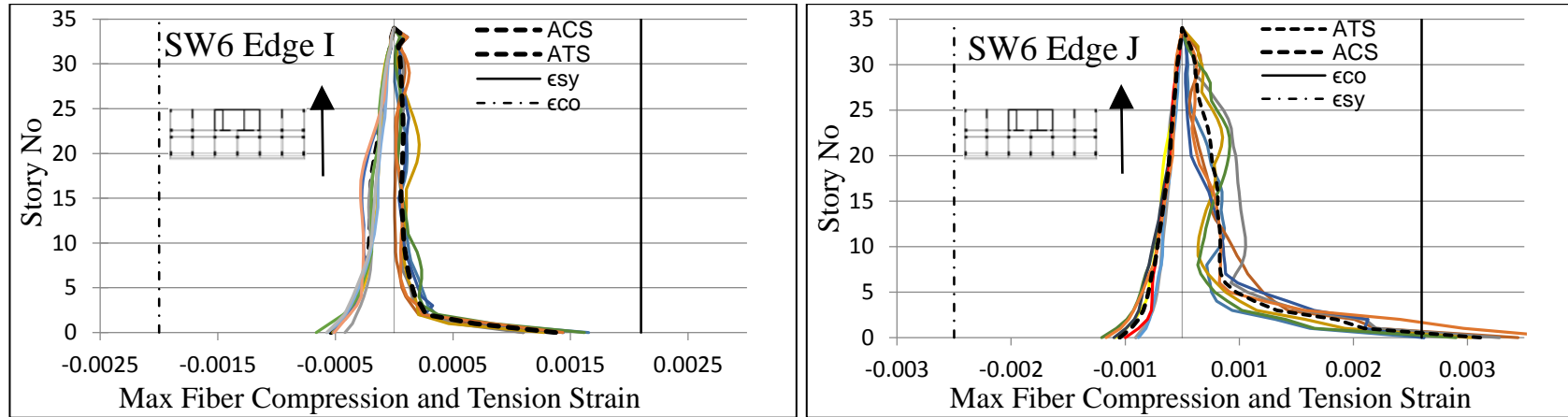


Figure 3.50. Axial strain at edge I (internal edge) and edge J (external edge) of shear wall SW6 under SLE shaking

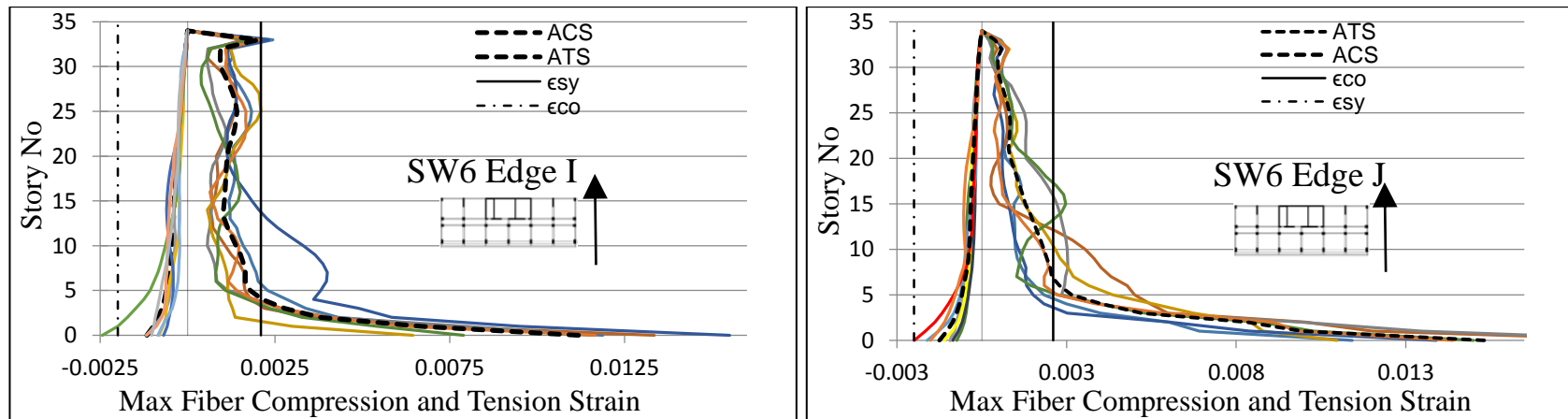


Figure 3.51. Axial strain at edge I (internal edge) and edge J (external edge) of shear wall SW6 under MCE shaking

3.6.5 Beam-end Average Curvature

In this part, maximum average curvature of three selected critical beams (B1, B2 and B3) in a representative story when subjected to earthquake excitation is presented through all floors. The inelastic properties of each of these beams do not change through all story levels. Each of these beams with their edges I and J, and the direction of earthquake horizontal components are shown in Figure 3.52. It is important to note that excitations are applied only in the positive x and y directions. Thus, the conclusions do not comprise the effect of earthquake direction, which is out-of-scope of this dissertation. Each end of the beams also has a hinge which receives negative and positive actions. The sign convention for a beam element is shown in Figure 3.53.

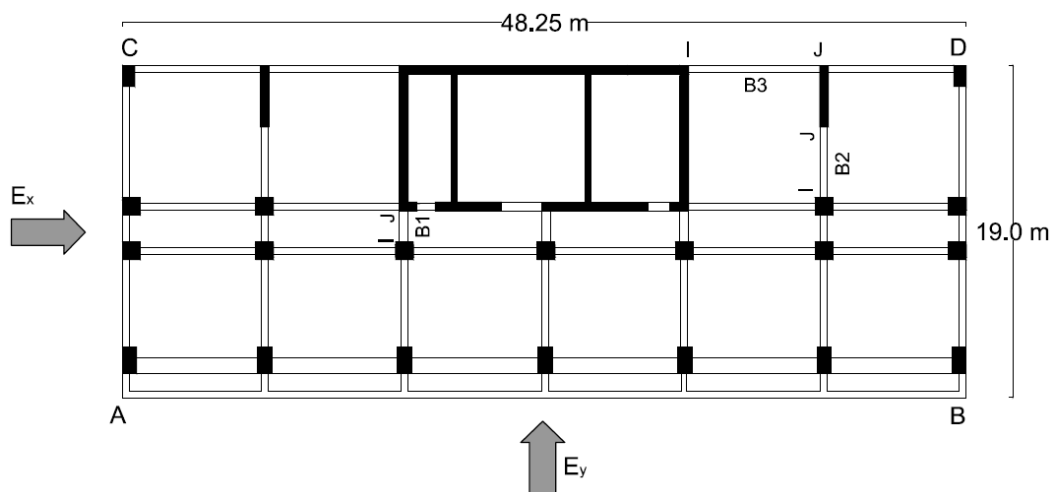


Figure 3.52. Selected critical beams and direction of earthquake horizontal components

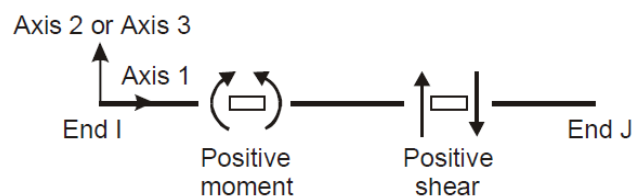


Figure 3.53. Sign convention

Instead of using average strain or rotation values in order to assess the member behavior under an expected earthquake shaking, some researchers propose to employ

some limit values depend on curvature. The following curvature limits can be utilized to assess the member behavior in this study [Sucuoğlu, 2014].

$$\phi_{av} < \phi_y : \text{No damage}$$

$$\phi_y < \phi_{av} < 0.75\phi_{max} : \text{Significant damage region}$$

$$0.75\phi_{max} < \phi_y < \phi_{max} : \text{Severe damage region}$$

Figure 3.54 and 3.55 illustrate the maximum values of average moments and curvatures for beam B1 obtained under the SLE and MCE shakings. In these figures, the distribution of positive moment and curvature values at the end I, negative moment and curvature values at the end I, positive moment and curvature values at the end J and negative moment and curvature values at the end J along the height of the building are shown in rows 1-4, respectively. Also, yield curvature and moment limits for beams are marked with solid vertical lines on these graphs.

As it is illustrated in Figure 3.54, some minor yielding (mean results are used for assessment) occurs under SLE excitations. These damages which are slightly beyond yield point may be acceptable for service level evaluation. It can be easily seen from Figure 3.54 that in positive end I and negative end J cases, although mean curvatures are detected to be beyond the yield limit, mean moment values are apparently below yield moment, which is one of the major drawbacks of presenting averaged results. As it is illustrated in Figure 3.55, significant plastic deformations occur in negative end I and positive end J under MCE excitations. Relatively slight plastic deformation is observed in positive end I and negative end J. These damage states are acceptable for the collapse prevention level. In addition, results indicate that the contribution of higher modes on the response of the beam members is significant. Similar results are also observed for B2, which are illustrated in Figures 3.56 and 3.57.

The obtained results of B3 differ from B1 and B2 results since direction of joist beam is extended along the longitudinal direction of structure and the beam is located between SW3 and SW7. As it can be seen in Figures 3.58, these damages which are below yield point are acceptable for SLE. In addition, no damage is observed in positive end I under SLE and MCE excitations. On the other hand, some minor plastic deformation is observed under MCE excitations. These damage states are also acceptable for the collapse prevention level.

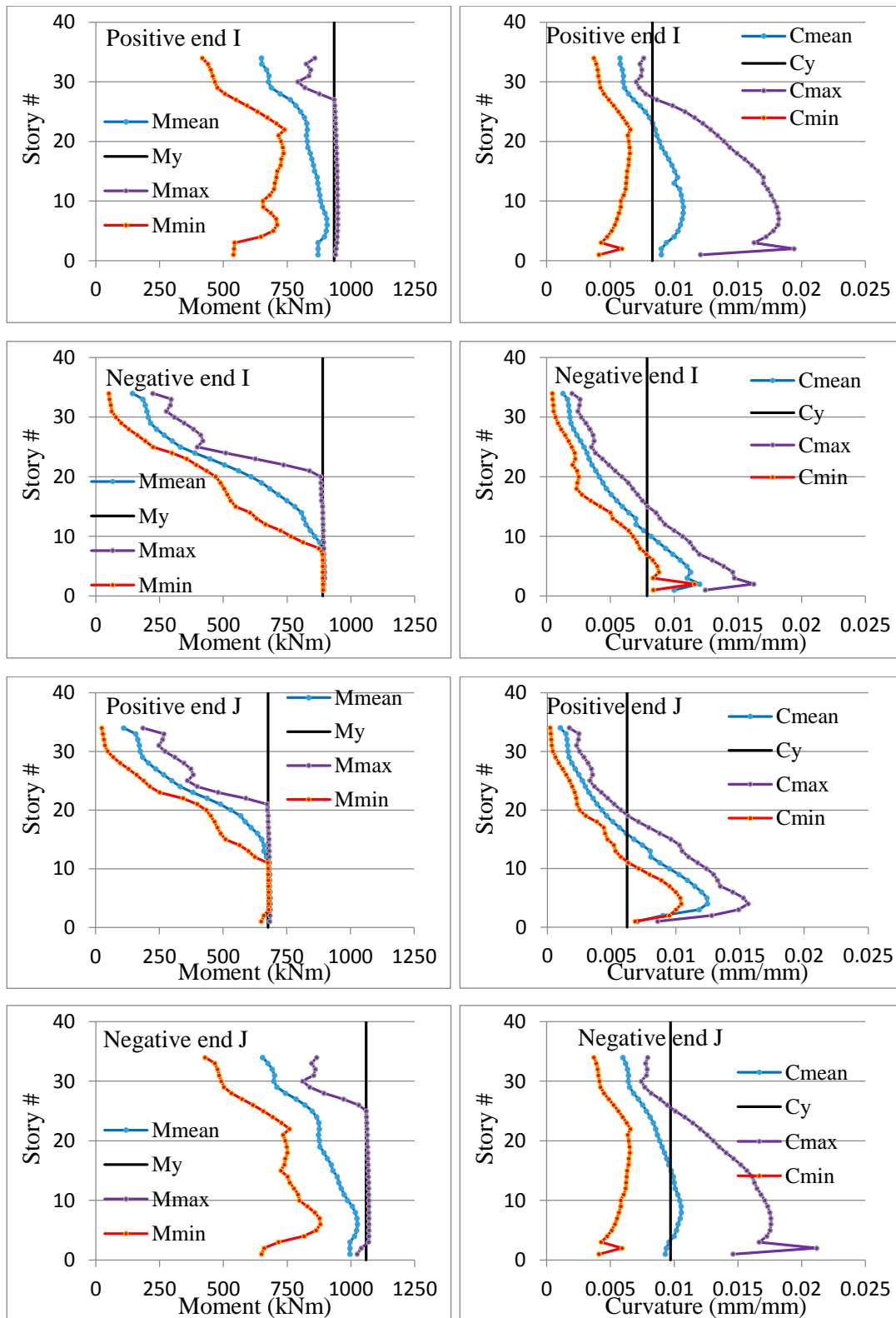


Figure 3.54. The distribution of positive moments and curvatures at the end I, negative moments and curvatures at the end I, positive moments and curvatures at the end J and negative moments and curvatures at the end J along the height of the building under SLE shaking (Beam B1).

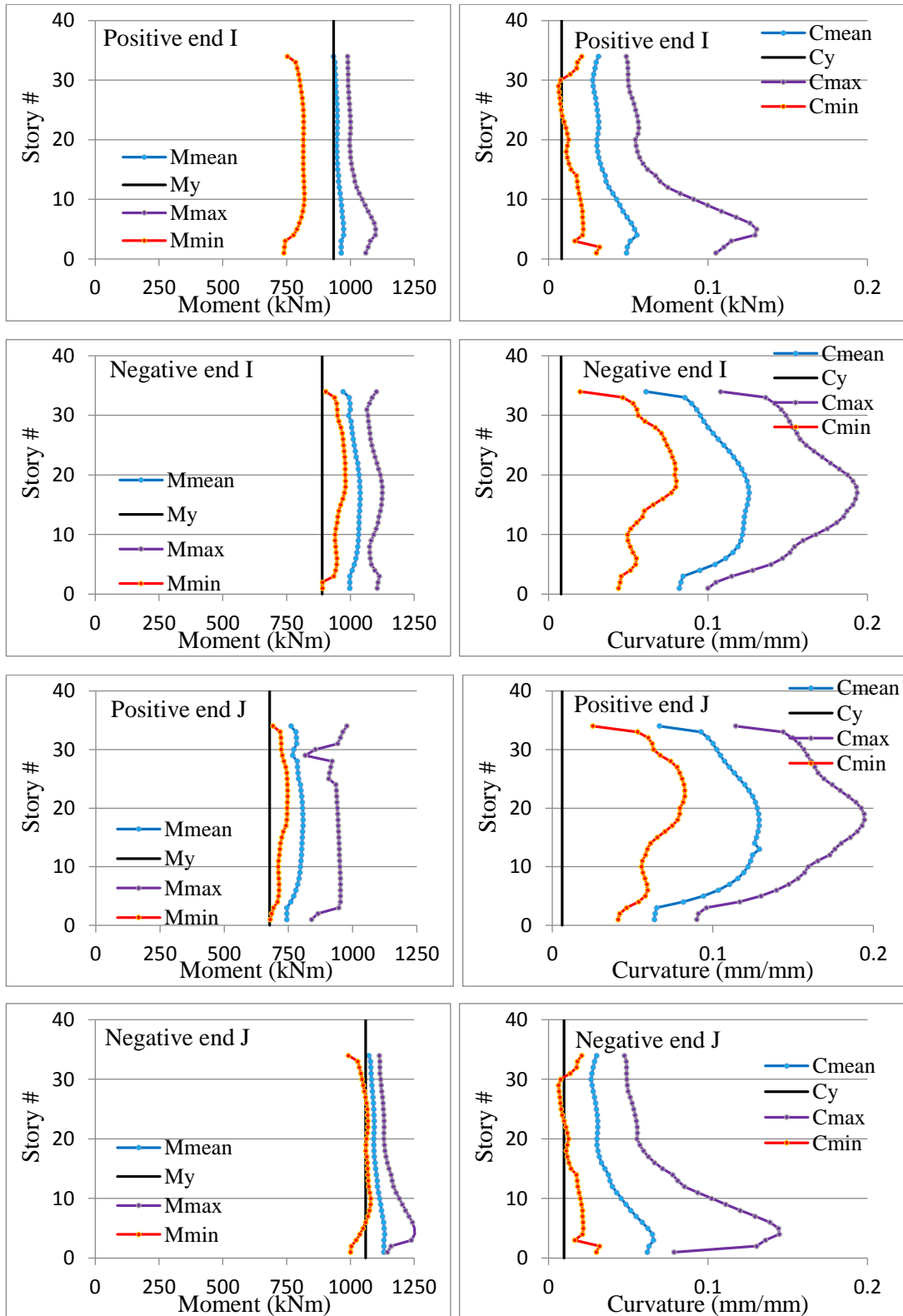


Figure 3.55. The distribution of positive moments and curvatures at the I end, negative moments and curvatures at the I end, positive moments and curvatures at the J end and negative moments and curvatures at the J end along the height of the building under MCE shaking (Beam B1)

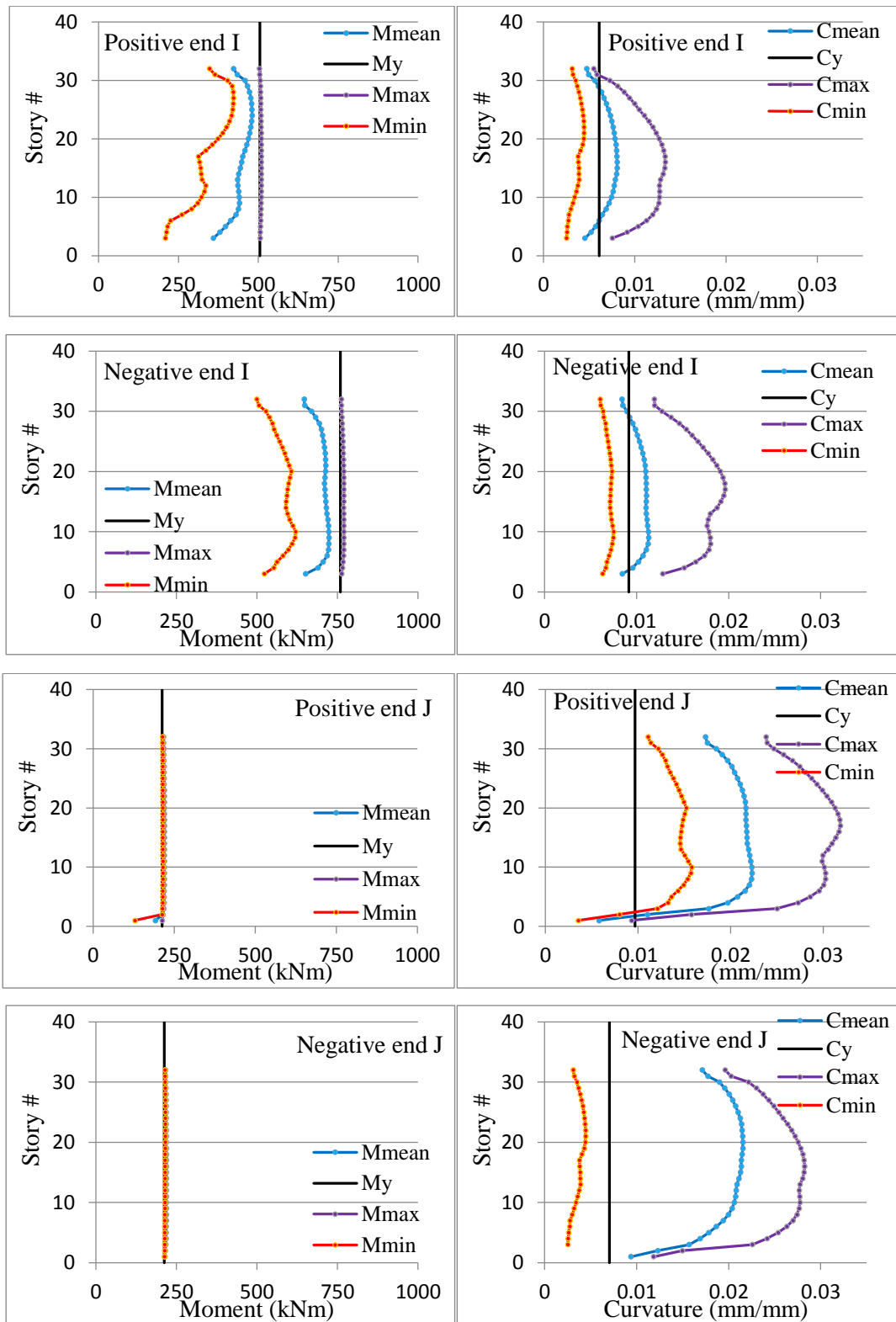


Figure 3.56. The distribution of positive moments and curvatures at the end I, negative moments and curvatures at the end I, positive moments and curvatures at the end J and negative moments and curvatures at the end J along the height of the building under SLE shaking (Beam B2)

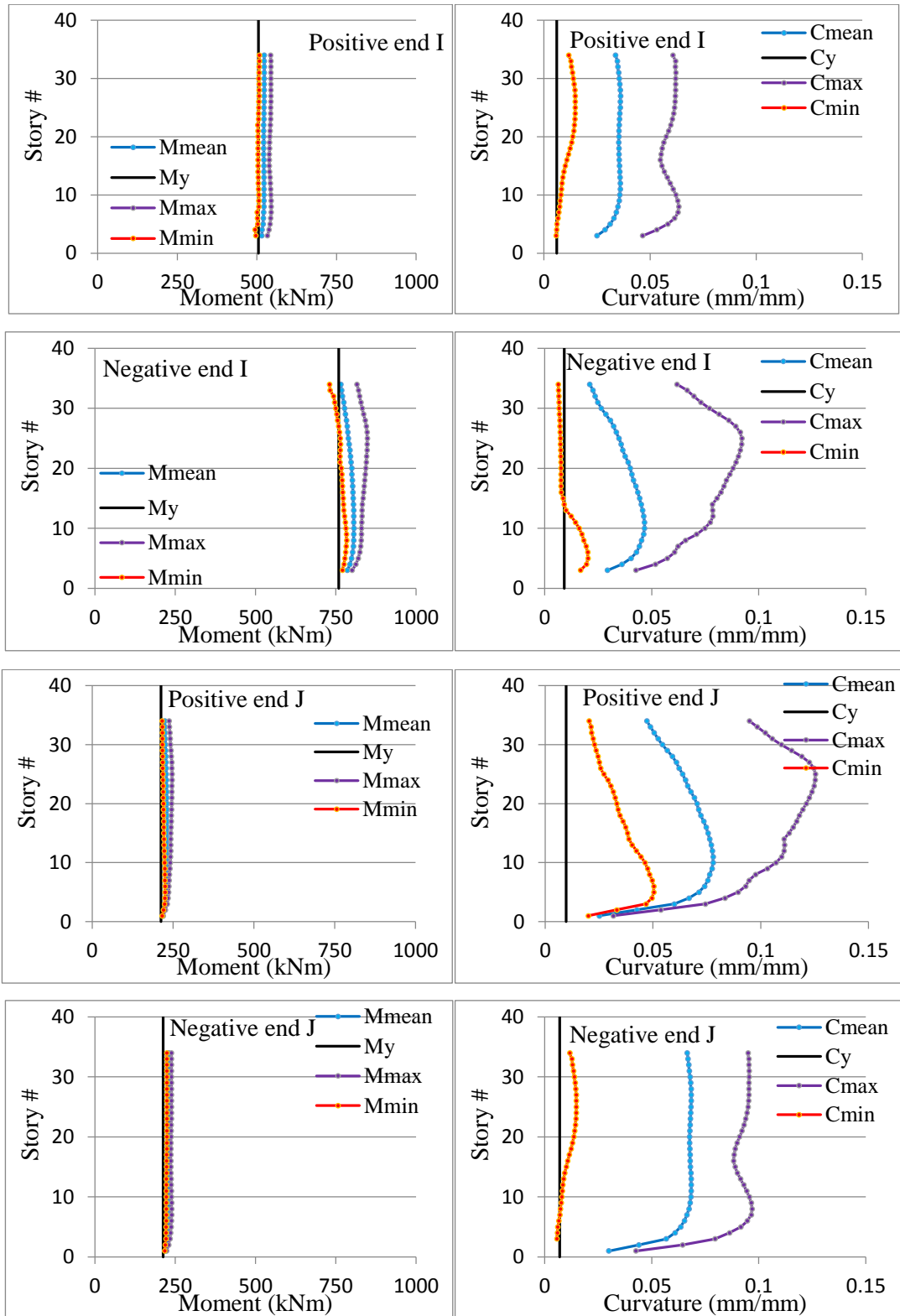


Figure 3.57. The distribution of positive moments and curvatures at the end I, negative moments and curvatures at the end I, positive moments and curvatures at the end J and negative moments and curvatures at the end J along the height of the building under MCE shaking (Beam B2).

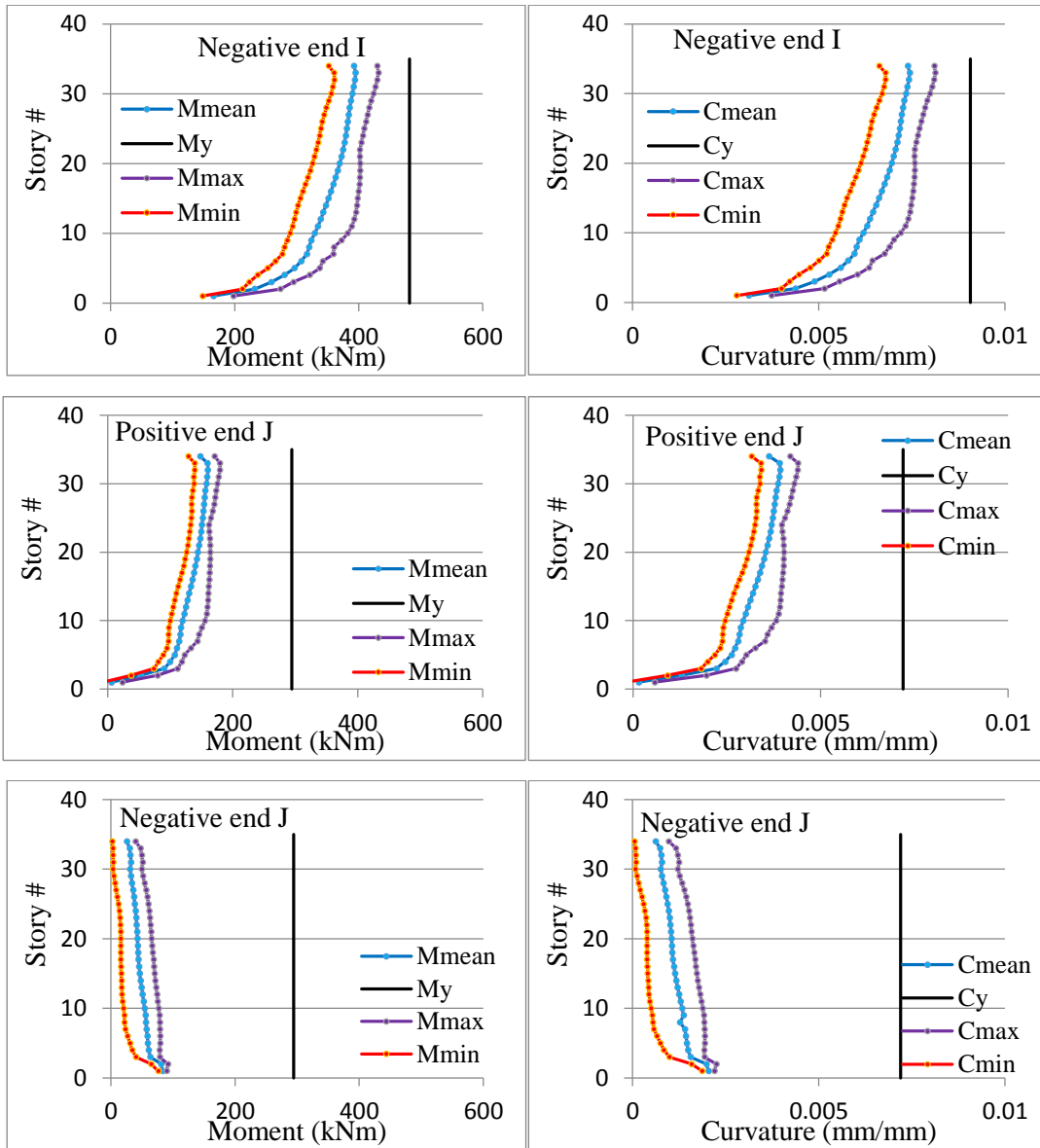


Figure 3.58. The distribution of negative moments and curvatures at the end I, positive moments and curvatures at the end J and negative moments and curvatures at the end J along the height of the building under SLE shaking (Beam B3)

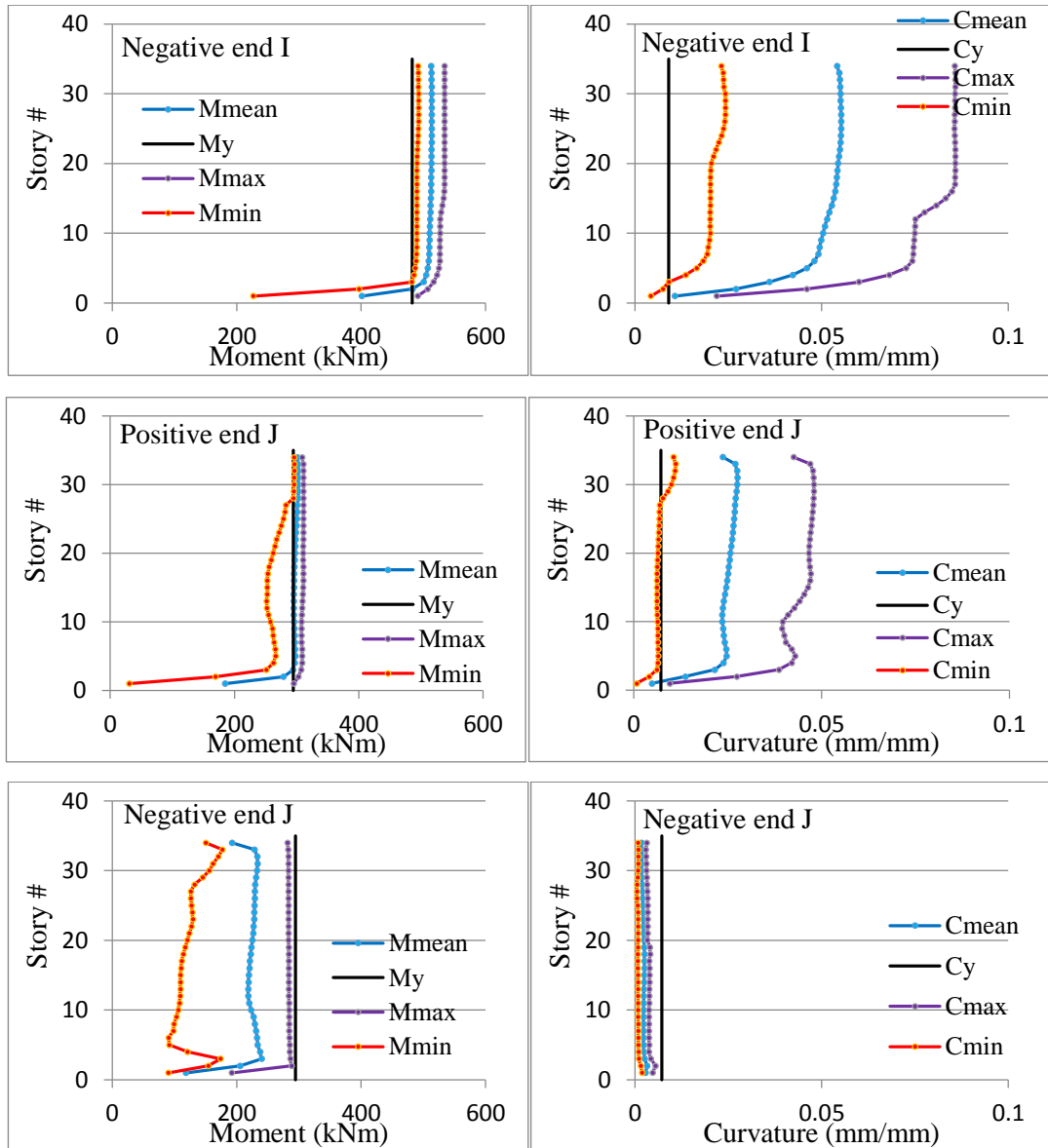


Figure 3.59 The distribution of negative moments and curvatures at the end I, positive moments and curvatures at the end J and negative moments and curvatures at the end J along the height of the building under MCE shaking (Beam B3)

3.6.6 Coupling Beam Results

The expected performance of coupling beams under SLE shaking is to remain elastic. Moreover, the coupling beams can yield under MCE shaking but they are supposed to be controlled by shear. Accordingly, shear displacement hinge was defined at the mid-point of each coupling beam. The mean chord displacement results obtained from analyses are presented in Figures 3.60 - 3.64 for both performance levels. The sign conventions for coupling beam elements are similar to beam members, which was shown in Figure 3.53. Damages occurred in CB3 under SLE shaking are below the immediate occupancy limit state and damages occurred in CB3 under MCE shaking are below the collapse prevention limit state. Accordingly, the building maintains its serviceability condition under SLE shaking and its stability under MCE shakings. Targeted limit states are satisfied for coupling beams. In addition, the contribution of higher modes to response of the coupling beams is also observed.

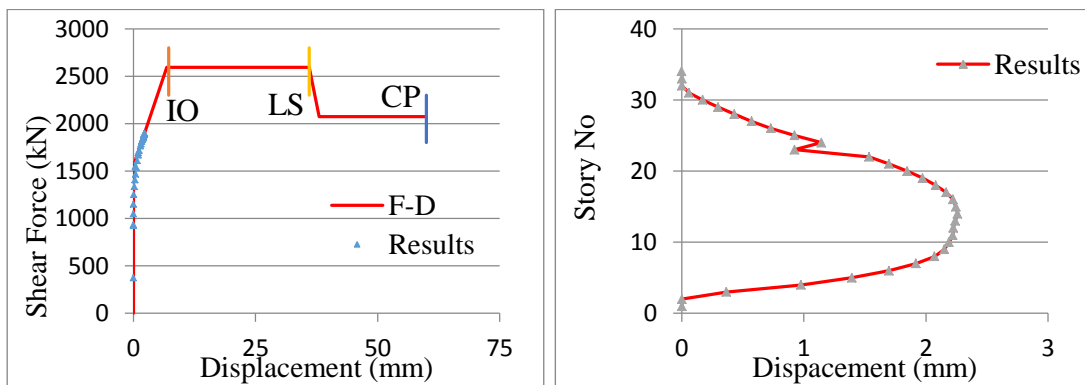


Figure 3.60 Maximum average positive chord displacement hinge for CB3 under SLE shaking.

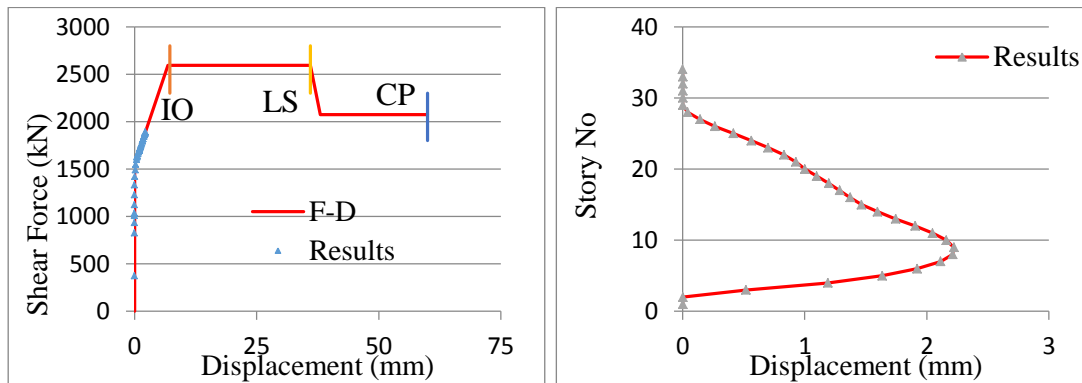


Figure 3.61 Maximum average negative chord displacement for CB3 under SLE shaking.

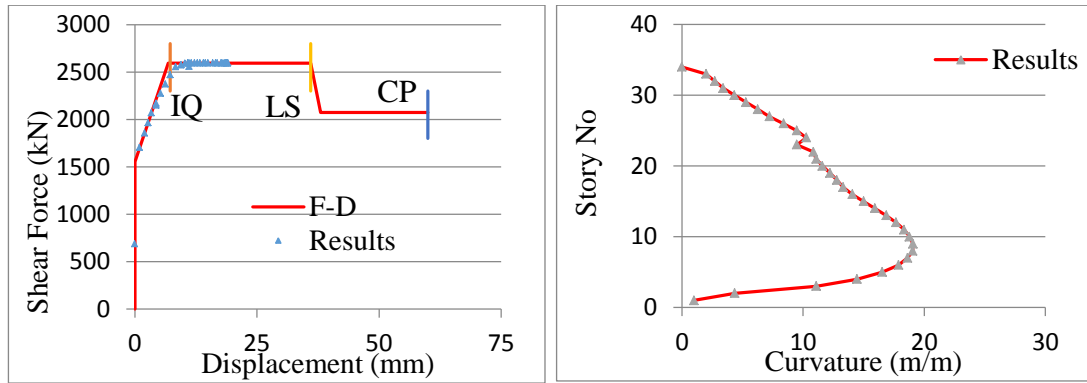


Figure 3.62 Maximum positive chord displacement for CB3 under MCE shaking.

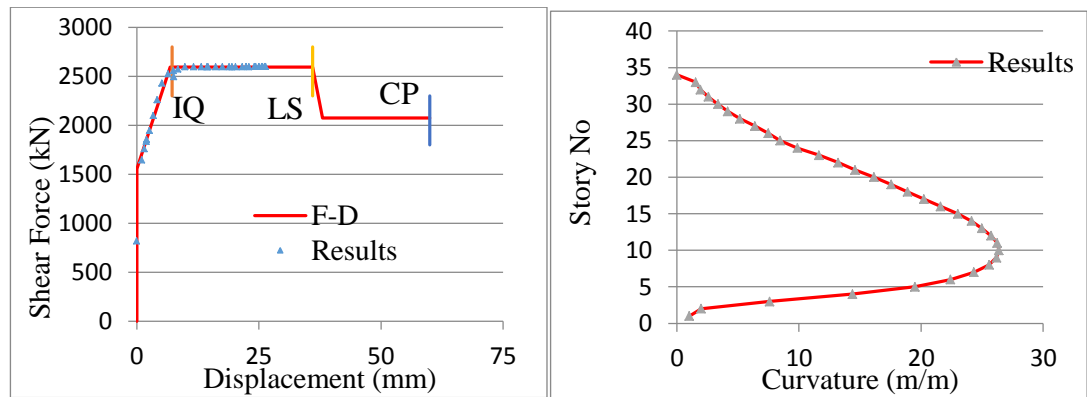


Figure 3.63 Maximum negative chord displacement for CB3 under MCE shakings.

3.7 Comparison of Results from the Original and Revised Case Studies

In light of results of the case study and revised case study, interstory drift ratios and axial strains, axial load ratio and shear stress of shear wall SW2, SW3 and SW6 are compared with each other. The results indicate that although the section dimensions have increased, axial tensile strain of core shear wall segments, especially at the bottom of each shear wall (SW2, SW3 and SW6), and interstory drift ratios (points C and D in the X direction and points A and C in the Y direction) have also increased slightly because of the increased torsional irregularity. This is because; the building tends to show more torsional rotations due to the shift in the center of rigidity caused by the stiffness increase in the shear wall SW3. In other words, the increase in the sizes of columns and shearwalls causes a modification of the seismic properties of the selected case study building but the capacity improvement is evidently more than

the demand increase as expected. On the other hand, shear stress and axial load ratio on each shear wall has reduced due to the increased section thicknesses. The selected results are presented below.

3.7.1 Comparison of Drift Results

The following symbols are used in comparing results of drift ratios.

CS: maximum average transient interstory drift ratio of case study

RS: maximum average transient interstory drift ratio of revised case study

LS: Limit state value

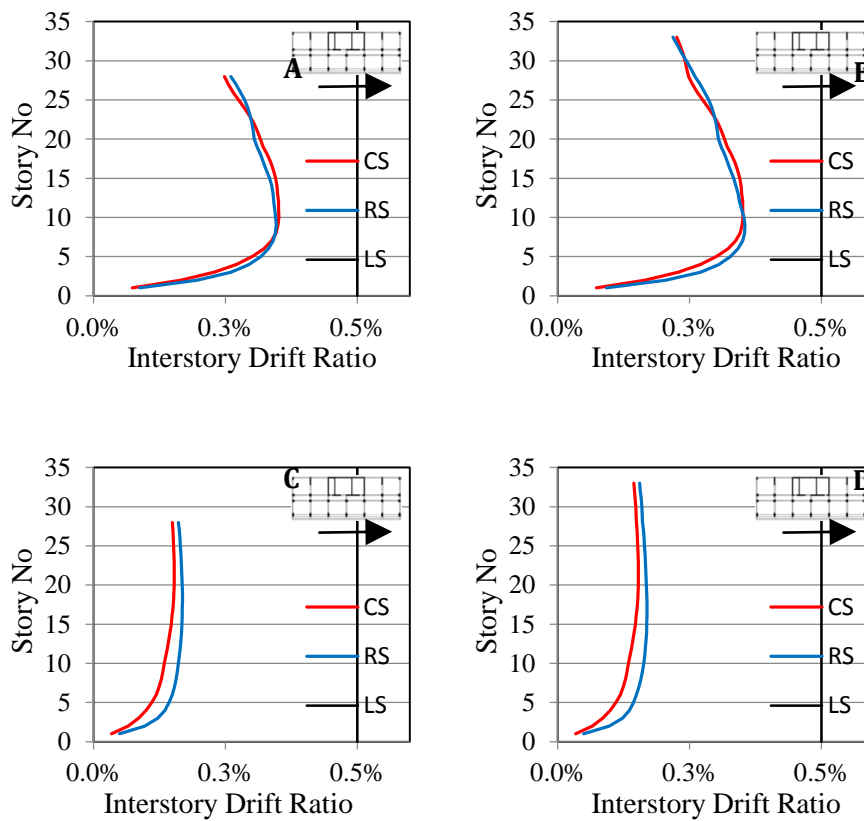


Figure 3.64 Comparison mean interstory drift results of original case study with revised case study under SLE shakings in X direction

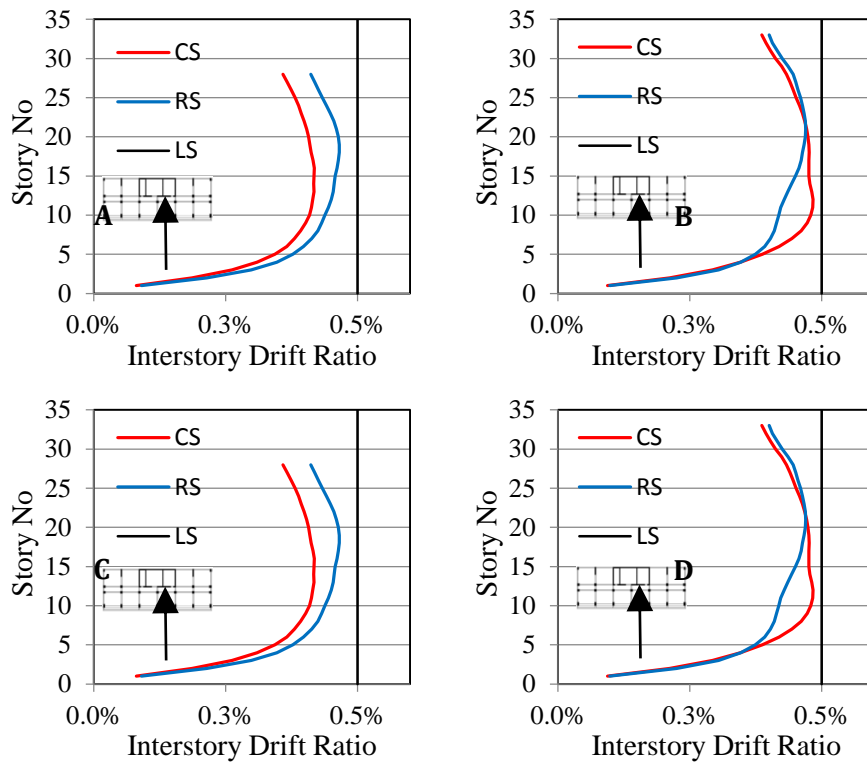


Figure 3.65 : Comparison mean interstory drift results of original case study with revised case study under SLE shaking in Y direction

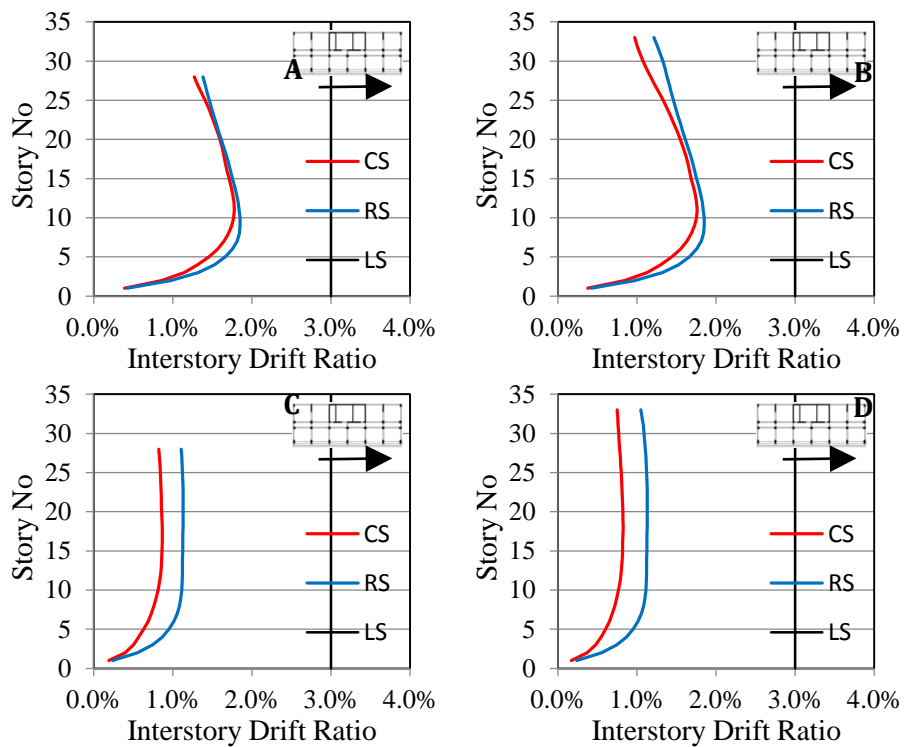


Figure 3.66 : Comparison mean interstory drift results of original case study with revised case study under MCE shakings in X direction

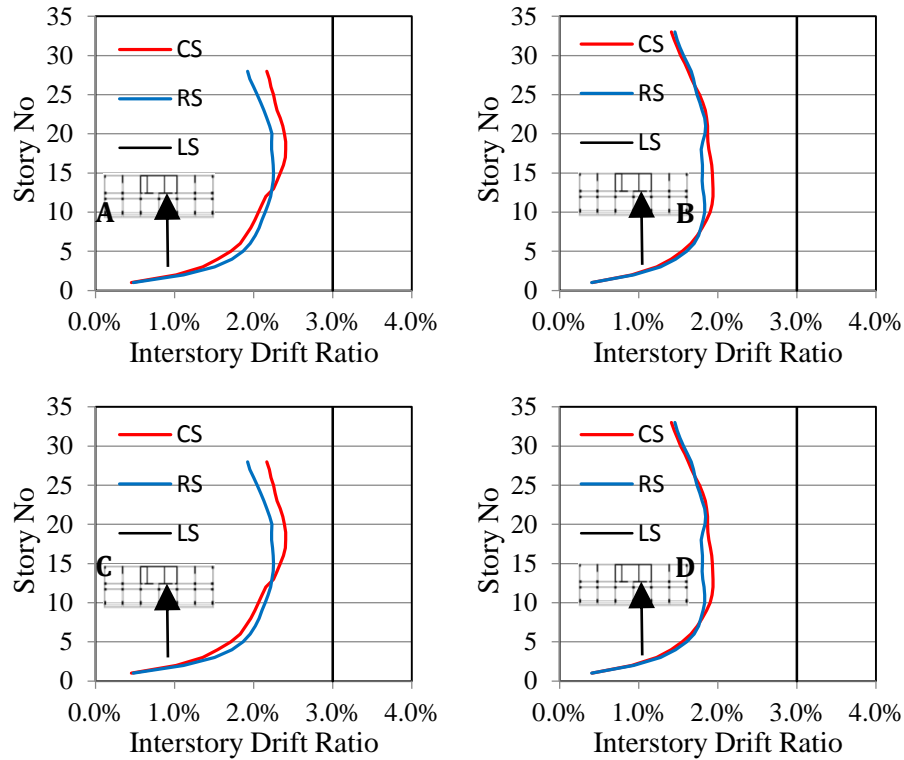


Figure 3.67 Comparison mean interstory drift results of original case study with revised case study under MCE shakings in Y direction

3.7.2 Comparison of Average Shear Stress and Axial Loads and Axial Strain of Shear Walls

The following symbols are used in comparing results of shear stress and axial load level of shear walls:

CS, RS: Mean shear stress results of the original and revised case study respectively.

CS-C, RS-S: Mean compressive axial load level of the original and revised case study respectively.

CS-T, RS-T: Mean tensile axial load level results of the original and revised case study respectively

τ_{cr} , τ_u : The cracking shear stress and ultimate shear stress respectively.

C-LS, T-LS : Compression limit state (30%) and tension limit state respectively.

CS-C, CS-T : Mean compressive and tensile strain of original case study.

RS-C,RS-T : Mean compressive and tensile strain of revised case study respectively.

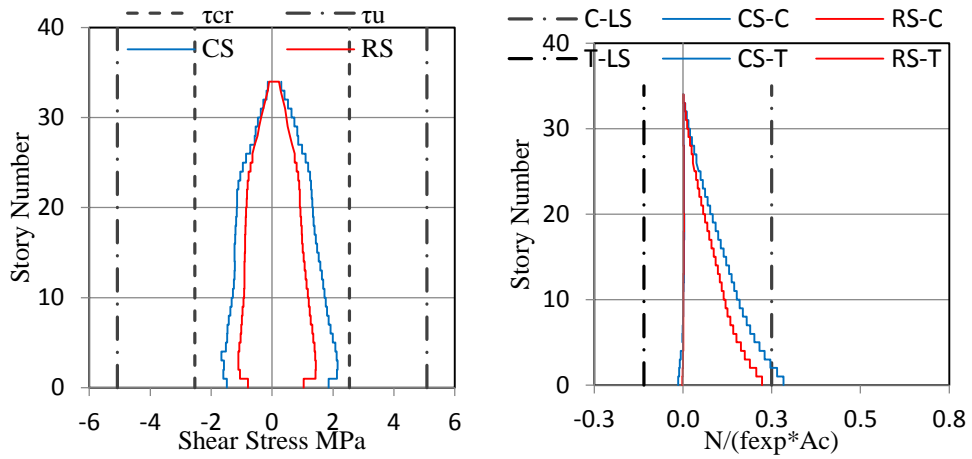


Figure 3.68 Comparison average shear stress and axial load level of shear wall SW2 results of case study model with revised case study model under SLE shaking

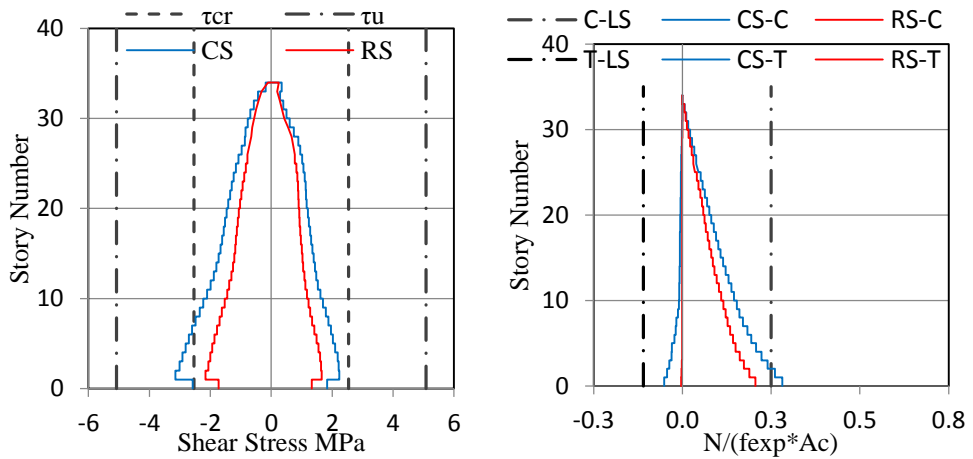


Figure 3.69 Comparison average shear stress and axial load level of shear wall SW3 results of case study model with revised case study model under SLE shaking

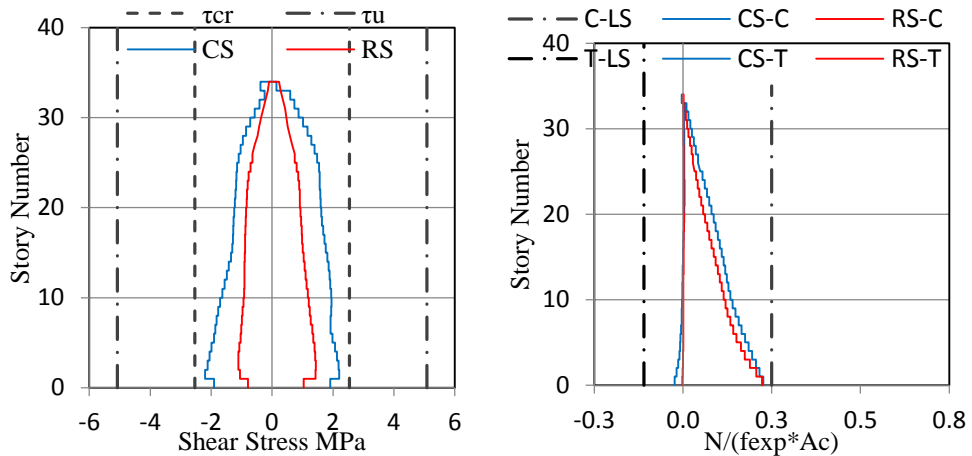


Figure 3.70 Comparison average shear stress and axial load level of shear wall SW6 results of case study model with revised case study model under SLE shaking

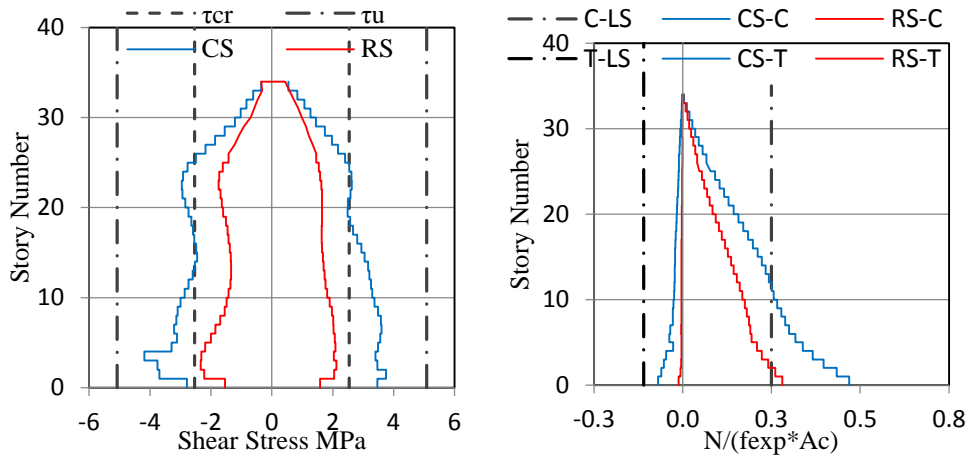


Figure 3.71 Comparison average shear stress and axial load level of shear wall SW2 results of case study model with revised case study model under MCE shaking

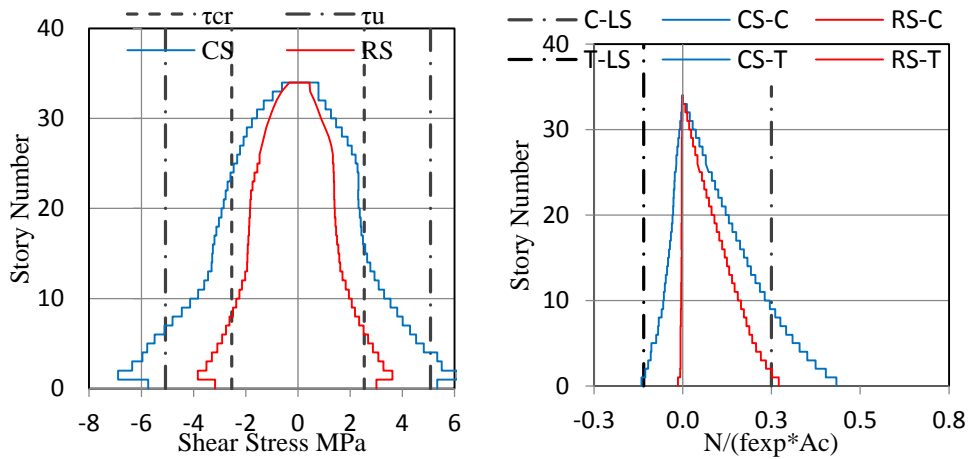


Figure 3.72 Comparison average shear stress and axial load level of shear wall SW3 results of case study model with revised case study model under MCE shaking

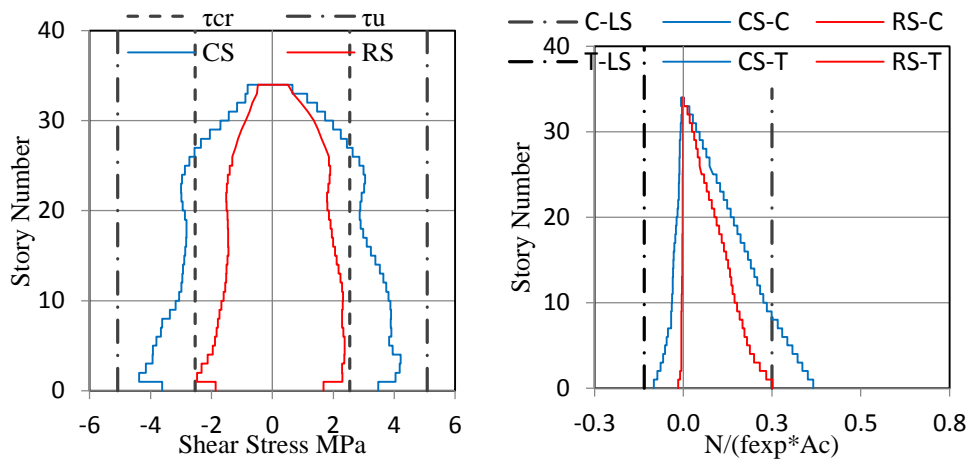


Figure 3.73 Comparison average shear stress and axial load level of shear wall SW6 results of case study model with revised case study model under MCE shaking

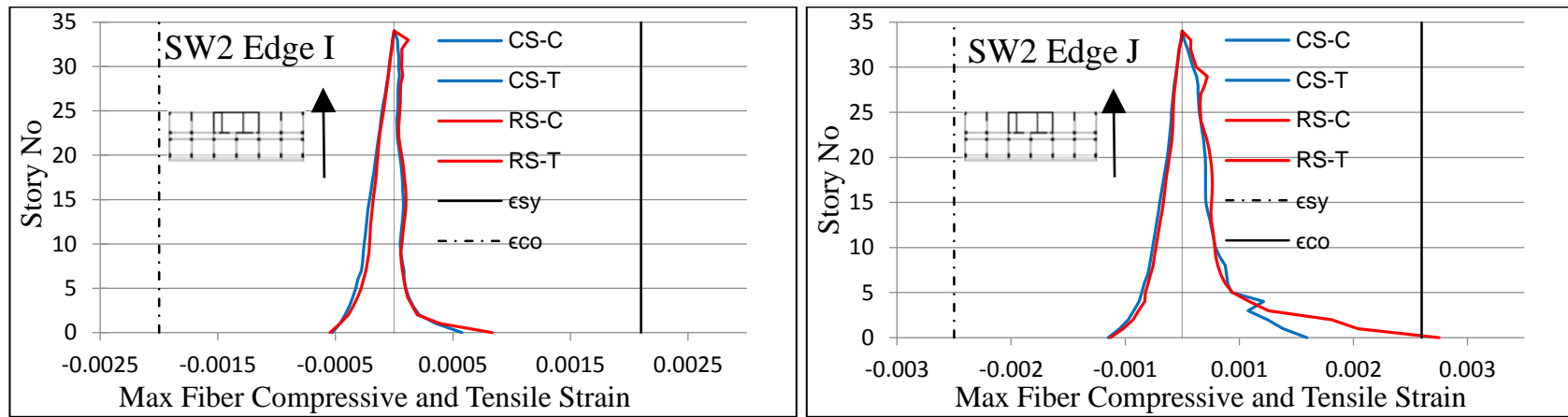


Figure 3.74 Comparison mean axial strain results of case study model with revised case study model under SLE shaking

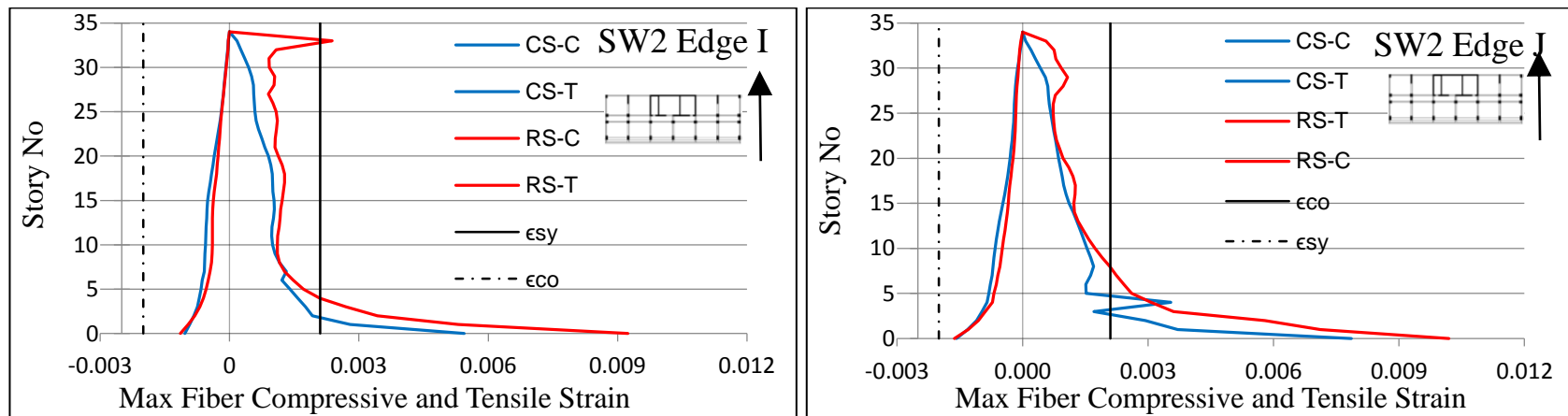


Figure 3.75 Comparison max fiber compressive and tensile strain of SW2 under MCE shaking.

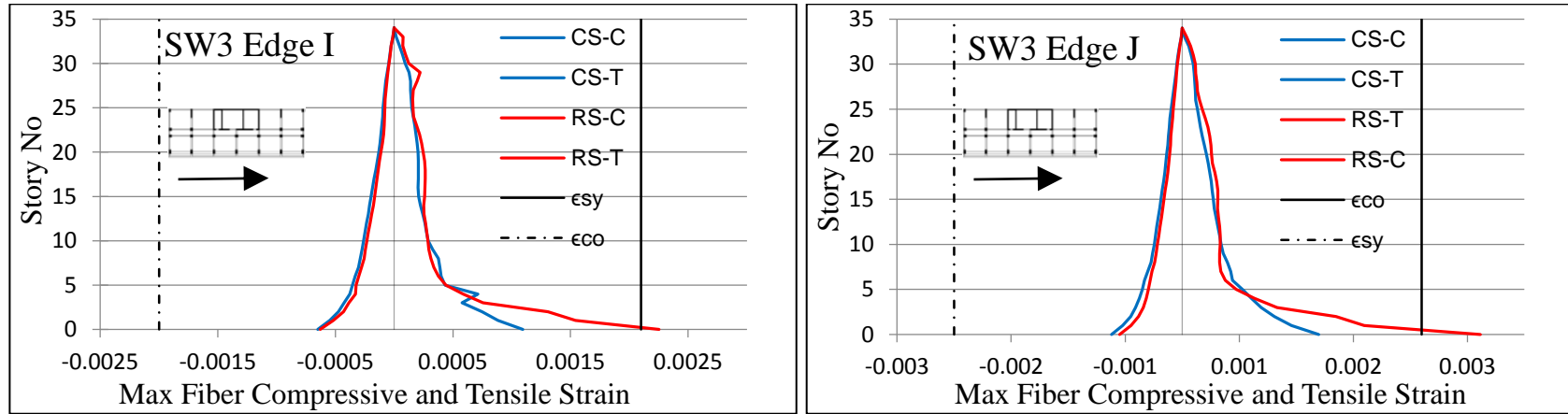


Figure 3.76 Comparison max fiber compressive and tensile strain of SW3 under SLE shaking.

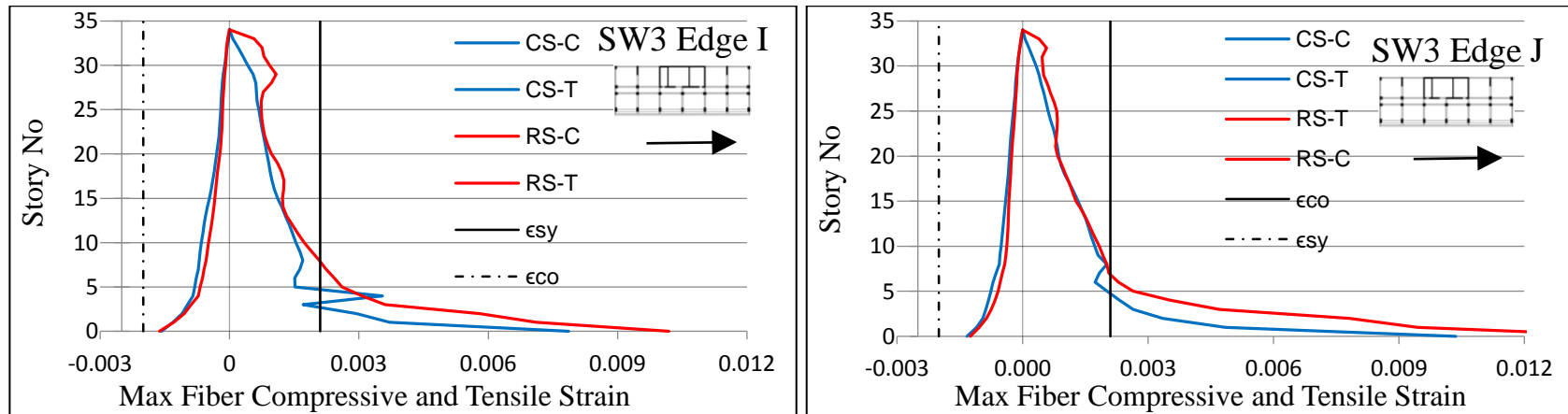


Figure 3.77 Comparison max fiber compressive and tensile strain of SW3 under MCE shaking.

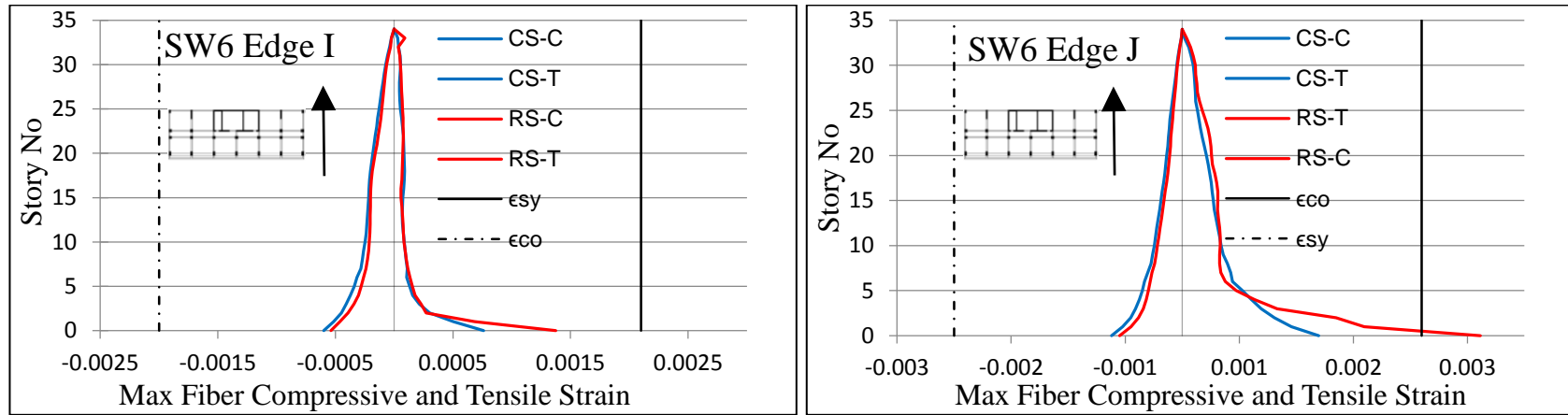


Figure 3.78 Comparison max fiber compressive and tensile strain of SW6 under SLE shaking.

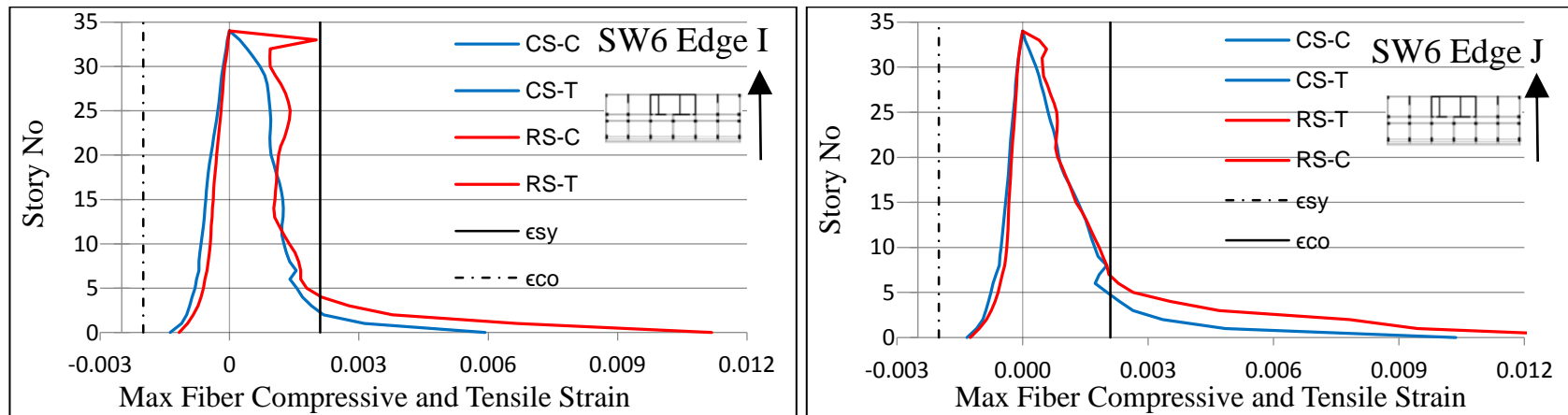


Figure 3.79 Comparison max fiber compressive and tensile strain of SW6 under MCE shaking

CHAPTER 4

SUMMARY AND CONCLUSIONS

4.1 SUMMARY

Performance based seismic design of tall buildings by employing nonlinear time history analysis (NLTHA) as an analysis tool is summarized in this study. The need for tall buildings is increasing gradually and most of those buildings are located in seismic regions. Unlike regular buildings, tall buildings are special buildings due to specific architectural properties and building configurations. In addition, the contribution of higher mode effects influences the dynamic behavior of tall buildings significantly under earthquake excitations. On the other hand, current prescriptive seismic codes are too restrictive and inadequate to understand the anticipated behavior of tall buildings and apply a reasonable design. The studies show that the need for alternative designs and analysis methods, especially using NLTHA, in order to conduct a feasible design for tall buildings is an inevitable requirement. The reasons of this requirement were explained elaborately. In addition, the basic reasoning for issuing non-prescriptive alternative seismic design guidelines for tall buildings by official building departments or task groups is clarified.

The main concern in performance based seismic design is to evaluate a structure and members of the structure by comparing damage and/or internal forces or deformations with pre-defined target performance criteria under an expected earthquake scenario. Current conventional seismic codes do not allow a realistic anticipation and distribution of these effects properly. However, damage and internal forces can be controlled reasonably if a reliable performance based design approach is conducted. For this propose, the first step is to define performance levels and acceptance criteria depending on the expected earthquake shaking levels. Several performance levels may be defined for a structure but two performance levels are generally described for tall buildings. At service level evaluation stage, it is generally desirable that the tall buildings remain essentially elastic under small to

moderate earthquakes. In collapse prevention level stage, the target is that the tall buildings maintain their stability under expected strong earthquakes. In other words, collapse of the structures should be prevented. The controlling damage of the structure under any expected earthquake is satisfied by setting limit states on damage or/and force and deformation levels of members and global behavior of structure in order to maintain the anticipated functional requirement.

Performance based seismic design of tall buildings by conducting nonlinear dynamic analysis method is being increasingly used. It is a quite sophisticated and a time consuming process from creating nonlinear modeling to interpreting the results for expected structural performance. However, there are also a variety of uncertainties from modeling of the components to the selection of ground motions. For this purpose, advantages and disadvantages of nonlinear modeling options for reinforced concrete structural components was compared with each other. Moreover, the capabilities of the only commercially available software, PERFORM-3D, for nonlinear analysis of tall buildings was presented. For nonlinear modeling of reinforced concrete shear walls, several parametric case studies and sensitivity analyses (by comparing analytical result with test results which was done previously) have been performed in order to specify the number of fibers in a cross section, wall elements and energy and stiffness degradation factors. Instead of using more sophisticated material models, commercially available software utilizes simplified uniaxial bilinear or trilinear material models in fiber modeling. Accordingly, sensitivity analyses have been also implemented to show the effect of material models on the accuracy of results. For frame members, the characteristic properties of concentrated hinge model and shear displacement hinge model were indicated. The selection and modification of ground motion time series with respect to performance levels and the importance of P-delta effects on the nonlinear behavior of tall buildings were also mentioned. Afterward, performance levels and acceptance criteria for buildings and tall buildings with respect to official building codes and alternative non-prescriptive seismic guidelines for tall buildings were evaluated. Finally, a reinforced concrete unsymmetrical-plan tall building with 34 stories is designed according to the Turkish Seismic Code under design earthquake. At both service level and collapse prevention level, NLTHA is employed by using a suite set

of seven ground motions for checking the results in compliance with the determined target performance levels.

4.2 CONCLUSIONS

This study is about performance based seismic design of tall buildings by using nonlinear time history analysis. The following conclusions are drawn in accordance with the results obtained in this study.

- The need for tall buildings is growing consistently. Approximately, a thousand buildings over 100 meters are being constructed and thousands of buildings are planned currently all over the world. In addition, tall buildings which have been constructed in Turkey are located in the regions with high seismicity.
- Tall buildings are long period structures thus the contribution of higher modes are substantial.
- Current conventional seismic codes are too restrictive and insufficient. For example, innovative structural systems that are not recognized in current conventional seismic and building codes have been employed increasingly to enhance seismic performance of the building.
- Using nonlinear time history analysis in tall buildings is necessity if damage is expected when subjected to severe earthquake excitations. Current conventional seismic codes do not permit estimating distribution of the expected damage level and internal forces accurately. In tall buildings, predicting both the level of damage related to internal deformations and internal forces in the members are important to evaluate the seismic performance of structure.
- Performance based seismic design of tall buildings by conducting nonlinear time history analyses are based on many assumptions and simplifications at different stages. Accordingly, this method must be carried out by an expert structural engineer who has proven his/her specialty in this field.
- Tall buildings are long period structures thus it may be troublesome to select appropriate ground motion records to obtain correct response from these structures. The modifications employed for generating ground motion time

series is a debatable issue, thus ground motions must be selected by a ground motion specialist.

- The case study results show that although the case study is designed according to the provisions of TSE-500 (2000) and TEC-2007, it does not provide adequate resistance under expected earthquake levels.
- The overall behavior of the building obtained from the results obtained show that the building rotates about the strong axis of building where SW3 is located. The overall behavior structure is controlled by interstory drift ratio obtained under SLE shakings. Interstory drift limits under MCE shakings are more conservative.
- The contribution of higher modes on interstory drift ratio is significant.
- Results show that, axial load level on several columns and shear walls exceeds the pre-determined limit state for collapse prevention level. In addition, shear stress of SW3 exceeds the upper limits for shear strength of shear walls.
- Because of overturning moment and unsymmetrical building plan, the axial load level on column members especially near the core shear wall increase dramatically under maximum earthquake levels.
- Expected governing and controlling type of action is axial force for shear walls and columns.
- The shear stress results of the shear walls when subjected to MCE shaking also indicate that the contribution of higher modes to the total shear response is significant because the shear stress of walls decrease from the second story until nearly the 15th story, but then increase above this story.
- The results also indicate that shear stresses reach maximum value at the second story level due the presence of a podium level.
- The results also show that a plastic zone which is nearly equal to 15 % of building height developed at the base of each shear wall under the MCE excitation.
- Each shear wall has yielded but the amount of yielding of each shear wall is acceptable for collapse prevention level.

- Some minor yielding occurred in beam members under SLE excitations but these damages which are slightly beyond yield point may be acceptable for service level evaluation.
- Significant damages occurred in the beam members under MCE shakings but these damages are below the limit states. Accordingly, the structure maintains its stability under expected strong earthquakes.
- There is no significant damage in coupling beams.
- Several performance targets are not satisfied, hence the preliminary design was revised to achieve the objectives of performance evaluation levels.
- After the design is revised, the obtained results nearly satisfied all performance levels.
- When comparing the original case study results with revised case study, although the dimension of core shear wall and some columns is increased, the axial strain at the bottom of shear walls also increases and the interstory drift ratios increased slightly since the building tends to show more torsional rotations due to the shift in the center of rigidity caused by the stiffness increase in the shear wall SW3.
- The increase in the sizes of columns and shear walls causes a modification of the seismic properties of the selected the original case study building but the capacity improvement is evidently more than the demand increase as expected.
- Performance based seismic design utilizing nonlinear time history analysis is dependent on too many uncertainties and assumptions from modelling, ground motion selection, stiffness, material models to assessment stages, i.e. limit states, damage classification, etc. These assumptions could lead different analytical models, which directly affect the obtained results. In addition, the assessment results are purely related to the selected performance criteria. Therefore, this method should be carried out by authorized and certified design engineers.

REFERENCES

1. Ali M.M. and Moon K.K (2007). Structural Developments in Tall Buildings, Architectural Science Review, Vol. 50.3, pp. 205-223.
2. ACI (2008). Building Code Requirements for Structural Concrete (ACI 318-08) and Commentary (ACI 318R-08), American Concrete Institute, Farmington Hills, Michigan.
3. Alici F.S. (2013). Generalized Pushover Analysis, M.S. Thesis, Department of Civil Engineering, Middle East Technical University, Ankara.
4. American Society of Civil Engineers (2010). ASCE 7-10 Minimum Design Loads for Buildings and Other Structures, Reston, VA.
5. American Society of Civil Engineers (2013). ASCE/SEI Standard 41-13, Seismic Rehabilitation of Existing Buildings, Reston, VA.
6. Applied Technology Council (2010). ATC-72-1: Modeling and Acceptance Criteria for Seismic Design and Analysis of Tall Buildings, Redwood City, California.
7. Baker J.W. (2011). Conditional Mean Spectrum: Tool for Ground Motion Selection, Journal of Structural Engineering, 137(3), 322-331.
8. Chopra A.K. and Goel R.K. (2002). A Modal Pushover Analysis Procedure for Estimating Seismic Demands for Buildings, Earthquake Engineering and Structural Dynamics, Vol. 31, pp. 561-582.
9. Chopra A.K., Chintanapakdee C. (2004). Inelastic deformation ratios for design and evaluation of structures: single-degree-of-freedom bilinear systems, Journal of Structural Engineering, 130(9), 1309-1319.
10. Christopoulos C. (2015). Prota 30. Yıl Sempozyumu, Personal Communication.
11. Council on Tall Buildings and Urban Habitat. Available from: 11 August 2015 <http://skyscrapercenter.com>
12. CTBUH (2008). Recommendations for the Seismic Design of High-Rise Buildings, Report of the Working Group on the Seismic Design of Tall Buildings, prepared by Willford M., Whittaker A.S., and Klemencic R.,

edited by Wood A., for the Council on Tall Buildings and Urban Habitat, Chicago, Illinois.

13. Elwood K.J., Matamoros A.B., Wallace J.W., Lehman D.E., Heintz J.A., Mitchell A.D., Moore M.A., Valley M.T., Lowes L.N., Comartin C.D., and Moehle J.P. (2007). Update to ASCE/SEI 41 concrete provisions, *Earthquake Spectra*, Vol. 23, No. 3, pp. 493-523.
14. FEMA (2009). 'Effects of Strength and Stiffness Degradation on Seismic Response, FEMA P440A Report, prepared by the American Society of Civil Engineers for the Federal Emergency Management Agency, Washington, D.C.
15. Filippou F.C., Popov E.G., and Bertero V.V. (1983). Effects of Bond Deterioration on Hysteretic Behavior of Reinforced Concrete Joints, UCB/EERC Report 83/19, University of California, Berkeley, California.
16. Goel R. K. and Chopra A. K. (2005). Extension of Modal Pushover Analysis Procedure to Compute Member Forces, *Earthquake Spectra*, Vol. 21(1), pp. 125-139.
17. Gupta B. and Kunnath S. K. (2000). Adaptive Spectra-Based Pushover Procedure for Seismic Evaluation of Structures, *Earthquake Spectra*, Vol. 16, No. 2, pp. 367–391.
18. Haselton C.B., Liel A.B., Taylor Lange S., and Deierlein G.G. (2008). 'Beam-Column Element Model Calibrated for Predicting Flexural Response Leading to Global Collapse of RC Frame Buildings, PEER Report 2007/03, Pacific Earthquake Engineering Research Center, University of California, Berkeley, California.
19. Ibarra L.F., Medina R.A., and Krawinkler H. (2005). Hysteretic models that incorporate strength and stiffness deterioration, *Earthquake Engineering and Structural Dynamics*, Vol. 34, No. 12, pp. 1489-1511.
20. Ibarra L.F., and Krawinkler H. (2005). Global Collapse of Frame Structures under Seismic Excitations, John A. Blume Earthquake Engineering Center Report No. TR 152, Department of Civil Engineering, Stanford University, Stanford, California and PEER Report 2005/06 Pacific Earthquake Engineering Research Center, University of California, Berkeley, California.

21. Istanbul Metropolitan Municipality (IMM) (2008). Istanbul seismic design code for tall buildings, prepared by Kandilli Observatory and Earthquake Research Institute
22. Krawinkler H. (2006). Importance of Good Nonlinear Analysis, *The Structural Design of Tall and Special Buildings Journal* 15, 515-531.
23. Los Angeles Tall Buildings Structural Design Council (2005). *An Alternative Procedure for Seismic Analysis and Design of Tall Buildings Located in the Los Angeles Region*. Los Angeles Tall Buildings Council: Los Angeles, CA.
24. Los Angeles Tall Buildings Structural Design Council (2008). *An Alternative Procedure for Seismic Analysis and Design of Tall Buildings Located in the Los Angeles Region*. Los Angeles Tall Buildings Council: Los Angeles, CA.
25. Los Angeles Tall Buildings Structural Design Council (2011). *An Alternative Procedure for Seismic Analysis and Design of Tall Buildings Located in the Los Angeles Region*. Los Angeles Tall Buildings Council: Los Angeles, CA.
26. Los Angeles Tall Buildings Structural Design Council (2013). *An Alternative Procedure for Seismic Analysis and Design of Tall Buildings Located in the Los Angeles Region*. Los Angeles Tall Buildings Council: Los Angeles, CA.
27. Los Angeles Tall Buildings Structural Design Council (2014). *An Alternative Procedure for Seismic Analysis and Design of Tall Buildings Located in the Los Angeles Region*. Los Angeles Tall Buildings Council: Los Angeles, CA.
28. Los Angeles Tall Buildings Structural Design Council (2015). *An Alternative Procedure for Seismic Analysis and Design of Tall Buildings Located in the Los Angeles Region*. Los Angeles Tall Buildings Council: Los Angeles, CA.
29. Mander J.B., Priestley M.J.N. and Park R. (1988). Observed stress-strain behavior of confined concrete, *Journal of Structural Engineering, ASCE*, Vol. 114, No.8, pp. 1827-1849.
30. Massone L.M., Orakcal K., Wallace J.W. (2006). Modeling flexural/shear interaction in RC walls ACI-SP-236, *Deformation Capacity and Shear Strength of Reinforced Concrete Members under Cyclic Loadings*, American Concrete Institute: Farmington Hills, MI, Paper 7, 127-150, May 2006.
31. Massone L.M. (2006). *RC Wall Shear – Flexure Interaction: Analytical and Experimental Responses*, Ph.D. Dissertation, University of California, Department of Civil & Environmental Engineering, Los Angeles, California.

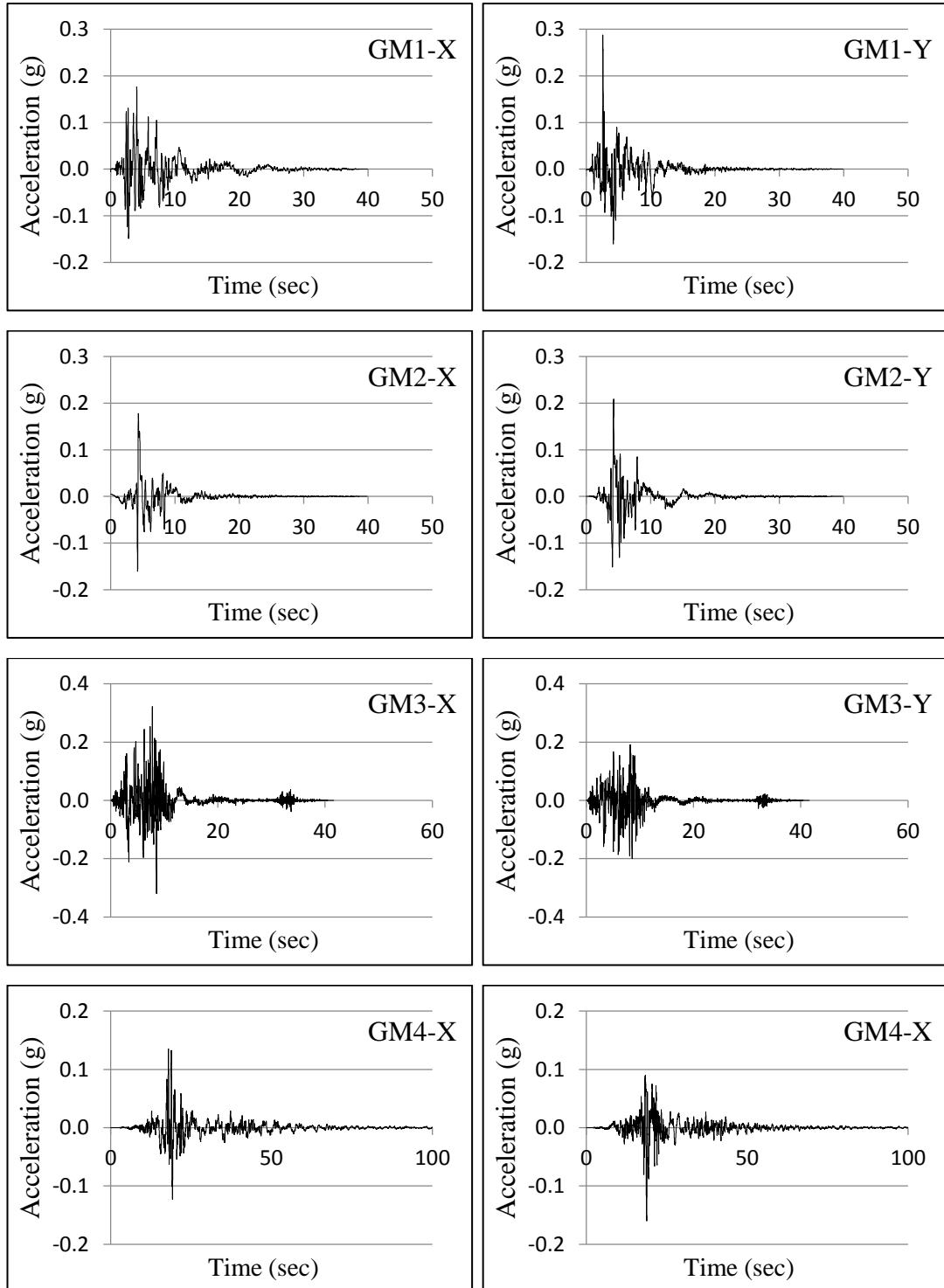
32. Menegotto M. and Pinto P. (1973). Method of analysis for cyclically loaded RC plane frames including changes in geometry and non-elastic behavior of elements under combined normal force and bending, Proceedings of Symposium on Resistance and Ultimate Deformability of Structures Acted on by Well-Defined Repeated Loads, IABSE Reports, Vol. 13, pp. 2557-2573.
33. Moehle J.P. (2005). Nonlinear Analysis for performance-based earthquake engineering, The Structural Design of Tall and Special Buildings Journal 14, 385-400.
34. NEHRP (2010). Nonlinear Structural Analysis for Seismic Design, NEHRP Seismic Design Technical Brief No. 4, NIST GCR 10-917-5, U.S Department of Commerce Gary Locke.
35. NEHRP (2013). Nonlinear Analysis Research and Development Program for Performance-Based Seismic Engineering, NIST GCR 14-917-27, December 2013, U.S Department of Commerce.
36. OpenSees (2005). Open System for Earthquake Engineering Simulation, 'http://opensees.berkeley.edu', November 15, 2011.
37. Orakcal K., and Wallace J.W. (2006). Flexural modeling of reinforced concrete walls-Experimental verification, Structural Journal, ACI, Vol. 103, No. 2, pp. 196-206.
38. Pacific Earthquake Engineering Center (2010). Seismic Design Guidelines for Tall Buildings, PEER Report 2010/05, prepared by the TBI Guidelines Working Group, Berkeley, California.
39. Pampanin S, Christopoulos C, and Priestley M.J.N. (2002). Residual Deformations in the Performance-Seismic Assessment of Frame Structures, Research Report No. ROSE-2002/02, European School for Advanced Studies in Reduction of Seismic Risk, Pavia, Italy.
40. PEER Strong Motion Database (2014). Available from: <http://peer.berkeley.edu/smcat>.
41. Perform 3D V5.0 (2011). Nonlinear Analysis and Performance Assessment for 3D Structures.
42. Perform 3D V5.0 (2011). Components and Elements for Perform 3D and Perform Collapse, Berkeley, California, USA.

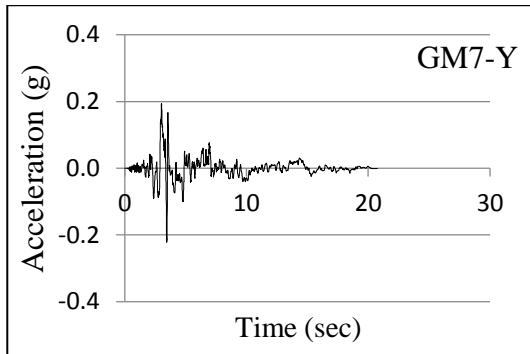
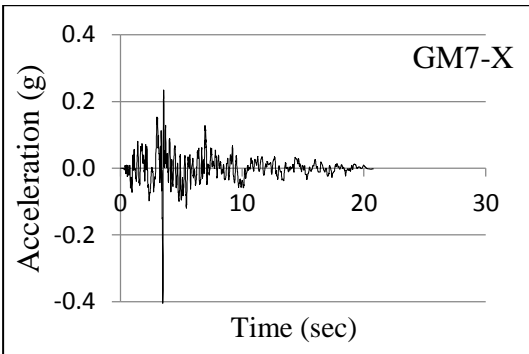
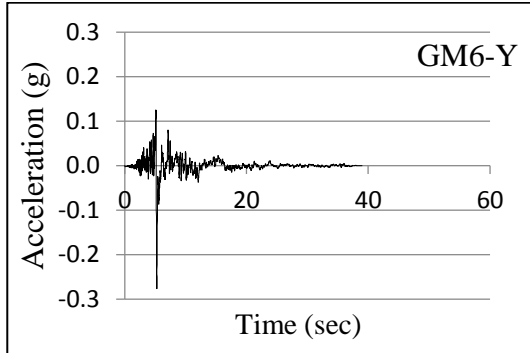
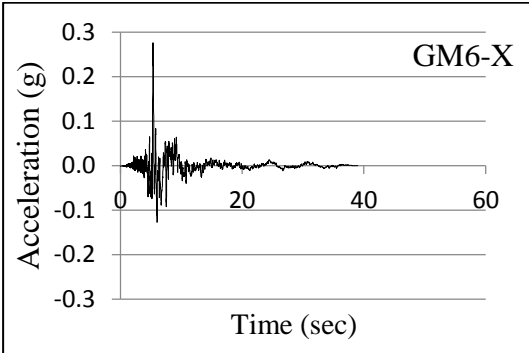
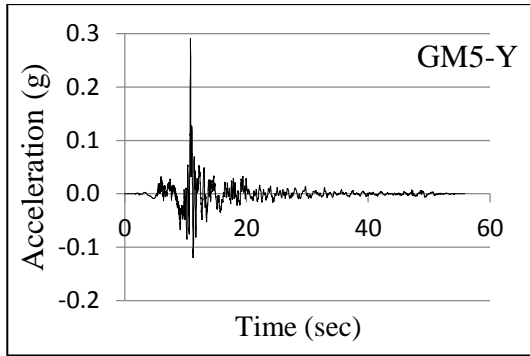
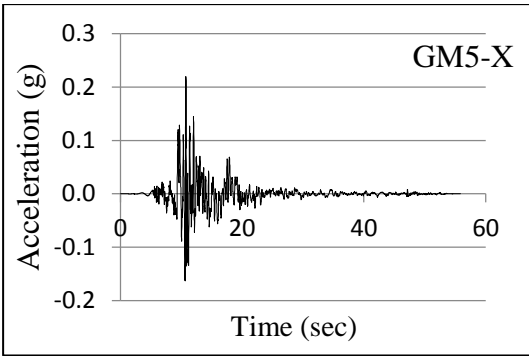
43. Perform 3D V5.0 (2011). User Guide for Perform 3D, Berkeley, California, USA.
44. Planning and Growth Management Committee of Toronto (2013). Tall Buildings Design Guidelines, Toronto.
45. Poursha M., Khoshnoudian F. and Moghadam A.S. (2009). A Consecutive Modal Pushover Procedure for Estimating the Seismic Demands of Tall Buildings, *Engineering Structures*, Vol. 31, pp. 591-599.
46. Powell G. (2012). Seminar Notes of Perform 3D.
47. Ruiz-Garcia J. and Miranda E. (2003). Inelastic displacement ratio for evaluation of existing structures, *Earthquake Engineering and Structural Dynamics*, 32(8), 1237-1258, 2003.
48. Ruiz-Garcia J. and Miranda E. (2006). Residual displacement ratios for the evaluation of existing structures, *Earthquake Engineering and Structural Dynamics*, Vol. 35, pp. 315-336.
49. Saatcioglu M. and Razvi S. (1992). Strength and ductility of confined concrete, *Journal of Structural Engineering*, ASCE, Vol.118, No.6, pp. 1590-1607.
50. San Francisco Department of Building Inspection (2013). San Francisco Building Code.
51. SAP 2000 V.15.1.0 (2015). Integrated Software for Structural Analysis and Design, Berkeley, California, USA.
52. Saritaş A. (2013). CE 7016 Nonlinear Structural Analysis Course Notes, Middle East Technical University, Ankara.
53. Scott B.D., Park R., and Priestley M.J.N. (1982). Stress-strain behavior of concrete confined by overlapping hoops at high and low strain rates, *ACI Journal Proceedings*, Vol. 79, No. 1, pp. 13-27.
54. Salas M.C. (2008). Modeling of Tall Reinforced Concrete Wall Buildings, MSCE Thesis, Department of Civil and Environmental Engineering, University of California, Los Angeles, California.
55. Structural Engineers Association of Northern California (SEAONC) (2007). Recommended Administrative Bulletin on the Seismic Design and Review of Tall Buildings using Non-Prescriptive Procedures, AB-083 Task Group.

56. Sucuođlu H. and Gđnay M. S. (2011). Generalized Force Vectors for Multi-Mode Pushover Analysis, Earthquake Engineering and Structural Dynamics, Vol. 40, pp. 55-74.
57. Sucuođlu H. and Akkar S. (2014). Basic Earthquake Engineering from Seismology to Analysis and Design, Springer.
58. Sucuođlu H. (2015). Performans esaslı deprem mđhendisliđinin temel kavramları, Sekizinci Ulusal Deprem Mđhendisliđi Konferansı.
59. Priestley M.J.N., Calvi G.M., Kowalsky M.J. (2007). Displacement-Based Seismic Design of Structures, IUSS Press.
60. Thomsen IV J.H. and Wallace J.W. (2004). Experimental Verification of Displacement-Based Design Procedures for Slender Reinforced Concrete Structural Walls, Journal of Structural Engineering, ASCE, Vol. 130, No. 4, pp. 618-630.
61. Yassin M.H.M. (1994). Nonlinear analysis of pre-stressed concrete structures under monotonic and cyclic loads, Ph.D. Dissertation, University of California, Berkeley, California.

APPENDIX A

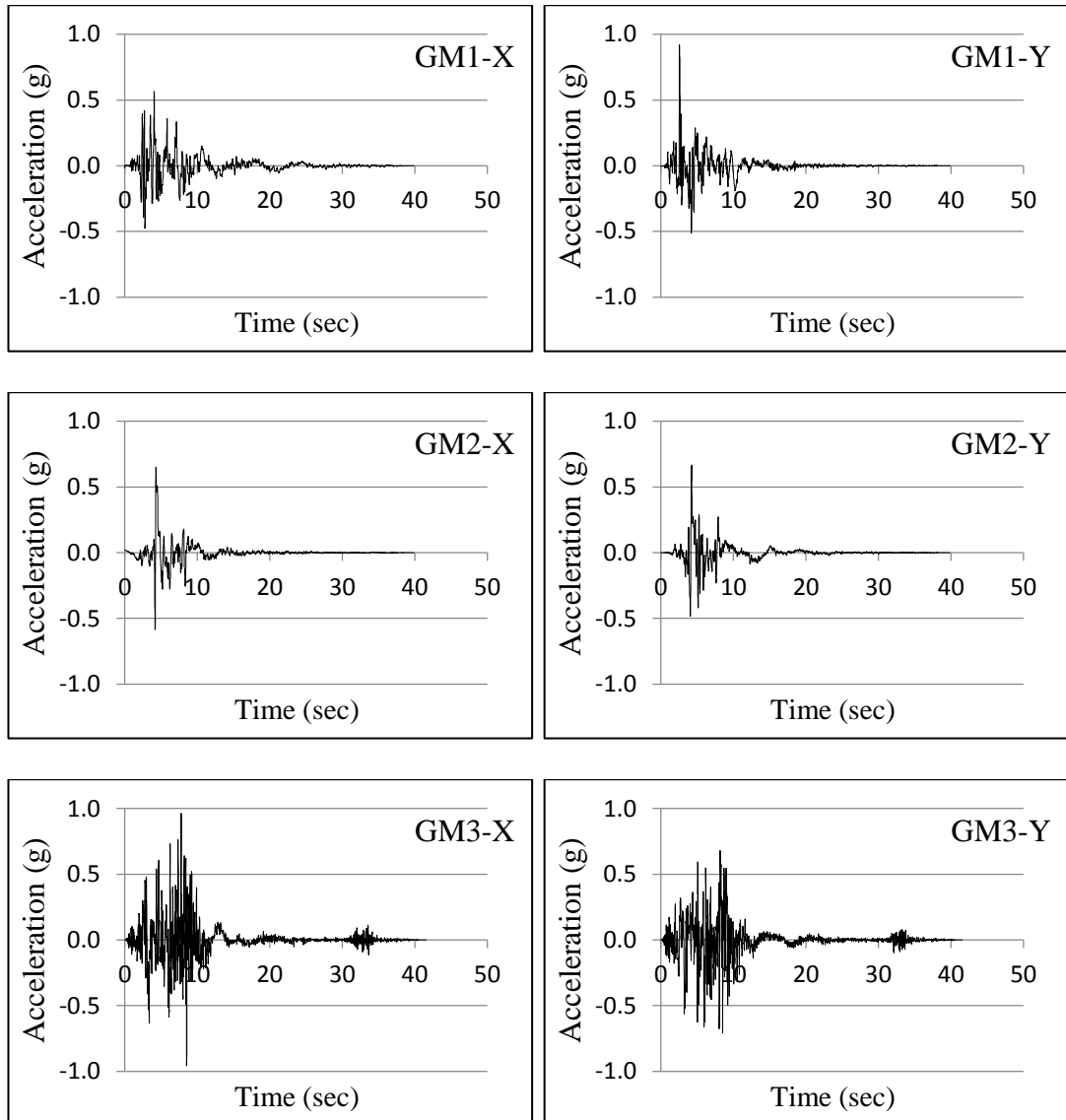
SERVICE LEVEL EARTHQUAKE GROUND MOTIONS TIME SERIES

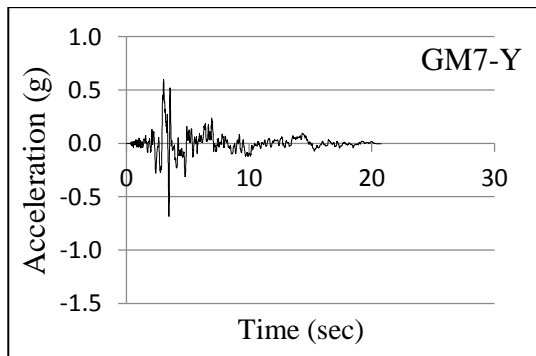
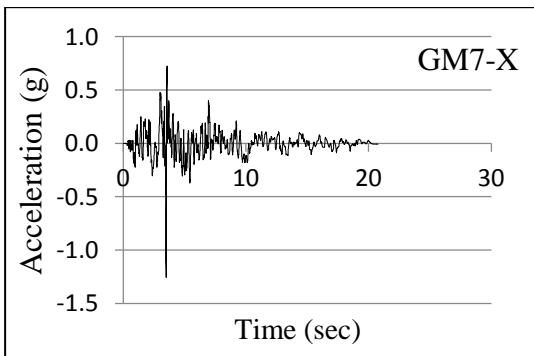
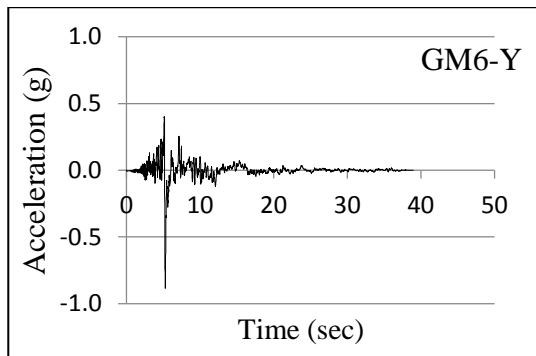
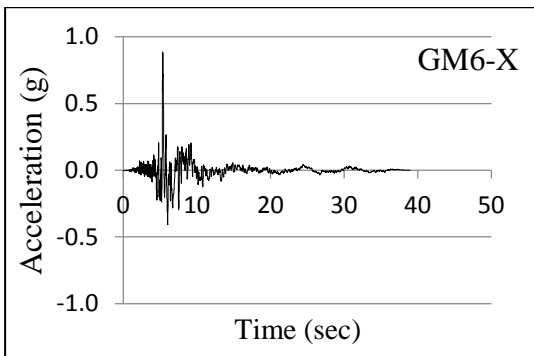
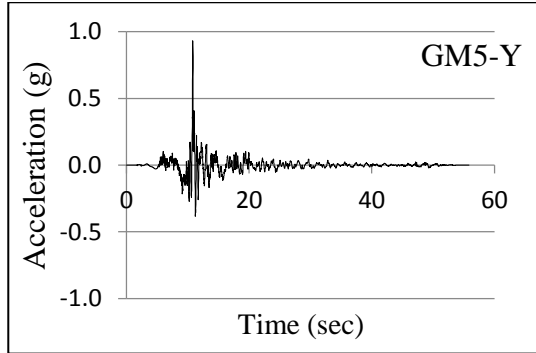
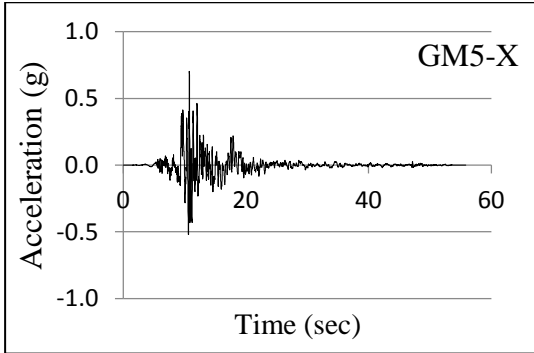
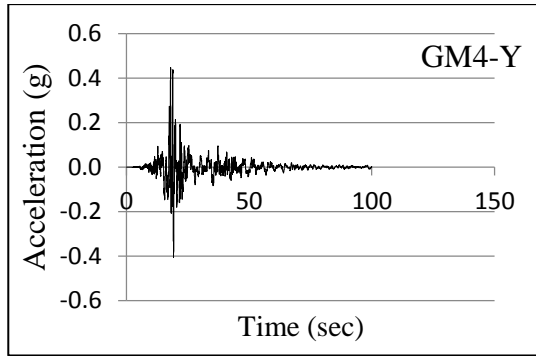
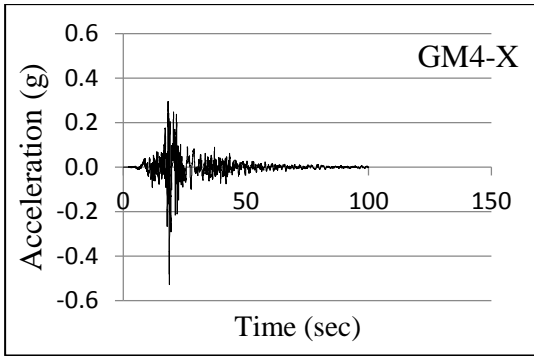




APPENDIX B

MAXIMUM CONSIDERED EARTHQUAKE GROUND MOTIONS TIME SERIES





APPENDIX C

SELECTED CRITICAL SECTION DETAILS

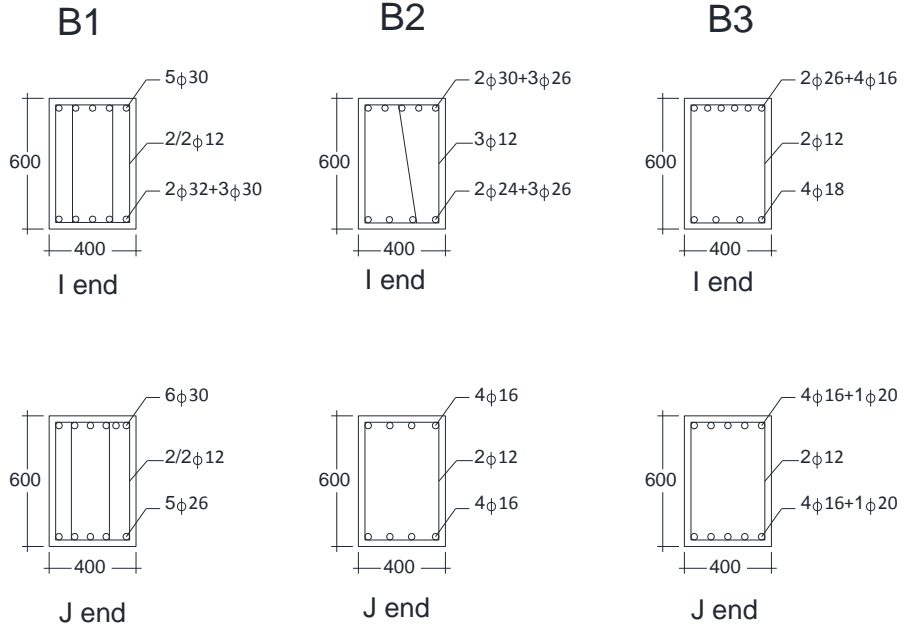


Figure A.1 Selected critical beam section details at the support region

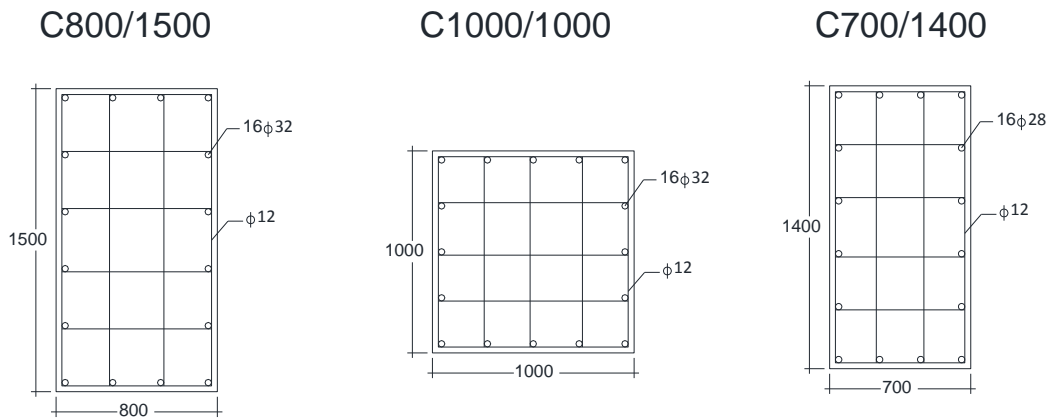


Figure A.2 Selected column section details

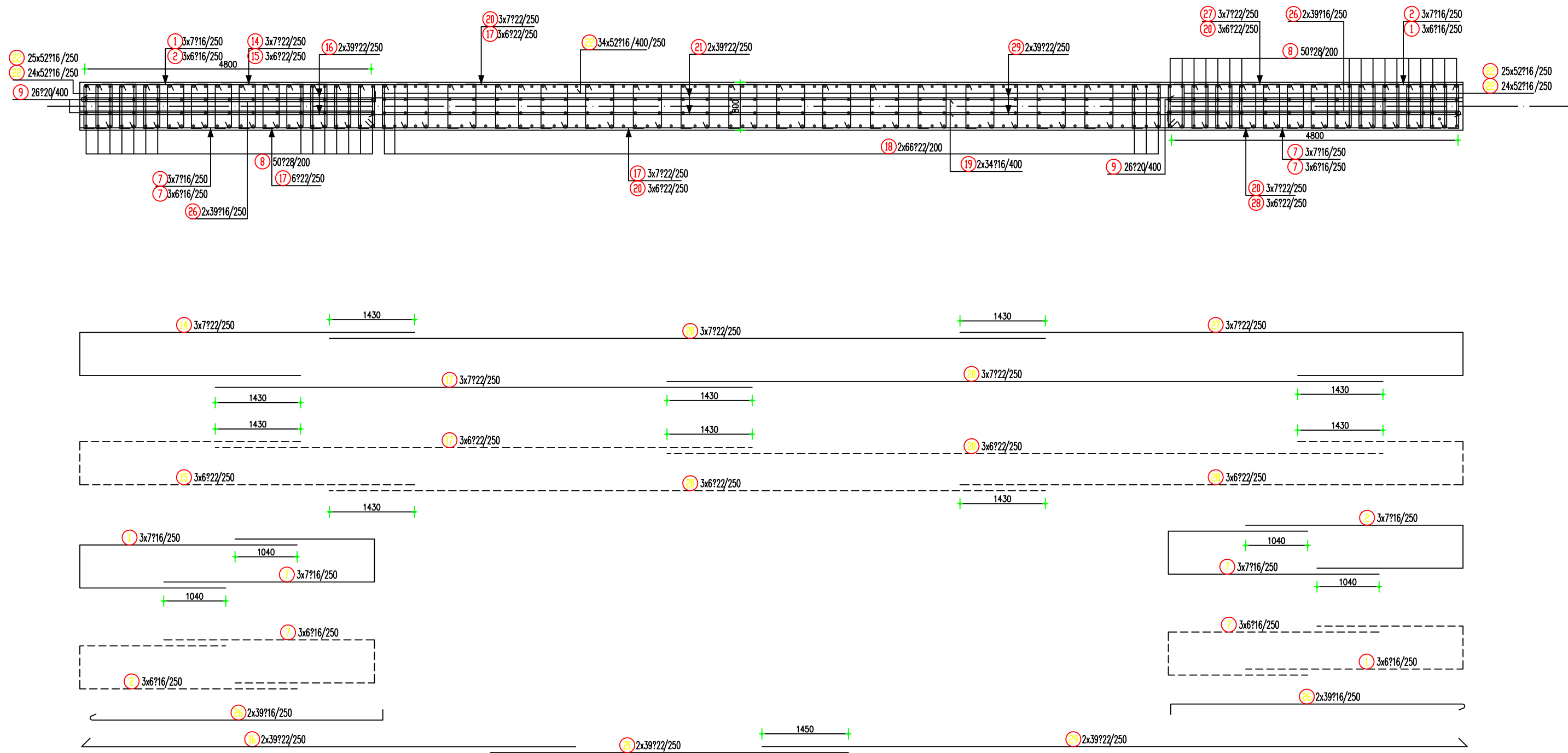


Figure A.4 Section details of parametric case study

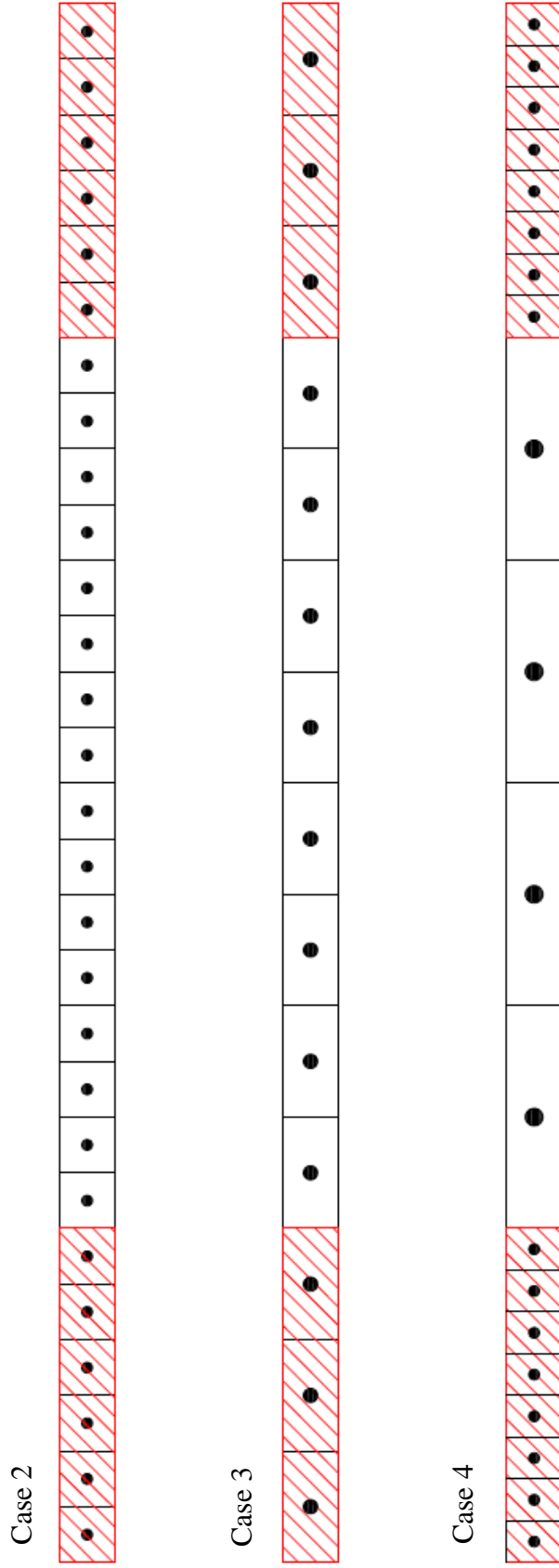


Figure A.5 The detailed fiber properties of parametric case study